Method Development for Characterization of N-linked Glycoproteins in Mass Spectrometry

By

2007

Ying Zhang

Ph.D., University of Kansas 2007

Submitted to the Department of Chemistry and the
Faculty of the Graduate School of the University of Kansas
in partial fulfillment of the requirements for the degree of
Doctor of Philosophy

_____
Heather Desaire (Chairperson)

_____
Robert C. Dunn

_____
Cindy L. Berrie

_____
David D. Weis

_____
Roberto N. De Guzman

Date defended _____

The Dissertation Committee for Ying Zhang certifies that this is the approved version of the following dissertation:

Method Development for Characterization of N-linked Glycoproteins in Mass Spectrometry

Committee:

_____
Heather Desaire (Chairperson)

_____
Robert C. Dunn

_____
Cindy L. Berrie

_____
David D. Weis

_____
Roberto N. De Guzman

Date Accepted _____

Abstract

Method Development for Characterization of N-linked Glycoproteins in Mass Spectrometry

by

2007

Ying Zhang

Doctor of Philosophy in Chemistry

University of Kansas

Advisor: Dr. Heather Desaire, Chair

Protein glycosylation is one of the most important post-translational modifications, and it is involved in many biological processes, including inter-/intra cell signaling, protein recognition, and receptor binding, etc. It is estimated that 50-60% of cell-surface and secreted proteins are glycosylated. Alteration in the glycan structures on these proteins has been implicated in various disease states, such as, cancer, Alzheimer's disease, rheumatoid arthritis, and chronic obstructive pulmonary disease, etc. Thus, characterizing glycans and monitoring the changes of glycan profiles on proteins are essential to elucidate their biological significance and facilitate disease diagnosis.

Mass spectrometry is a powerful tool for characterizing glycans on proteins, due to its high sensitivity, selectivity and small sample requirements for analysis. In order to elucidate a variety of glycan profiles (including both neutral and acidic glycans) on glycoproteins, several efficient MS-based approaches have been developed, and they are described herein. These approaches include an ion-pairing strategy in conjunction with ESI-MS/MS to identify the acidic functional groups (sulfate, and phosphate) in carbohydrates and glycopeptides; and a glycopeptide-

based MS approach (liquid chromatography followed by MALDI-TOF/TOF) to characterize glycans on different glycoproteins that vary in the number of glycosylation sites and their corresponding glycan profiles.

Aside from protein glycosylation, disulfide connectivity is another important modification present in proteins, and it plays a key role in establishing/maintaining protein structures in their biologically active forms. Therefore, determination of disulfide bond arrangement provides chemical structural information about proteins, and it may lead to insights into their functional roles. To achieve this goal of determining disulfide bonding patterns in proteins, a mass spectrometric approach using liquid chromatography followed by electrospray ionization-Fourier transform ion cyclotron resonance mass spectrometry (LC/ESI-FTICR-MS) has been validated and used to determine the disulfide bond arrangement in an HIV envelope protein. This study contributes to the understanding of this protein's structure, and these findings are essential in understanding and improving the protein's immunogenicity.

Acknowledgment

First of all, I would like to express my deep and sincere gratitude to my advisor, Dr. Heather Desaire for her broad knowledge, invaluable guidance, continuous support, and encouragement throughout this study. Without those knowledge and guidance from her, this study would not have been successful.

I would also like to express my deep gratitude to Dr. Eden P. Go for her detailed and constructive suggestions in my research, and helping me with MALDI instrument, editing my papers, and providing suggestions in my oral comprehensive examination, etc. I am also thankful to Dr. Hui Jiang for his generous assistance at the beginning of my research and helping me to initiate my first project in graduate school. I warmly thank Dr. Todd Williams and Dr. Marc Anderson for their kind support and guidance in the instruments used in my research. I would also like to thank Dr. Barton F. Haynes, Dr. Hua-Xin Liao, and Laura L. Sutherland at Duke Human Vaccine Research Institute (Duke University, Durham, NC) for supplying HIV Env proteins for my research. I warmly thank Dr. George R. Bousfield, and Dr. Vladimir Y. Butnev from Wichita State University for supplying the glycoprotein hormones for my study.

I am thankful to all my graduate friends for sharing literatures, invaluable opinions, comments, and assistance in my course work and my research. I am also thankful to all my Chinese friends in Lawrence Chinese Evangelical Church for prayers and their continued support in my life.

I would like to express my love and gratitude to my beloved family for their understanding, support, encouragement, trust, and endless love in my entire life, especially my mother, thank you for always being there for me. I would also like to

express my loving thanks to my fiancé Xuefeng Xue for his support, understanding, encouragement, and love through the duration of my last two years' graduate studies. Without his encouragement and understanding, it would be impossible for me to finish writing this dissertation. Thank you for being willing to share your opinions, comments and suggestions in my life. Thank you for bringing lots of happiness in my life.

Last but not least, I would like to give all my deep and sincere thanks to God for my life. You have made my life bountiful and blessed.

Table of Contents

I. Introduction

1.1 Mass spectrometry……1

1.2 Matrix-assisted laser desorption/ionization (MALDI)……...2

1.3 Electrospray ionization (ESI)……17

1.4 Principle of quadrupole ion-trap mass spectrometry……18

1.5 Principle of Fourier transform mass spectrometry……20

1.6 Background information on carbohydrates and glycoproteins…….....22

1.7 Analyzing carbohydrates and glycoproteins by mass spectrometry……25

1.8 Overview and summary of the following chapters……27

1.9 References……30

II. A novel mass spectrometric method to distinguish isobaric monosaccharides that are phosphorylated or sulfated using ion-pairing reagents.

2.1 Introduction……...35

2.2 Experimental……..37

2.3 Results and discussion……..38

2.4 Conclusions……...56

2.5 References……57

III. Distinguish phosphorylation and sulfation in carbohydrates and glycoproteins using ion-pairing and mass spectrometry.

3.1 Introduction……60

3.2 Experimental……..63

3.3 Materials and methods……65

3.4 Conclusions……...76

3.5 References……76

IV. Maximizing coverage of glycosylation heterogeneity in MALDI-MS analysis of glycoproteins with up to 27 glycosylation sites.

4.1 Introduction……...80

4.2 Experimental section……..84

4.3 Results and discussion……..89

4.4 Conclusions……112

4.5 References……...115

V. Determination of disulfide bond arrangement of HIV Env protein CON-S gp140 ΔCFI by LC/ESI-FTICR mass spectrometry.

5.1. Introduction……120

5.2. Experimental section……...124

5.3. Results and discussion……...126

5.4. Conclusions……145

5.5. References……..147

VI. Conclusions……151

Chapter I

Introduction

1.1 Mass spectrometry

During past two decades, mass spectrometry has emerged as a powerful and variable tool, which has been widely used in fundamental studies and analytical applications.[1-3] This technique measures the molecular mass of a molecule according to its mass-to-charge ratio (*m/z*). Typically, a mass spectrometer consists of three basic components: an ionization source, mass analyzer, and detector;[1] see Figure 1. Gas-phase ions are initially generated from a solid or liquid form in the ionization source by gaining or losing a charge on the neutral molecules.[4] The charged gas-phase ions are electrostatically drawn into a mass analyzer, separated based on the *m/z* ratio and then detected by a detector.[1] The generated mass spectrum provides the molecular masses of these ions.

There are several soft ionization techniques that have been widely used in the studies of glycomics, proteomics and glycoproteomics, etc. These soft ionization techniques consist of fast atom bombardment (FAB)[5-8], matrix-assisted laser desorption/ionization (MALDI)[1, 9-17] and electrospray ionization (ESI)[1, 3, 14]. Among these ionization sources, two ionization processes -MALDI and ESI- are used in the research presented herein. Therefore, the fundamentals of these two ionization sources will be discussed in the following sections. The principles as well as the application of FAB can be found in references 5 through 8.

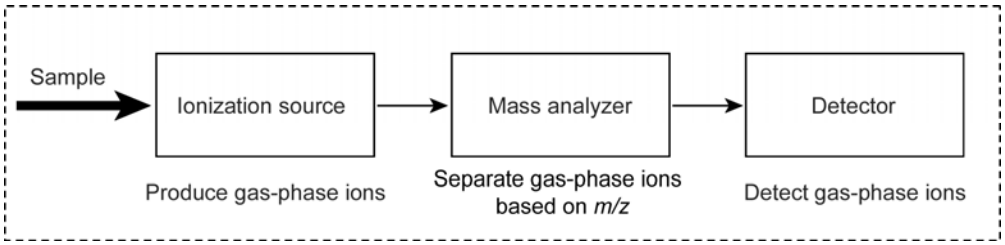

Figure 1. Schematic representation of the three basic components in mass spectrometry and their functions; the ions are produced in the ionization source, separated in the mass analyzer according to their *m/z* ratio, and then detected in a detector.

1.2 Matrix-assisted laser desorption/ionization (MALDI)

MALDI is one of the soft ionization processes to produce charged ions for biologically relevant molecules with molecular masses up to 300 kDa.[18, 19] MALDI mass spectrometry (MALDI-MS) was invented in 1988 by Tanaka, Karas, and Hillenkamp.[19] Since then, it has become one of the essential techniques in the identification of proteins and their corresponding post-translational modifications (PTMs) with high sensitivity, selectivity and throughput.[4, 15, 18, 20] The invention of this technique was a landmark, in that it provided an opportunity to apply mass spectrometry to the analysis of non-volatile, complex biological samples.[4, 18]

The MALDI ionization process initiates with mixing the sample with an excess amount of matrix solution and spotting the sample:matrix mixtures on the MALDI target plate. The crystallized sample:martrix mixtures are then irradiated by a laser beam to extract and ionize the analytes, as well as matrix molecules, into the gas phase, as shown in Figure 2. Although this process is still not well understood, it is generally believed that the matrix molecules absorb a large amount of the photon energy from the laser beam and subsequently transfer that energy to the analytes in a certain way that the sample molecules sublime to the gas phase as intact ions.[18, 19,

[21]

Two mechanisms have been proposed to explain how the charged analytes are formed in MALDI ionization process.[22, 23] The first mechanism shows a two-step ionization event: a primary ionization process, followed by a secondary in-plume ion-molecule reaction.[22] The matrix molecules are ionized in the first step and then undergo a secondary ion-molecule charge-transfer reaction with neutral analyte molecules in the expanding gas plume produced on the matrix surface; See Equation (1.1).

$$M^+ + A \rightarrow M + A^+ \qquad (1.1)$$

Where M^+ is the charged matrix molecule that could be protonated, sodiated, or deprotonated; A is the neutral analyte which participates the ion-molecule reaction to obtain the charge from the matrix molecule (M). The ion-molecule reactions between the charged matrix molecule and the neutral analyte might be proton transfer, cation transfer, electron transfer, or electron-capture reactions. In this model, the primary ionized matrix molecules are produced by laser excitation and the in-plume ion-molecule reaction plays a predominant role in the analyte ionization process.[18, 19, 21]

The second mechanism of analyte ionization is to produce the matrix-analyte clusters, followed by ionization of these clusters.[23] Two models have been proposed in this mechanism to explain how to charge the formed matrix-analyte clusters in MALDI ionization process. One model assumes that the analytes are present in a multiply charged form in the matrix.[23] The clusters are produced through trapping the multiply charged analytes as well as their counter-ions in the matrix. The generated and charged clusters are released in the plume by laser irradiation. During this process, the charged analyte molecules are generated from these matrix-rich

clusters via desolvation. The highly charged initial analytes cannot survive in the plume due to high charge-charge repulsion in the gas phase.[18, 22, 23] Therefore, these highly charged analytes undergo a charge reduction process, in which they are neutralized by the electrons produced by laser irradiation on the matrix.[22] During this process, only the singly charged ions are the lucky survivors in the plume. This explains why most gas phase ions produced in MALDI are singly charged. The second model of charging the formed matrix-analyte clusters is photoionization with normally used laser systems, such as N_2 (337 nm) laser and the frequency-tripled Nd:YAG (355 nm) laser, etc.[18, 19, 21]

In the desorption and ionization process discussed above, the generated analyte ions are mainly singly charged molecules. With the increases in the molecular masses of the sample molecules, the likelihood of forming oligomeric ions (e.g. doubly and triply charged ions) in MALDI becomes higher. Sodiated adducts are also a characteristic feature in the analysis of the biologically relevant samples by MALDI. In addition to the analysis of positively charged ions, the analysis of negatively charged ions is also possible with the MALDI ionization technique.[1, 9-11, 18-20]

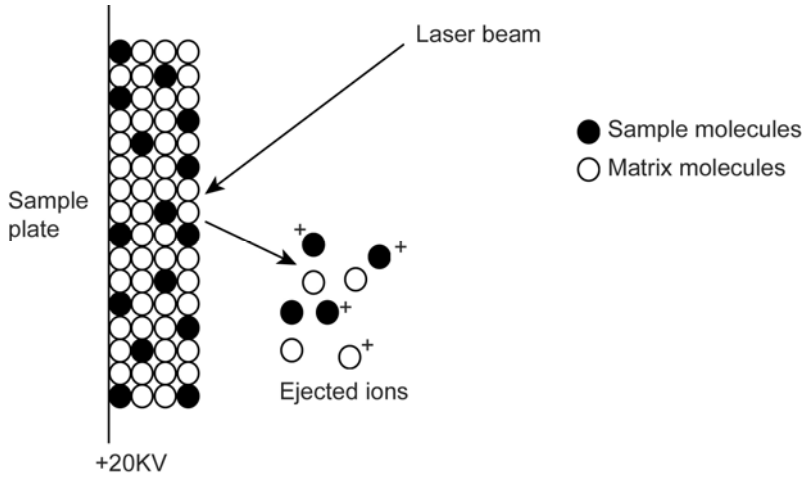

Figure 2. Matrix-assisted laser desorption/ionization process. (Adapted from Chhabil Dass, *Fundamentals of Contemporary Mass Spectrometry*, Wiley-interscience, New York, 2007.)

1.2.1 Laser systems in MALDI

In MALDI analysis, there are several important factors that need to be considered when performing the experiments, such as the laser system and the selected matrix solution. A diversity of laser systems has been applied in MALDI analysis, including UV lasers and IR lasers. UV lasers include the N_2 laser (337 nm), the ArF excimer laser (193 nm), and the frequency-tripled (355 nm) / frequency-quadrupled (266 nm) Nd:YAG lasers. IR lasers consist of the transversely excited atmospheric (TEA) CO_2 laser (10.6 μm), the Q-switched Er:YAG laser (2.94 μm), and the Cr:LiSAF / Nd:YAG pumped optical parametric oscillator (OPO) lasers (3.28 μm). These lasers are commonly used in MALDI systems and can produce the similar spectra in the analysis of biological samples.[12, 18, 19]

1.2.2 Matrices for MALDI

The MALDI matrix is another important part of the MALDI ionization process. Typically, the matrix used in MALDI desorption and ionization is a non-volatile solid material. It absorbs a large amount of photon energy from the laser beam and minimizes sample damage. The use of matrix can also reduce the inter-molecular forces among the sample molecules, thus decreasing sample aggregation. An ideal MALDI matrix is comprised of several characteristics: strong adsorption of laser energy to reduce sample damage; good solvent compatibility with analytes, to form well-defined crystals; low sublimation temperature, to facilitate the formation of a plume of the sample:matrix mixture by laser irradiation; and the ability to transfer charges to the analytes with high efficiency, through photochemical reactions.[18, 19, 21]

According to the characteristics of the ideal MALDI matrix, four classes of matrices have been widely used in the MALDI ionization process so far, including solid organic matrices, liquid organic matrices, ionic liquids, and inorganic materials. Solid organic matrices include α-cyano-4-hydroxycinnamic acid (CHCA), and 2,5-dihydroxybenzoic acid (DHB), etc. These compounds are the most common types of matrices retaining an aromatic ring in the structure to facilitate absorbing laser irradiation. While a wide range of species can be analyzed with this type of matrices, (such as proteins, peptides, oligosacchrides, glycoproteins, and glycopeptides, etc),[12] inhomogeneous distribution of the sample:matrix molecules in the crystallized solid phase exists when these matrices are used in MALDI analysis. Thus, spot-to-spot variations and sample-to-sample variations are present during analysis. Liquid organic matrices (e.g. 2-nitrophenyloctyl ether and 3-nitrobenzyl alcohol) and ionic liquids produced by mixing an organic solid matrix with an organic base (such as butylamine), can be used to overcome inhomogeneous distribution in the sample preparation.[18] Aside from organic compounds used in MALDI matrices, inorganic matrices such as metals, metal oxides, and graphitized carbon dispersed in a nonvolatile liquid are also used to mix with analytes and facilitate their detection in MALDI analysis.[12, 18, 19, 21]

1.2.3 Advantages and disadvantages of MALDI

MALDI produces charged molecules with little or no fragment ions; thus, it is a soft ionization technique that is applicable for the analysis of biomolecules, up to 300 kDa in mass. It also has a high salt tolerance and high sensitivity, detecting samples at a femtomole to low picomole levels, which is suitable for the analysis of samples present in low abundance in complex mixtures. Since matrix is necessary in

MALDI experiments, matrix interference would be a problem for the analysis of compounds in a lower mass range (< 700 Da). In addition, the use of an acidic matrix in MALDI may also cause sample degradation on a certain types of compounds. Therefore, selecting a suitable matrix material to be compatible with the analytes, to avoid the sample degradation, is very important. Aside from matrix interference, the laser beam used in MALDI may cause sample photodegradation. Therefore, the laser energy needs to be controlled carefully in the experiments, to reduce sample damage.[19]

1.2.4 Principles of time of flight (TOF) mass spectrometry

Time of flight (TOF) is a widely used mass analyzer coupled with MALDI ionization sources. Briefly, this technique works based on the principle that the generated ions from MALDI are accelerated and electrostatically drawn to the TOF tube in a field free drift region, in which the ions are separated based on the mass-to-charge ratio (*m/z*). Specifically, a positive voltage (V) is placed on the backing plate to produce an electric field within the source region, as shown in Figure 3. Prior to entering the field free drift region, all of the generated ions are accelerated to the same kinetic energy:

$$\frac{1}{2} mv^2 = qV \qquad (1.2)$$

where m= mass of the ion, v= velocity of the ion, q= charge of the ion, V= potential of the electric field. When the ions pass through the extraction grid, their velocities (v) are inversely proportional to the square root of their *m/q* (or *m/z*) values:

$$v = (2qV/m)^{1/2} \qquad (1.3)$$

Subsequently, the ions travel in a long, field free drift region of length L and reach the detector at different times, depending on their velocity, as described below:

$$t = L/v = L\bullet [m/(2qV)]^{1/2} \quad (1.4)$$

Since L and V are constants, the time spent to reach the detector relies on the square root of *m/q* (or *m/z*) of the ions. The lower *m/q* (or *m/z*) ions migrate faster and reach the detector earlier than the higher *m/q* (or *m/z*) ions in the field free drift region. The resultant time spectrum can be converted to a mass spectrum by an equation as shown below:

$$m/q = (2V) \bullet (t/L)^2 \quad (1.5)$$

From this equation, the *m/q* (or *m/z*) of the ions is proportional to the time they take to reach the detector. V and L are constants, determined by the experimental parameters in the instruments. Typically, the potential of the electric field V (accelerating voltage V) ranges from 3 kV to 30 kV, and the length of the TOF tube ranges from 15 cm to 8 m.[1, 9-11, 18-20]

Although the conventional linear TOF mass spectrometer can be employed to separate and detect the gas-phase ions on the basis of *m/z*, it generally has poor mass resolution (less than 500) which is related to the temporal width of two ions of the same *m/z* values (Δt) upon reaching the detector. The mass resolution of a TOF mass spectrometer is shown in below:

$$R = t/(2\Delta t) = m/\Delta m \quad (1.6)$$

Where R = mass resolution, t = time that the ions spend to reach the detector, Δt = the time interval of two ions of same *m/z* (s). Theoretically, if the ions of the same *m/z* value arrive at the detector simultaneously ($\Delta t \rightarrow 0$), the mass resolution can be increased according to equation (1.6). However, practically, when the ions are generated and accelerated in the source region, due to the intrinsic distribution in time (instant of ion formation), space (initial locations of the ions in the source

region), and velocity (different initial kinetic energies on the ions), the two ions with the same mass will not reach the detector at the same time. These factors result in the poor mass resolution in the linear TOF mass spectrometer. To mitigate these limitations and improve the mass resolution in MALDI-TOF analysis, delayed extraction and reflectron devices are designed and incorporated in the MALDI-TOF instrument.[1, 9-11, 18-20]

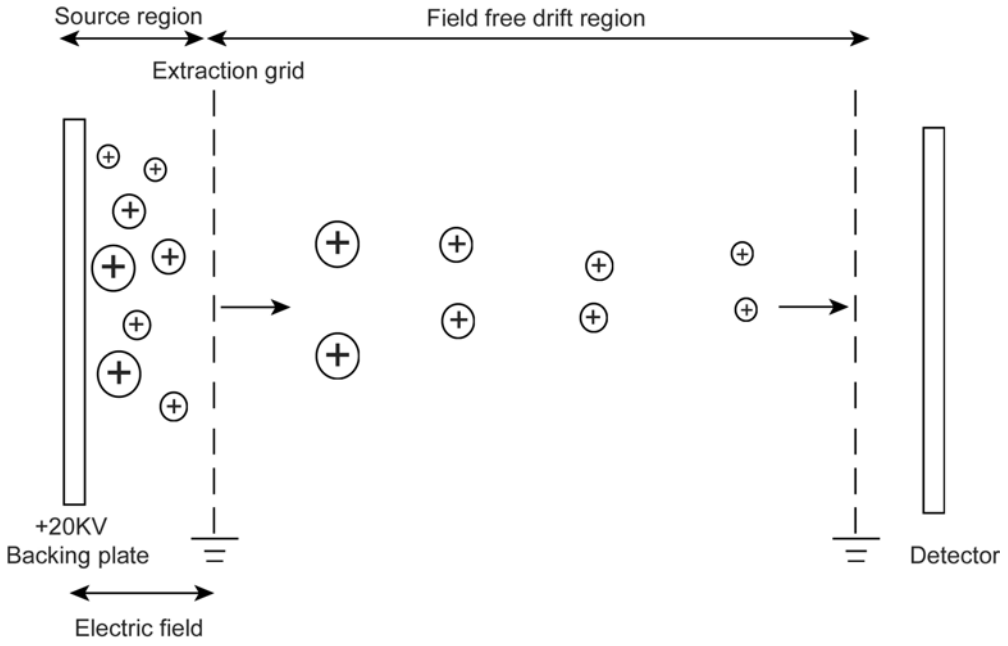

Figure 3. Schematic representation of mass separation in TOF analyzer; The ions are separated based on *m/z*. The ions with lower *m/z* (small circles) migrate faster than those with higher *m/z* (large circles). (Adapted from Chhabil Dass, *Fundamentals of Contemporary Mass Spectrometry*, Wiley-interscience, New York, 2007.)

1.2.5 Delayed extraction

Delayed extraction is an efficient approach to increase the mass resolution of a linear TOF mass spectrometer, in which the ionization source region has been divided into two regions, a field-free extraction region and an acceleration region; as shown in Figure 4A. In the ionization process, the crystallized sample:matrix mixture

is irradiated by a laser beam to form gas-phase ions. During this process, no potential is applied to the extraction region. The ions oscillate randomly in the field-free extraction region, in which the isomass ion with a higher initial velocity (e.g. ion a) moves faster than those with a lower initial velocity (e.g. ion b), therefore, the distance they travel away from the backing plate is different; see Figure 4A.

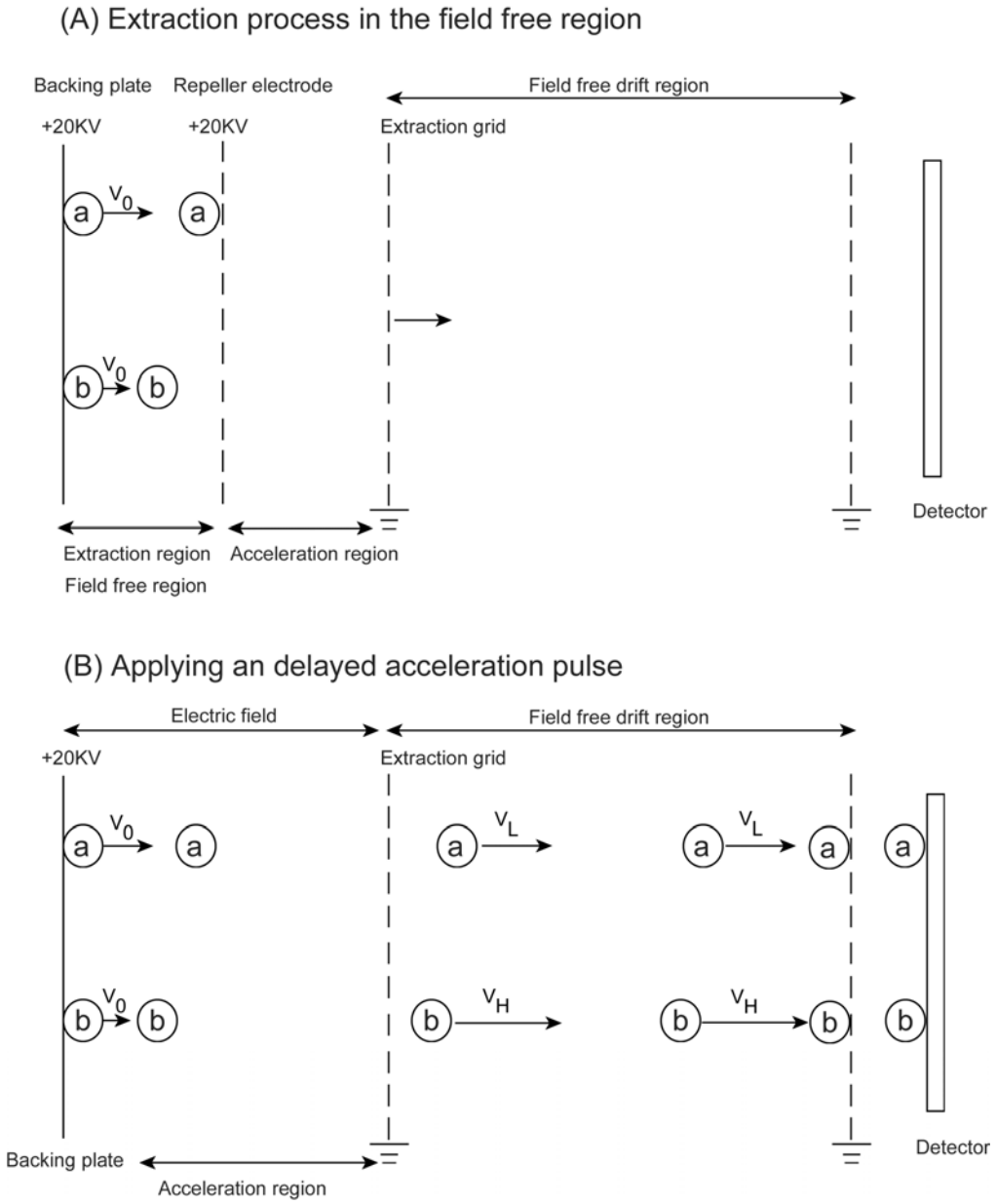

Figure 4. Schematic representation of delayed extraction in MALDI-TOF; The ions with the different initial velocities (v_0) are extracted in a field free environment in the extraction region. After a few nanoseconds of delay, an acceleration pulse is applied. The ion b with a lower v_0 is subjected into a higher potential field and accelerated to a higher velocity (v_H). While the ion a is subjected into a lower potential field and accelerated to a low velocity (v_L) prior to entering the field free drift region. In the field free drift region, the ion b continues to migrate closer to ion a and eventually they reach the detector at the same time.

After a short period of delay, an acceleration potential is applied to accelerate the ions. Thus, the isomass ions are electrostatically drawn away from the ionization source. Due to the different distances away from the backing plate, the isomass ions with lower initial velocities (e.g. ion b) are subjected to a higher potential field than those with higher initial velocities (e.g. ion a); See Figure 4B. As a result, the ions with a lower initial velocity (e.g. ion b) are sped up to a higher velocity than those with a higher initial velocity (e.g. ion a). In the field free drift region, all of the ions with the same *m/z* values migrate closer to each other and eventually reach the detector at the same time.[1, 9-11, 18, 20]

1.2.6 The reflectron

Reflectron is another widely used device to mitigate the intrinsic spatial and energy distribution of gas-phase ions; thus, it improves the mass resolution in MALDI-TOF analysis. A reflectron is comprised of a series of retarding electrostatic mirrors with a progressively increasing potential, as shown in Figure 5. These mirrors are located at the end of the field free drift region, and they slow down the ions to zero velocity. The ions are then reaccelerated in the opposite direction, and they migrate in the second field free drift region. According to the differences in the initial spatial and kinetic energy distribution, the isomass ions with higher initial energy (e.g. ion a) will travel in a longer pathway in the reflectron region than those with lower initial energy (e.g. ion b). Therefore, the shorter flying time of the isomass ions

with higher initial energy (e.g. ion a) in the first field free drift region is compensated by penetrating the retarding field in the reflectron to a greater depth than those with lower initial energy (e.g. ion b). As a result, all of the ions with the same *m/z* values reach the second detector (D2) simultaneously. This process enhances the mass resolution in MALDI-TOF.

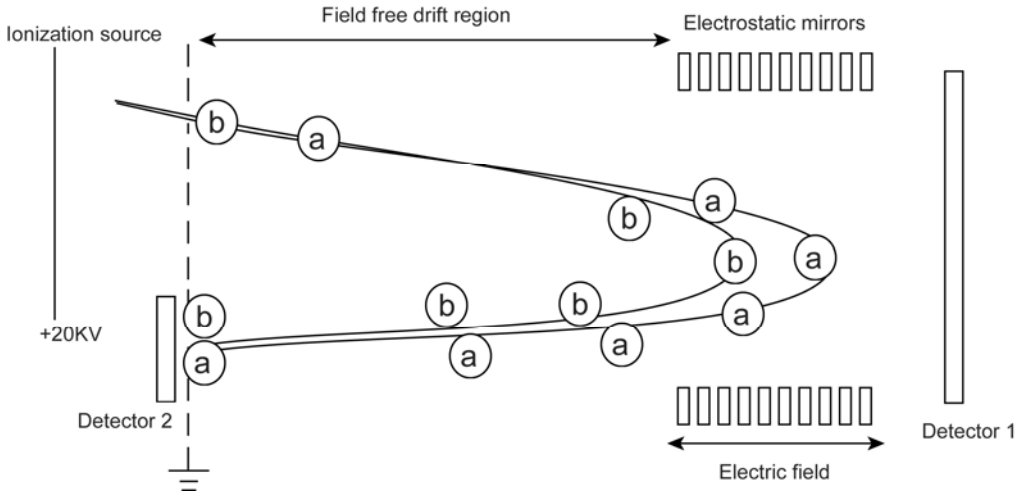

Figure 5. Schematic representation of the reflectron in a MALDI-TOF instrument; The ions a and b have the same *m/z* value but different initial kinetic energies. In the refletron mode, they are moving in a different pathway, but reach the second detector simultaneously. (Adapted from Chhabil Dass, *Fundamentals of Contemporary Mass Spectrometry*, Wiley-interscience, New York, 2007.)

To date, both reflectron and delayed extraction have been incorporated into MALDI-TOF mass spectrometers to improve mass resolution in MALDI-TOF MS analysis. This provides a unique opportunity for applying MALDI in the characterization of proteins and their corresponding post-translational modifications, because these devices allow sufficient mass resolution to distinguish isotopes for large molecules, and they can detect biological samples in low abundance. [1, 9-11, 18, 20]

1.2.7 Principle of post-source decay (PSD)

In addition to performing an MS^1 experiment on MALDI-TOF, tandem mass

spectrometry (MS^2) is also possible with a MALDI-TOF reflectron mass analyzer. This process can be accomplished with post-source decay (PSD), in which the ions formed in the ion source undergo the metastable dissociation in the field free drift region, which is located between the ionization source and the reflectron device; see Figure 6.[18, 19, 21] The generated charged fragments possess the same velocities but different kinetic energies with the precursor ions. Thus these fragments can be detected in the reflectron TOF analyzer which has the capability of distinguishing the ions with different kinetic energies. Consequently, a reflectron can be used as a tandem mass spectrometry to detect the ions produced in the metastable fragmentation to obtain the structural information of the ion of interest.[18, 19, 21]

In PSD technique, a series of electrodes (precursor ion selector) are located after the ionization source, along the ion flight path, as shown in Figure 6. A potential is applied continuously to deflect ions. For instance, if the ions generated from the ionization source retain positive charges, a negative potential is applied on the precursor ion selector to eliminate the ions. This potential is active all the time except for a short of period when the selected precursor ion is passing by. The selected precursor ion undergoes metastable dissociation in the field free drift region and generates both neutral and charged product ions. A scanning spectrum is initiated when the neutral fragment molecules hit detector 1 (Figure 6). Since the mass of the precursor ion is always higher than the charged fragment ion, and both of them have the same velocities, the precursor ion possesses a higher kinetic energy than the charged fragment ions, which results in the precursor ion traveling in a longer pathway in the reflectron. Based on the different migration pathways, the charged product ions and the precursor ion are separated in the reflectron and detected by

detector 2. To facilitate metastable fragmentation of MALDI-generated ions, the PSD experiment is performed using a "hot" MALDI matrix (e.g. α-cyano-4-hydroxycinnamic acid, etc). In addition, blowing air or an inert gas into the flying tube in the field free drift region may also enhance metastable fragmentation of the precursor ion.[9, 18, 21]

Although PSD is useful in performing MALDI-MS/MS experiment, there are several limitations with this approach: poor mass resolution of the precursor ion selection and the inefficiency of the metastable fragmentation process, which results in poor quality MS/MS data, compared to other methods of MS/MS analysis.[18, 19, 21] To overcome these limitations, the tandem time of flight (TOF/TOF) instrument was designed to perform improved MS/MS experiments and facilitate structural analysis of various species.

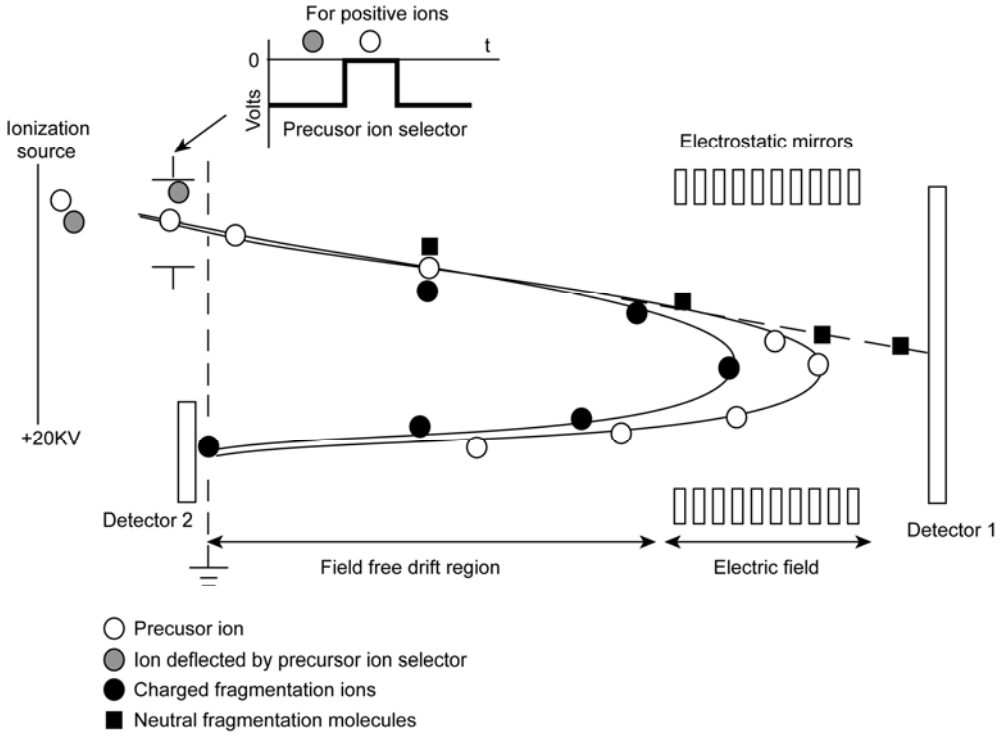

Figure 6. Schematic representation of post-source decay (PSD): the precursor ion

(white circle) is selected in the precursor ion selector and undergoes the metastable dissociation in the flying tube of field free drift region. The charged product ions (black circles) travel a short pathway in the reflectron than the precursor ion due to the lower kinetic energy and then detected by detector 2. The neutral molecules (black squares) strike the detector 1, which initiates the MS/MS spectrum scanning event. (Adapted from Edmond de Hoffmann and Vincent Stroobant, *Mass Spectrometry principles and applications*, John Wiley & Sons, Chichester, England, 2002.)

1.2.8 Principle of the tandem time of flight (TOF/TOF) mass spectrometry

MALDI-TOF/TOF is derived from the MALDI-TOF instrument, by incorporating a second time of flight tube and a series of components between the ionization source and the electrostatic mirrors located in the reflectron at the end of the second flight tube; as shown in Figure 7. These components consist of timed-ion selector (TIS), the deceleration mirrors, a floating collision cell, a second pulsed ion accelerator, and a pair of deflection electrodes for metastable suppression, etc.

Briefly, MALDI-TOF/TOF works based on the principle that the precursor ion is produced in the first TOF, fragmented in the collision cell, and analyzed in the second TOF. Specifically, the precursor ions generated in the MALDI ionization source are focused in the center of the TIS, which contains a double-sided deflection gate. The precursor ions are trapped by TIS through a time delay generator, which is programmed to open the gate of the TIS when the lowest mass of interest arrives to the gate and close the gate when the highest mass of interest passes through the gate. The non-selected ions are deflected away from the floating collision cell. The TIS-selected ions are decelerated by retarding mirrors, prior to entering the collision cell. In the collision induced dissociation process, the ions are activated and collided by the collision gas (N_2 or inert gas) with selected energy, which can be varied by

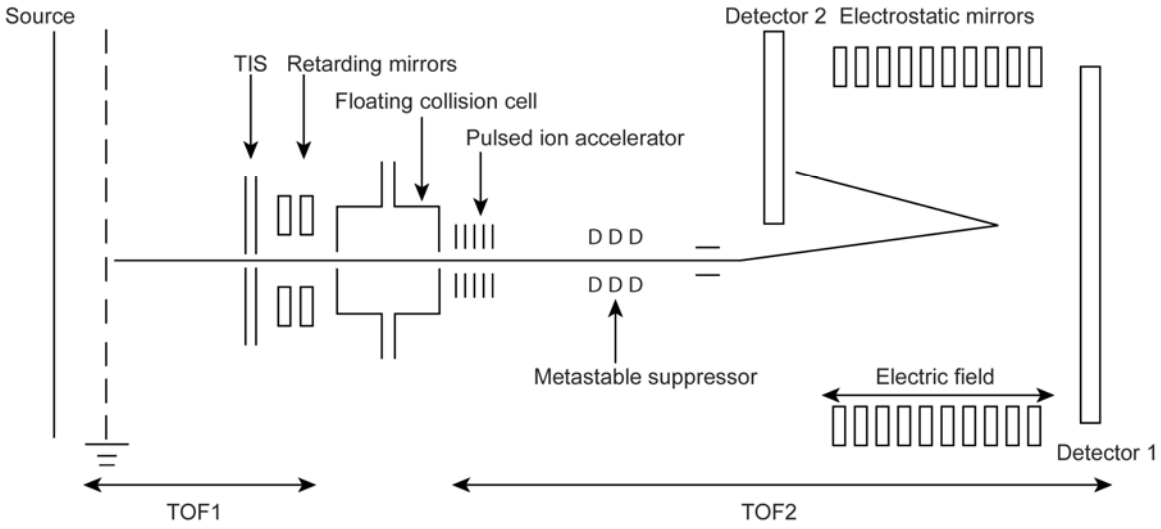

Figure 7. Schematic representation of MALDI-TOF/TOF instrument; (Adapted from Marvin L. Vestal *et al*, *Tandem time-of-flight mass spectrometry*. *Methods Enzymol*. **2005,** *402,* 79-108.)

adjusting the relative potential between the ionization source and the collision cell. The fragment ions as well as the precursor ions exit the collision cell, pass through a short field free drift region and are then reaccelerated by a second pulsed ion accelerator into the second TOF region. Consequently, the reflectron mode in the second TOF region is performed to generate high resolution MS/MS spectra. The metastable suppressor consisting of a set of deflection electrodes is used to deplete the “metastable” ions, which are produced outside of the collision cell, thus, improving the quality of the MS/MS spectra.[4, 10, 18, 20]

Aside from performing MS^2 experiments on MALDI-TOF/TOF instrument, the linear and reflectron modes in the MS^1 experiment can also be performed in the MALDI-TOF/TOF system without applying any voltages on the components added between ionization source and electrostatic mirrors for the MS^2 experiment. The performance of a MALDI-TOF/TOF system in MS^1 experiments in linear mode and reflectron mode is the same as the MALDI-TOF instrument described in the previous

sections, *1.2.4* and *1.2.6*, respectively.[4, 18, 20]

1.3 Electrospray ionization (ESI)

In addition to the MALDI ionization process, ESI is the softest ionization source that has been applied in the analysis of non-volatile biological samples, such as proteins, glycoproteins, carbohydrates, and peptides, etc. In this ionization process, the analytes are transferred from the solution phase to the gas phase via a metal capillary, to which a high voltage (from ~ 700 V to 5 KV) is applied; see Figure 8.[19] The liquid sample is infused through the capillary, which disperses the liquid solution into a mist of small, charged droplets. If a positive voltage is applied on the capillary, positively charged droplets are formed. The solvent on the positively charged droplets are evaporated by applying drying gas, heat or both, at atmospheric pressure.[19] As the solvent evaporates, the positively charged droplets shrink in size, and the charge density on their surface increases until it reaches the Raleigh limit, in which the repulsive Columbic forces between ions within the droplet exceed the surface tension of the droplets.[18, 19, 21] This causes fission of the droplets to form smaller charged droplets. As the solvent on the smaller droplets continues to be evaporated, the charged droplets keep breaking down into the smaller droplets and ultimately become a single ion.[21] This process is called Coulomb fission.[2, 13, 15, 24] Another proposed mechanism for ion formation is ion evaporation, in which the charged droplets become smaller by releasing one charged ion at a time, until the whole droplet contains one charged solute molecule in it. The produced charged ions from the ionization process are electrostatically directed to the mass analyzer and detected in the detector.[2, 15, 18, 19, 24]

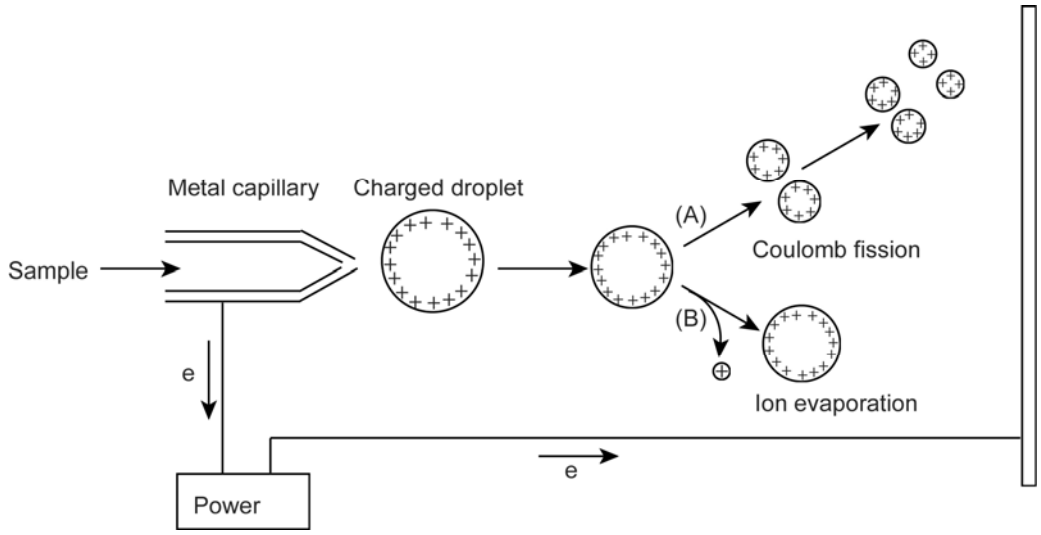

Figure 8. Schematic representation of ESI ionization process; the ions are transferred from liquid phase to gas phase via two mechanisms: (A) Coulomb fission and (B) Ion evaporation. (Adapted from Chhabil Dass, *Fundamentals of Contemporary Mass Spectrometry*, Wiley-interscience, New York, 2007.)

1.4 Principle of quadrupole ion-trap mass spectrometry

The quadrupole ion-trap (QIT) mass analyzer was invented in 1958 by Wolfgong Paul and his colleagues.[18, 19, 21] Since then, it has been utilized in a diversity of applications ranging from small compounds (e.g. drug metabolites, pharmaceuticals, etc) to large biologically relevant molecules, such as proteins, peptides, and their corresponding modifications, etc.[19]

Typically, the quadrupole ion trap consists of a ring electrode and two endcap electrodes; See Figure 9.[18] Mass separation in this instrument is accomplished by storing the ions in the trapping space, and ejecting one *m/z* at a time through small holes in the exit endcap, to a detector, by oscillating electric field created within the three electrodes.[18] Specifically, the ions created in the ionization source (e.g. ESI, MALDI, etc) are electrostatically drawn into the analyzer and trapped in a three-dimentional quadrupole filed, which is created by applying a voltage Φ_0 (Equation

1.7) to the ring electrode and maintaining the endcap electrodes at ground potential.[18]

$$\Phi_0 = U - V\cos\omega t \quad (1.7)$$

Where U is the amplitudes of the dc (constant) voltages and V is the amplitude of rf (alternating) voltages; ω is the angular frequency. A potential well is formed within the boundaries of the electrodes, and the lowest potential point of this well is located in the center of the trap. Once the ions enter the quadrupole field, the helium gas (at a pressure of 1mtorr) which is present in the trap is utilized to cool the kinetic energies of these ions and confine them in the center.[18] After the ions are focused in the center of the trap, a gradually increased rf voltage is applied on the ring electrode to eject the ions from the trap for detection. During this process, all the trapped ions migrate in a figure eight-shaped pathway; See Figure 9. The large *m/z*(s) migrate in a bigger pathway with a lower frequency, while the small *m/z*(s) migrate in a smaller pathway with a higher frequency. According to Equation 1.8,

$$m/z = 4eV/(q_{max}\omega^2 r_0^2) \quad (1.8)$$

where q_{max} is 0.908, and r_0 is the radius of the trap, under a given rf voltage (V), all the ions above a certain *m/z* value can be restored within the quadrupole field and the ions lower than this value become unstable and are ejected out from the trap.[18] Accordingly, as ramping the rf voltage V, the ions of sequentially increasing *m/z* are forced to be unstable, and ejected out from the ion trap for external detection.[18, 21] This approach of ejecting ions is known as “mass-selective instability mode”.[18] The alternative approach to eject ions is the “resonance ion ejection”, in which a supplementary rf voltage is applied to the endcap electrodes to eject ions with different *m/z*(s).[18]

In addition to performing MS^1 experiment, MS/MS (or MS^n) experiments are also performed in the QIT. In this process, all the ions but the *m/z*(s) of interest are ejected and a rf voltage is applied to the endcap electrode to excite the ions of interest, thus, facilitates generating fragmentation ions.[18, 21] The produced fragment ions as well as the precursor ions are then ejected from the QIT for external detection.

One salient feature of quadrupole ion trap is that it can perform multiple collision-induced dissociation experiments (CID) without requiring multiple analyzers.[19] Other predominant features of QIT instrument include its compact instrument size, and its capability to accumulate ions, thereby, enhances the signal-to-noise (S/N) in an analysis.[19]

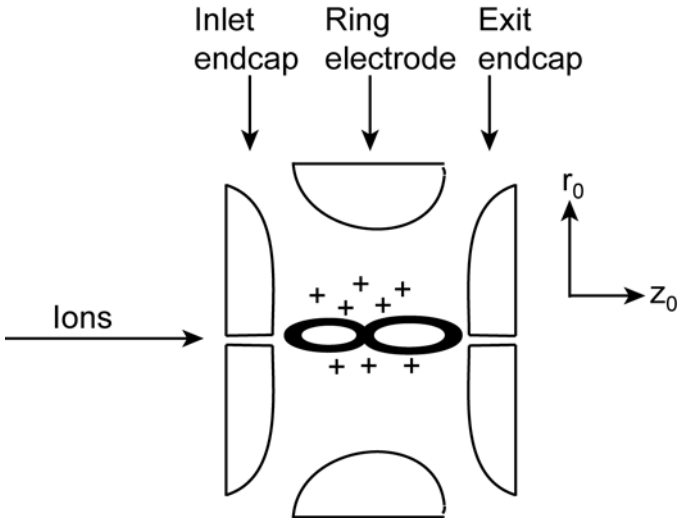

Figure 9. Schematic representation of quadrupole ion trap mass spectrometer. (Adapted from Chhabil Dass, *Fundamentals of Contemporary Mass Spectrometry*, Wiley-interscience, New York, 2007.)

1.5 Principle of Fourier transform mass spectrometry

Aside from the quadrupole ion trap, Fourier transform ion cyclotron

resonance mass spectrometry (FTICR-MS) is another technique which works based on the same principle of trapping ions. This instrument was invented in 1974 by Comisarow and Marshall.[18, 21] Since then, it has been widely used for the analysis of numerous species with the highest mass resolution and mass accuracy, compare to other mass analyzers.[19]

The key component of this instrument is a mass analyzer cell, which is housed inside a strong magnetic field.[18] This cubic cell consists of three pairs of electrodes, including two trapping plates (front and back electrodes), two excitation plates (the side electrodes), and two receiver plates (the top and bottom electrodes); See Figure 10.[18] The generated ions from the ionization source enter the analyzer cell along the same direction (z-axis) as the magnetic field, and they are confined to the center of the cell by applying a small voltage with the same polarity of the ions on the trapping plates. Prior to excitation, the trapped ions migrate along the z-axis at different frequencies, depending on their *m/z* values.[18] To excite and detect these trapped ions, the remaining four plates in the cell are utilized. In the excitation process, a range of radio frequency (rf) is applied to the two excitation plates. The ions absorb energy, which causes their cyclotron radius to enlarge and become coherent; therefore, the isomass ions cycle coherently at the same orbital radius.[18, 21] As the ions pass by the two receiver plates, an image current induced by the ions is detected as a function of time and Fourier transformed to the frequency domain to generate a mass spectrum.[18, 21] The generated image current oscillates at the same frequency as the coherently migrating ions, which relies on their *m/z* values. Since the ions are continuously migrating in a coherent circular pathway, they can be re-measured numerous

times, and this enhances the sensitivity and resolution of the instrument.

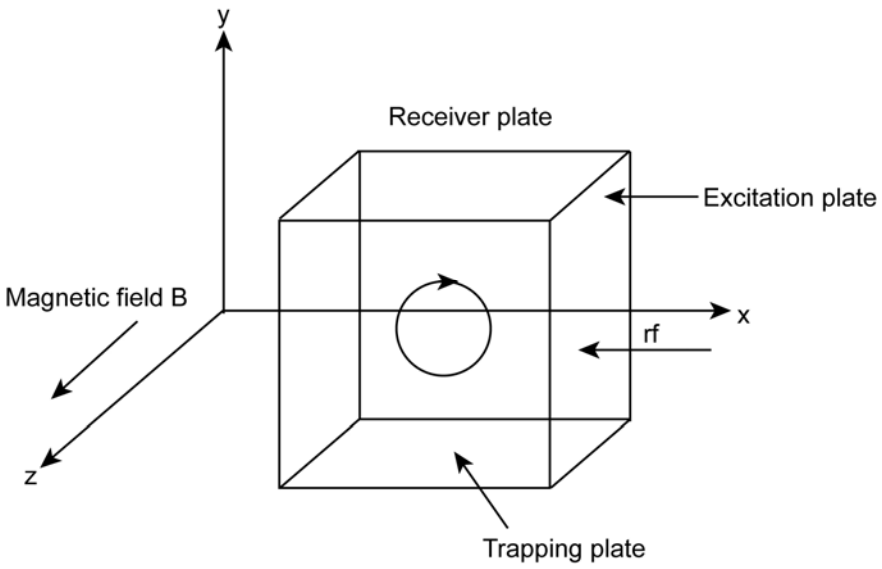

Figure 10. Schematic representation of Fourier transform ion cyclotron resonance mass spectrometry (FTICR-MS). (Adapted from Chhabil Dass, *Fundamentals of Contemporary Mass Spectrometry*, Wiley-interscience, New York, 2007.)

1.6 Background information on carbohydrates and glycoproteins

Carbohydrates are the most abundant and structurally complex species present in nature.[12, 13, 24-28] They are comprised of mono-, oligo-, and polymeric saccharides. In oligo-, and polysaccharides, branched structures can form, due to the different linkages that could be potentially present in the constituent monosaccharides; thereby, this results in a very large structural diversity in carbohydrates.[12, 13, 24] In addition to the complexity in the linkages among monosaccharides, carbohydrates can also be modified by addition of acidic functional groups to form sialylated, sulfated, or phosphorylated species. These acidic functional groups on carbohydrates influence their biological functional roles. Specifically, sialylation is involved in controlling the half-life circulation time and receptor binding.[29, 30] Sulfation is linked to biological recognition, and protein

clearance.[31] Alteration in phosphorylation of a carbohydrate correlates to diverse types of diseases, and the phosphorylation state of certain carbohydrates can be used as prognostic markers for breast cancer, ovarian cancer, and prostate cancer, etc.[32, 33]

Carbohydrates attach to proteins to generate either O-linked or N-linked glycoproteins. In O-linked glycosylation, the glycans are anchored via a hydroxyl oxygen of serine(S) / threonine (T) to form a glycosidic bond. In N-linked glycosylation, the carbohydrate is linked via an amide bond attached to the asparagine (N) sidechain. The asparagine must be present in the consensus sequence N X T/S, in which X can be any amino acid residues except for proline.[13] All the N-linked glycans contain a common trimannosyl chitobiose core consisting of [$HexNAc_2$+$Hexose_3$], which is boxed in scheme1.[13-16] Based on the differences in the outer branches of the glycans, the

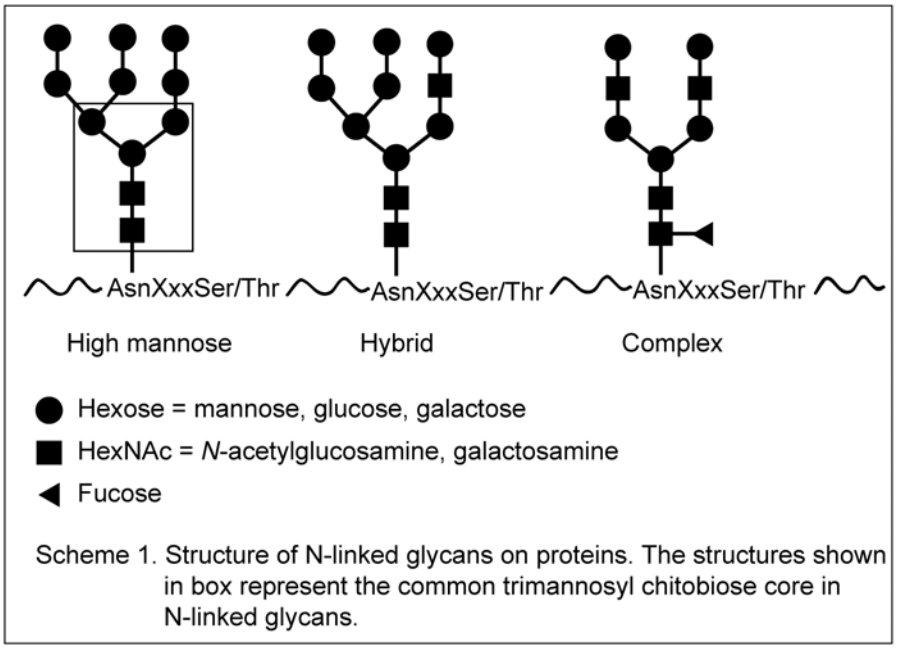

Scheme 1. Structure of N-linked glycans on proteins. The structures shown in box represent the common trimannosyl chitobiose core in N-linked glycans.

N-linked glycans can be classified as high mannose, hybrid and complex types.[13-16]

The research presented in this manuscript focuses on the N-linked glycoproteins, since these proteins are the most abundant species in mammalian cells.[13]

Glycosylation on proteins affects various biological functions of the proteins (e.g. protein binding, inter- or intra- cell signaling, etc),[28, 34-43] and it can serve as an indicator of disease.[34-38, 44-47] For example, human serum glycoproteins, immunoglobulin G (IgG), transferrin, and α_1-acid glycoprotein (AGP) are the most abundant and significant proteins in human plasma. Human IgG is the major immunoglobulin in human serum and serves as antibody. The neutral glycans on human IgG are involved in inter-/intra cell signaling. Transferrin is a metal carrying serum protein, transporting iron to tissues, via the circulation system.[48] Alteration in the glycosylation pattern on this protein affects iron homeostasis in the body. AGP, also known as orosomucoid, is one of the important positive acute phase proteins in human plasma.[44] Although the biological functions of AGP are not fully understood, changes in the glycosylation in some pathological conditions have been implicated, such as chronic inflammation, pregnancy, etc.[44] In addition, AGP has affinity for various basic or neutral lipophilic drugs from endo and exogeneous sources,[49-51] and these binding activities largely rely on the glycan structures. Therefore, characterization of the glycosylation in proteins is one important step in developing a comprehensive understanding of the biological significance of glycosylation and in facilitating disease diagnosis. Aside from human serum glycoproteins, several other glycoproteins, such as glycoprotein hormones,[52] and HIV Env proteins (CONS gp140 ΔCFI and JRFL gp140 ΔCF) [53] are also used in this study for glycan analysis by mass spectrometry.

1.7 Analyzing carbohydrates and glycoproteins by mass spectrometry

There are two basic approaches to characterizing glycans on glycoproteins by mass spectrometry, either cleaving of the glycans or analyzing glycopeptides; see Figure 11.[14-17, 54] For glycan analysis, the glycans are enzymatically or chemically released from the protein, followed by a separation technique and then detected by MS. Since the glycans ionize inefficiently, the reducing-terminus of the glycans is frequently derivatized in a reductive amination reaction by an aromatic amine; this facilitates detection of the glycans in mass spectrometry.[17] Although this approach is useful in characterization of glycans with high sensitivity, the glycosylation site-specific information, which defines where on the protein the glycans are attached can not be elucidated, unless the glycosylation sites are separated prior to glycan release.[31]

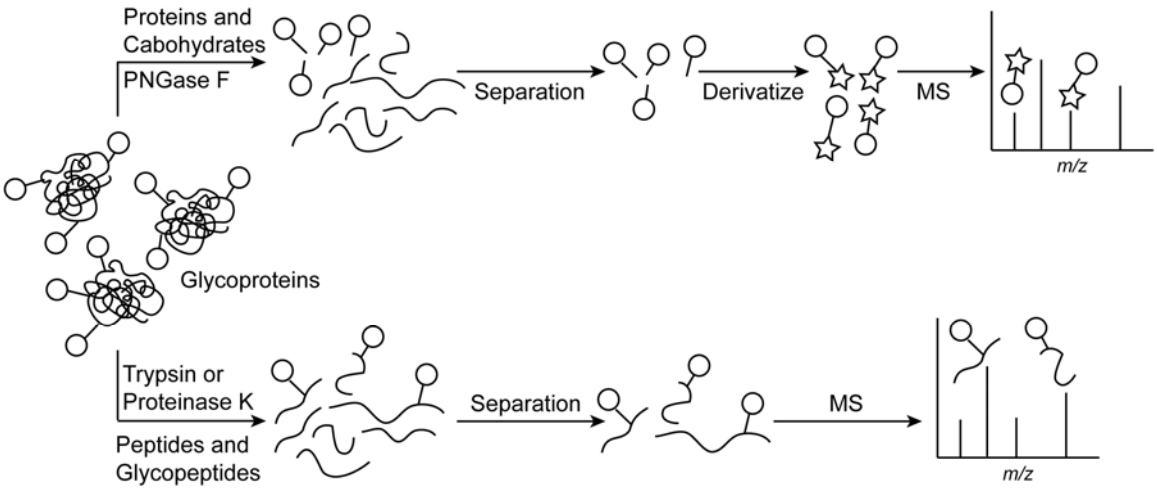

Figure 11. Schematic representation of characterization of glycans on glycoproteins by mass spectrometry: circle: glycans; star:derivatized reducing ends on the glycans.

The alternative approach to characterizing glycans on glycoproteins is to perform glycopeptide-based analysis, in which the glycans and their attached

glycosylation sites can be elucidated in the same experiment. This affords glycosylation site-specific information, which is useful in elucidating the functional properties of glycoproteins.[31, 55] Typically, the glycopeptide-based analysis entails enzymatic digestion by either specific or non-specific proteases, followed by a separation approach (e.g. high-performance liquid chromatography, etc) and then mass analysis. One salient feature of this approach is that the peptide portion in the glycopeptides is more readily ionized than underivatized glycans; so no extra derivatization step is needed.[17] As a result, this approach can be used for elucidation of glycan structures on proteins with relatively low detection limits.[17]

In addition to the advantages of using glycopeptide-based MS analysis, several challenges are encountered in this approach, including sample preparation and data analysis.[54] For sample preparation, due to the presence of glycans on glycopeptides and their high degree of heterogeneity, the mass spectral signals of glycopeptides are suppressed by the strongly ionizing peptides when both species co-exist in a complex mixture. Therefore, the enrichment/separation process is critical in the sample preparation of glycopeptide analysis. Detailed information for the comparison of different enrichment and/or chromatographic approaches is discussed in Chapter IV.

For data analysis, two “unknowns” are generated from glycopeptide-based analysis, the glycan moiety and the peptide moiety of a glycopeptide peak in the mass spectrum. This is due to the heterogeneity in both glycosylation and peptide potion of the glycopeptides generated in enzymatic digestion. In order to unambiguously assign the glycan compositions for the glycopeptides, the peptide must be identified first. Knowledge of the primary sequence of the protein is required

to generate the theoretical peptide masses, which are necessary for elucidating the peptide moiety of the glycopeptides.[17] This process of identifying the peptide composition can be accomplished by a web-based tool GlycoPep ID developed by our group. After identifying composition of the peptide moiety of glycopeptides, the process of assigning the glycan compositions of glycopeptides to MS^1 data is greatly facilitated. The detailed steps of data analysis in glycopeptide-based analysis can be found in reference [50] and [51].[56, 57]

1.8 Overview and summary of the following chapters

The research presented herein focuses on developing several efficient MS-based approaches to characterize post-translational modifications on glycoproteins. These approaches include ion-pairing strategy in conjunction with ESI-MS/MS to identify the acidic functional groups (sulfate, and phosphate) in carbohydrates and glycopeptides; (Chapter II, III) and a glycopeptide-based MALDI-TOF/TOF approach to characterize glycans on different glycoproteins varying in the number of glycosylation sites and their corresponding glycan profiles (Chapter IV).

In addition to glycosylation, disulfide connectivity is another important protein modification, and it plays a key role in establishing/maintaining protein structures in their biologically active forms. Therefore, the determination of disulfide bond arrangement will provide an efficient way to obtain the chemical structural information about proteins, and these studies may lead to insights into the proteins' functional roles. Towards this end, a mass spectrometric approach using liquid chromatography followed by eletrospray ionization-Fourier transform ion cyclotron resonance mass spectrometry (LC/ESI-FTICR-MS) was developed to determine the disulfide bond arrangement in proteins and glycoproteins, as described in Chapter V.

The content of each chapter in this manuscript is summarized below.

1.8.1 Using ion-pairing strategy to differentiate between phosphorylation and sulfation in mass spectrometry. (Chapter II and III)

The studies presented in Chapter II and III focus on the discrimination of sulfation from phosphorylation in mass spectrometry. Phosphorylation and sulfation are two important biological modifications present in carbohydrates, proteins, and glycoproteins. Typically, sulfation and phosphorylation cause different biological responses, so identification of these two functional groups is important for understanding structure/function relationships in various species. Mass spectrometry is one of the methods used to detect the presence of these two modifications in complex biological mixtures. However, phosphorylated and sulfated structures are isobaric; thus, differentiation between them in routinely used mass spectrometers is not possible. To overcome this problem, a novel mass spectrometric method, ion-pairing, in conjunction with ESI-MS/MS analysis, is developed on model phosphorylated/sulfated carbohydrates(Chapter II), and subsequently applied in discriminating sulfation from phosphorylation present in other biologically relevant molecules, including mono-, di-, saccharides, and the highly sulfated glycoprotein, ovine luteinizing hormone; see Chapter III. The ion-pairing strategy developed herein is the first study demonstrating that this robust approach can be used to differentiate the two isobaric functional groups, and this method is also useful in the detection of phosphorylated compounds in complex mixtures.[32, 33]

1.8.2 Method development in glycan profiling on glycoproteins. (Chapter IV)

The research presented in Chapter IV focuses on method development for characterization of N-linked glycans on glycoproteins, to facilitate understanding how

the glycan structures influence biological functional roles of glycoproteins. To date, glycopeptide-based MS analysis has proven to be a well-suited approach for characterizing glycans, since the glycan and its attachment site on the protein can be elucidated in the same experiment. However, when glycopeptides co-exist with peptides, glycopeptide signals are usually suppressed by the strongly ionizing peptides. Towards this end, it would be desirable to seek methods to improve glycopeptide detection. In Chapter IV, we performed an in-depth study of maximizing glycosylation coverage on model glycoproteins by optimizing all the aspects of glycopeptide-based analysis, including sample preparation methods, mass spectral techniques, and data analysis strategies. In doing so, we created a work-flow that is designed specifically to optimize the coverage of glycosylation heterogeneity in terms of the number of glycosylation sites detected and their corresponding glycan profiles. To test the effectiveness of this approach, a glycoprotein with 27 potential glycosylation sites was analyzed. This work demonstrates that our strategies significantly improve the glycopeptide detection to elucidate a variety of glycoforms present on proteins, thereby, facilitating the understanding of the functional properties of glycans on glycoproteins.

1.8.3 Method development in determination of disulfide bonds on glycoproteins. (Chapter V)

In addition to glycan profiling on the glycoproteins, determining the disulfide bonding pattern is another important feature in protein structural analysis. In Chapter V, aiming to understand how the HIV Env protein's structure influences its immunogenicity, we developed a highly efficient MS-based approach, liquid chromatography electrospray ionization Fourier transform ion cyclotron (LC/ESI-

FTICR) mass spectrometry, to determine the disulfide linkages on a synthetic form of the HIV Env protein, CON-S gp140 ΔCFI, which has marked improvement in antigenicity, compared to other similar wild-type proteins. This study is the first investigation of utilizing mass spectrometry to determine the disulfide bonding pattern in the HIV Env protein. The disulfide bonding pattern obtained from this study complements the glycan profiling (also performed in our lab) to reveal overall structural information, including functional domains and glycan shields present on CON-S gp140 ΔCFI. Thus, these studies may provide beneficial information for understanding the immunogenetic activity of this protein, which would lead to insights to guide the direction of future vaccine development.

1.9 References

1. Sachon, E.; Jensen, O.N. Protein and peptide analysis by matrix-assisted laser desorption/ionization tandem mass spectrometry (MALDI MS/MS). *Spectral Tech. Proteomics.* **2007,** 67-79.

2. Nguyen, D.N.; Becker, G.W.; Riggin, R.M. Protein mass spectrometry: applications to analytical biotechnology. *J. Chromatogr., A* **1995,** *705,* 21-45.

3. Nedlkov, D.; Nelson, R.W. Isolation of glycoproteins and identification of their N-linked glycosylation sites. In New and emerging proteomic techniques; Humana Press Inc: New Jersey, 2006; pp177-186.

4. Vestal, M. L.; Campbell, J.M. Tandem time-of-flight mass spectrometry. *Methods Enzymol.* **2005,** *402,* 79-108.

5. Carr, S.A.; Barr, J.R.; Roberts, G.D. Anumula, K.R.; Taylor, P.B. Identification of attachment sites and structural classes of asparagine-linked carbohydrates in glycoproteins. *Methods Enyzmol.* **1990,** *193,* 501-518.

6. Angel, A.S.; Nilsson, B. Linkage positions in glycoconjugates by periodate oxidation and fast atom bombardment mass spectrometry. *Mehods Enyzmol.* **1990,** *193,* 587-607.

7. Egge, H.; Peter-Katalinic, J.; Karas, M.; Stahl, B. The use of fast atom bombardment and laser desorption mass spectrometry in the analysis of complex

carbohydrates. *Pure Appl. Chem.* **1991,** *63*, 491-498.

8. Dell, A.; Rogers, M.E. Fast atom bombardment mass spectrometry of protein and carbohydrate biopolymers. *TrAC, Trends Anal. Chem.* **1989,** *8,* 375-378.

9. Pasch, H.; Schrepp, W. Mass spectrometric instrumentation. In MALDI-TOF mass spectrometry of synthetic polymers; Springer-Verlag Berlin Heidelberg: New York, 2003; pp19-53.

10. Coon, J.J.; Skyka, J.E.P.; Shabanowitz, J.; Hunt, D.F. Tandem mass spectrometry for peptide and protein sequence analysis. *BioTechniques*. **2005,** *38,* 519, 521, 523.

11. Cotter, R.J. Time-of-flight mass spectrometers. In Time-of-flight mass spectrometry: Instrumentation and applications in biological research; American Chemical Society, 1997; pp19-44.

12. Harvey, D.J. Matrix-assisted laser desorption/ionization mass spectrometry of carbohydrates. *Mass Spectrom. Rev.* **1999,** *18,* 349-450.

13. Harvey, D.J. Identification of protein-bound carbohydrates by mass spectrometry *Proteomics.* **2001,** *1,* 311-328.

14. Harvey, D. J., Structural determination of N-linked glycans by matrix-assisted laser desorption/ionization and electrospray ionization mass spectrometry. *Proteomics* **2005,** *5,* 1774-1786.

15. Harvey, D.J. Proteomic analysis of glycosylation: structural determination of N- and O-linked glycans by mass spectrometry. *Expert Rev. Proteomics* **2005,** *2,* 87-101.

16. Harvey, D.J. Analysis of carbohydrates and glycoconjugates by matrix-assisted laser desorption/ionization mass spectrometry: an update covering the period 1999-2000 *Mass Spectrom. Rev.* **2006,** *25,* 595-662.

17. Harvey, D.J.; Kuster, B.; Wheeler, S.F.; Hunter, A.P.; Bateman, R.H.; Dwek, R.A. Matrix-assisted laser desorption/ionization mass spectrometry of N-linked carbohydrates and related compounds. *Mass Spectrom. Biol. Med.* **2000,** 403-437.

18. Dass, C. Fundamentals of contemporary mass spectrometry; John Wiley & Sons, Inc: Hoboken, New Jersey, 2007; pp35-45, 80-86, 133-136.

19. Siuzdak, G. Mass spectrometry for biotechnology; MCC Press; 2003; pp13-33.

20. Vestal, M.L.; Juhasz, P.; Martin, S.A. Delayed extraction matrix-assisted laser desorption time-of-flight mass spectrometry. *Rapid Commun. Mass Spectrom.* **1995,** *9,* 1044-1050.

21. De Hoffmann, E.; Stroobant, V. Mass spectrometry principles and applications; John Wiley & Sons, Inc: Southern Gate, Chichester, 2002; pp28-32, 33-44, 89-99.

22. Karas, M.; Gluckmann, M.; Schafer, J. Ionization in matrix-assisted laser desorption/ionization: singly charged molecular ions are the lucky survivors. *J. Mass Spectrom.* **2000**, *35*, 1-12.

23. Karas, M.; Kruger, R. Ion formation in MALDI: the cluster ionization mechanism. *Chem. Rev.* **2003,** *103*, 427-440.

24. Zaia, J. Mass spectrometry of oligosaccharides. *Mass Spectrom. Rev.* **2004,** *23,* 161-227.

25. Dell, A.; Morris, H.R.; Glycoprotein structure determination by mass spectrometry. *Science,* **2001,** *291,* 2351-2356.

26. Helenius, A.; Aebi, M. Intracellular functions of N-linked glycans. *Science* **2001,** *291,* 2364-2356.

27. Rudd, P.M.; Dwek, R.A.; Glycosylation: Heterogeneity and the 3D structure of proteins. *Crit. Rev. Biochem. Mol. Biol.* **1997,** *32,* 1-100.

28. Weerapana, E.; Imperiali, B. Asparagine-linked protein glycosylation: From eukaryotic to prokaryotic systems. *Glycobiology.* **2006,** *16,* 91R-101R.

29. Dalpathado, D.S.; Irungu, J.; Go, E.P. Butnev, V.Y.; Norton, K.; Bousfield, G.R.; Desaire, H. Comparative Glycomics of the Glycoprotein Follicle Stimulating Hormone: Glycopeptide Analysis of Isolates from Two Mammalian Species. *Biochemistry* **2006,** *45,* 8665-8673.

30. Compton, Steven J. Glycosylation and proteinase-activated receptor function. *Drug Dev. Res.* **2003,** *59,* 350-354.

31. Irungu, J.; Dalpathado, D. S.; Go, E. P.; Jiang, H.; Ha, H.; Bousfield, G. R.; Desaire, H. Method for characterizing sulfated glycoproteins in a glycosylation site-specific fashion, using ion pairing and tandem mass spectrometry. *Anal. Chem.* **2006,** *78*, 1181-1190.

32. Zhang, Y.; Go, E.P.; Jiang, H.; Desaire, H. A novel mass spectrometric method to distinguish isobaric monosaccharides that are phosphorylated or sulfated using ion-pairing reagents. *J. Am. Soc. Mass. Spectrom.* **2005,** *16,* 1827-1839.

33. Zhang, Y.; Jiang, H. Go, E.P.; Desaire, H. Distinguishing phosphorylation and sulfation in carbohydrates and glycoproteins using ion-pairing and mass spectrometry. *J. Am. Soc. Mass. Spectrom.* **2006,** *17,* 1282-1288.

34. Kameyama, A.; Kaneda, Y.; Yamanaka, H.; Yoshimine, H.; Narimatsu, H.; Shinohara, Y. Detection of oligosaccharides labeled with cyanine dyes using matrix-

assisted laser desorption/ionization mass spectrometry. *Anal. Chem.* **2004,** *76,* 4537-4542.

35. Kameyama, A.; Kikuchi, N.; Nakaya, S.; Ito, H.; Sato, T.; Shikanai, T.; Takahashi, Y.; Takahashi, K.; Narimatsu, H. A strategy for identification of oligosaccharide structures using observational multistage mass spectral library. *Anal. Chem.* **2005,** *77,* 4719-4725.

36. Nilsson, B. Analysis of protein glycosylation by mass spectrometry. *Mol. Biotechnol.* **1994,** *2,* 243-280.

37. Palm, A. K.; Novotny, M. V. A monolithic PNGase F enzyme microreactor enabling glycan mass mapping of glycoproteins by mass spectrometry. *Rapid Commun. Mass Spectrom.* **2005,** *19,* 1730-1738.

38. Shinohara, Y.; Furukawa, J.; Niikura, K.; Miura, N.; Nishimura, S. Direct N-glycan profiling in the presence of tryptic peptides on MALDI-TOF by controlled ion enhancement and suppression upon glycan-selective derivatization. *Anal. Chem.* **2004,** *76,* 6989-6997.

39. Yu Y. Q.; Gilar, M.; Kaska, J.; Gebler J. C. A rapid sample preparation method for mass spectrometric characterization of N-linked glycans. *Rapid Commun. Mass Spectrom.* **2005,** *19,* 2331-2336.

40. Haslam, S. M.; North, S. J.; Dell, A. Mass spectrometric analysis of N- and O-glycosylation of tissues and cells. *Curr. Opin. Struct. Biol.* **2006,** *16,* 584-591.

41. Jones, J.; Krag, S. S.; Betenbaugh, M. J. Controlling N-linked glycan site occupancy. *Biochim. Biophys. Acta, Gen. Subj.* **2005,** *1726,* 121-137.

42. Helenius, A.; Aebi, M. Roles of N-linked glycans in the endoplasmic reticulum. *Annu. Rev. Biochem.* **2004,** *73,* 1019-1049.

43. Vigerust, D. J.; Shepherd, V. L. Virus glycosylation: role in virulence and immune interactions. *Trends Microbiol.* **2007,** *15,* 211-218.

44. Imre, T.; Schlosser, G.; Pocsfalvi, G.; Siciliano, R.; Molnar-Szollosi, E.; Kremmer, T.; Malorni, A.; Vekey, K. Glycosylation site analysis of human alpha-1-acid glycoprotein (AGP) by capillary liquid chromatography - electrospray mass spectrometry. *J. Mass Spectrom.* **2005,** *40,* 1472-1483.

45. Larsen, M. R.; Hojrup, P.; Roepstorff, P. Characterization of gel-separated glycoproteins using two-step proteolytic digestion combined with sequential microcolumns and mass spectrometry. *Mol. Cell Proteomics.* **2005,** *4,* 107-119.

46. Wada, Y.; Tajiri, M.; Yoshida, S. Hydrophilic affinity isolation and MALDI multiple-stage tandem mass spectrometry of glycopeptides for glycoproteomics. *Anal. Chem.* **2004,** *76,* 6560-6565.

47. Sparks, S. E. Inherited disorders of glycosylation. *Mol. Genet. Metab.* **2006,** *87,* 1-7.

48. Van Rensburg, S. J.; Berman, P.; Potocnik, F.; MacGregor, P.; Hon, D.; De Villiers, N. 5- and 6-glycosylation of transferrin in patients with Alzheimer's disease. *Metab. Brain Dis.* **2004,** *19,* 89-96.

49. Dage, J. L.; Ackermann, B. L.; Halsall, H. B. Site localization of sialyl Lewisx antigen on a1-acid glycoprotein by high performance liquid chromatography-electrospray mass spectrometry. *Glycobiology* **1998,** *8,* 755-760.

50. Fournier, T.; Medjoubi, N. N.; Porquet, D. Alpha-1-acid glycoprotein. *Biochim. Biophys. Acta.* **2000,** *1482,* 157-171.

51. Nagy, K.; Vekey, K.; Imre, T.; Ludanyi, K.; Barrow, M. P.; Derrick, P. J. Electrospray Ionization Fourier Transform Ion Cyclotron Resonance Mass Spectrometry of Human a-1-Acid Glycoprotein. *Anal. Chem.* **2004,** *76,* 4998-5005.

52. Bousfield, G.R.; Butnev, V.Y.; Butnev, V.Y.; Nguyen, V.T.; Gary, C.M.; Dias, J.A.; MacColl, R.; Eisele, L.; Harvey, D.J. Differential effects of α subunit asparagines^{56} oligosaccharide structure on equine lutropin and follitropin hybrid conformation and receptor-binding activity. *Biochemistry* **2004,** *43,* 10817-10833.

53. Liao, H.; Sutherland, L.L.; Xia, S.; Brock, M. E.; Scearce, R. M.; Vanleeuwen, S.; Alam, S. M.; McAdams, M.; Weaver, E. A.; Camacho, Z. T.; Ma, B.; Li, Y.; Decker, J. M.; Nabel, G. J.; Montefiori, D. C.; Hahn, B. H.; Korber, B. T.; Gao, F.; Haynes, B. F. A group M consensus envelope glycoprotein induces antibodies that neutralize subsets of subtype B and C HIV-1 primary viruses. *Virology* **2006,** *353,* 268-282.

54. Budnik, B. A. ; Lee, R. S. ; Steen, J. A. J. Global methods for protein glycosylation analysis by mass spectrometry. *Biochim. Biophys. Acta.* **2006,** *1764,* 1870-1880.

55. Novotny, M. V.; Mechref, Y. New hyphenated methodologies in high-sensitivity glycoprotein analysis. *J. Sep. Sci.* **2005,** *28,* 1956-1968.

56. Go, E. P.; Rebecchi, K. R.; Dalpathado, D. S.; Bandu, M. L.; Zhang, Y.; Desaire, H. GlycoPep DB: a tool for glycopeptide analysis using a "smart search". *Anal. Chem.* **2007,** *79,* 1708-1713.

57. Irungu, J.; Go. E. P.; Dalpathado, D. S.; Desaire, H. Simplification of mass spectral analysis of acidic glycopeptides using *GlycoPep ID. Anal. Chem.* **2007,** *79,* 3065-3074.

Chapter II

A novel mass spectrometric method to distinguish isobaric monosaccharides that are phosphorylated or sulfated using ion-pairing regents

2.1 Introduction:

Phosphorylation and sulfation are functionally significant biological modifications commonly found in metabolites, carbohydrates, proteins, and glycoproteins. Phosphorylation is linked to signal transduction, gene expression, cell cycle, cytoskeletal regulation, and apoptosis [1-8]. In particular, phosphorylated carbohydrates are integral components of nucleic acids [1,5], oligosaccharides [1,5], glycopeptides [2,3,4,6], and glycoproteins [2-4]. They are also involved in glycolysis processes in the extracellular matrix [7,8]. Sulfation effects protein recognition and helps facilitate clearance of proteins and metabolites from the body [9-14]. Specifically, sulfated carbohydrates represent a class of biologically active and pharmaceutically important molecules [10]. They are essential in neuropathology and used as therapeutic agents [9]. Because phosphorylation and sulfation have been linked to different biological functions, differentiating these structures is essential for understanding structure/function relationships in proteins, carbohydrates, and metabolites.

Numerous studies [1-4, 6-7, 9-18] have been utilized to characterize the phosphorylation and sulfation. These methods indicate that selective and sensitive detection of phosphorylated and sulfated compounds in complex matrices is

paramount. Radiolabelling [3,6,11-14] is one of the commonly used methods to identify phosphorylated and sulfated carbohydrates with good specificity. While this method is hazardous and time-consuming, phosphorylated or sulfated species can be selectively discriminated in the presence of many other compounds in the matrix, using radiolabeling.

Mass spectrometry, which is highly selective and sensitive, could possibly provide information about phosphorylation and sulfation without the need for radiolabelling [3,15-17]. Recent MS experiments to identify phosphorylated compounds include exact mass differentiation [2] and discrimination using ion-molecule reactions [1] by using Fourier Transform Ion Cyclotron Resonance Mass Spectrometry (FTICR-MS). While these two methods are useful in differentiating the presence of phosphorylated and sulfated compounds, only a few groups have access to these sophisticated instruments. Thus, developing the mass spectrometric methods on more readily available instruments will benefit investigators who are interested in this field.

Herein, we utilize basic peptides [9,19-23] as ion-pairing reagents to complex to phosphorylated or sulfated carbohydrates via non-covalent interactions [9,19-23] and perform MS/MS experiments on each complex to obtain the structural information. This is the same ion-pairing technique employed in MALDI and ESI that is used to enhance the signal of sulfated carbohydrates [19, 20]. Since both phosphate and sulfate are highly acidic compounds with different proton affinities, differences in their chemical reactivities with the ion-pairing reagents may be used to distinguish their structures by MS/MS experiments. This is the first study to illustrate that ion-pairing can be used in conjunction with MS/MS to differentiate isobaric

phosphorylated and sulfated compounds. In addition to its application to simple carbohydrates, this method is also potentially applicable in identifying phosphorylation and sulfation in glycosaminoglycans and glycoproteins in biological samples.

This work complements other mass spectrometric studies that have discriminated phosphorylation from sulfation using FTICR-MS [1,2], and most recently MALDI-MS in which the differentiation was accomplished by monitoring the differences in the ionization behavior between the two functional groups [24]. In addition to discriminating these isobars, ion pairing has the added advantage of simultaneously enhancing the mass spectral signal of these acidic groups, even when they are present in complex mixtures of other compounds [20].

2.2 Experimental Section

Chemicals and Materials

All of the phosphorylated and sulfated monosaccharides and peptides were purchased from Sigma-Aldrich (St. Louis, MO), except for the three basic peptides Arg-Arg-Arg (R3), Arg-Ser-Lys (RSK) and Arg-Gly-Lys (RGK). These three small peptides were synthesized at the University of Kansas Biological Research Service Laboratory using solid phase peptide synthesis. All chemicals were used without further purification and all solvents were HPLC grade.

Sample Preparation

All of the compounds including basic peptides were dissolved in a minimal amount of HPLC grade water. Peptide stock solutions were further diluted with methanol : water (MeOH:H_2O) mixture (1:1) containing 0.5% acetic acid, to a final

concentration of 2 mM. All phosphorylated and sulfated monosaccharides were diluted to 1 mM. Prior to MS analysis, ion-pair complexes were formed by combining 5 μL of basic peptide solution and 5 □L of monosaccharides solution. The mixture was thoroughly mixed and 1-2 μL was directly injected into the mass spectrometer.

Mass Spectrometry

A surveyor MS-pump (Thermo, San Jose, CA) was used to deliver the mobile phase of MeOH : H_2O (1:1) containing 0.5% acetic acid at a flow rate of 20 μL/min. 1-2 □L of samples were directly injected into mass spectrometer. All samples were analyzed on a Thermo Finnigan LCQ Advantage quadrupole ion trap mass spectrometer (Thermo, San Jose, CA). Electrospray ionization in both positive and negative ion mode was achieved by using a spray voltage of ~ 4.0 kV. Nitrogen was used as a nebulizing gas, at a pressure of 20 psi. A capillary temperature of 200-230°C was maintained. Ion-pairing experiments were performed in positive ion mode, and MS data of the native carbohydrates was performed in negative ion mode.

Collision-induced dissociation (CID) was performed to obtain structural information. Specifically, doubly charged precursor ions were activated for 30 ms with 20% normalized collision energy. A q_z value of 0.25 and an isolation width of 3 Da were used. The singly charged precursor ions were activated with 15% normalized collision energy.

2.3 Results and Discussion

MS data for isobaric monosaccharides without ion-pairing

To demonstrate the effectiveness of the ion-pairing technique in

differentiating between phosphorylated and sulfated compounds, two sets of isobaric phosphorylated and sulfated monosaccharides were chosen as model compounds (Scheme 1). In the first set of experiments, the fragmentation characteristics of the isobaric monosaccharides without ion-pairing were examined. MS/MS data revealed that the two sets of isobaric monosaccharides, glucose-6-phosphate (Glc6P) / glucose-6-sulfate (Glc6S), and N-acetyl-glucosamine-6-phosphate (GlcNAc6P) / N-acetyl-glucosamine-6-sulfate (GlcNAc6S) produce identical MS/MS data (Figure 1A-D).

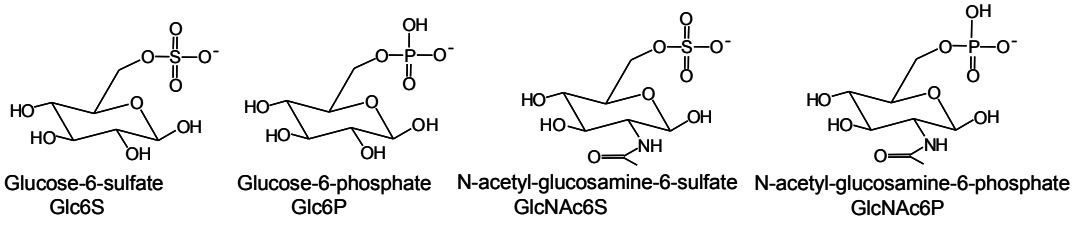

Scheme1. Phosphorylated and sulfated monosaccharide standards used for the ion-pairing experiments.

As a result, these isobaric monosaccharides cannot be distinguished using standard MS/MS methods.

Ion-pairing for sulfated and phosphorylated carbohydrates

To overcome this problem, ion-pairing [9,19-23] was employed for the analysis. Ten different basic peptides: Lys-Lys (K2), Lys-Lys-Lys (K3), Lys-Tyr-Lys (KYK), Arg-Ser-Lys (RSK), Arg-Gly-Lys (RGK), Arg-Arg-Arg (R3), Lys-Lys-Lys-Lys (K4), Arg-Lys-Arg-Ser-Arg-Lys-Glu (P1), Ser-Arg-Val-Ser-Arg-Arg-Ser-Arg (P2), Lys-Arg-Thr-Leu-Arg- Arg (P3), were evaluated for their potential to form ion-pairing complexes with the acidic carbohydrates and facilitate their discrimination in MS/MS experiments. These peptides were complexed with the isobaric carbohydrates in Scheme 1.

Typical MS data of the carbohydrate and peptide ion-pairs depict the formation of abundant ion-pair complexes. An example of the carbohydrate:peptide complex between the phosphorylated carbohydrate, Glc6P, and the tripeptide, R3, is shown in Figure 2. Since the basic side chain of the peptide is easily protonated under the conditions used in this analysis, both doubly and singly charged ion-pair complexes are formed in the spectrum. This is the first example that demonstrates ion-pairing, which is typically used to facilitate MS detection of sulfated compounds [9,20,21], also can be used for phosphorylated species. Structural information on each carbohydrate:peptide complex was obtained from MS/MS experiments. The data are presented in Table 1 and 2. To determine which peptide could be used in the differentiation study, the fragmentation pattern of each singly and doubly charged ion-pair complex was compared. The most effective ion-pairing reagents were identified as those that could discriminate both sets of isobaric monosaccharides, in Scheme 1. A summary of all the MS/MS data is in Table 1 and 2. Peptides that produced unique product ions for one of the isobaric compounds were deemed "useful", because they could discriminate the isobars by MS/MS.

Table 1 shows data for the singly charged complexes. Several peptides were ruled out as potentially useful ion-pairing candidates because their MS/MS data were identical for both sets of the isobaric carbohydrate:peptide ion-pairs. In fact, only the three peptides, R3, K3, and KYK, in Table 1, could be used to differentiate all the isobars in this study. The same comparison was made for the doubly charged complexes in Table 2. The peptides P1, P2, P3 and K3 in Table 2 were useful for discriminating the doubly charged isobaric complexes. Combining the results from both tables, indicate that K3 can be used to differentiate isobaric carbohydrates,

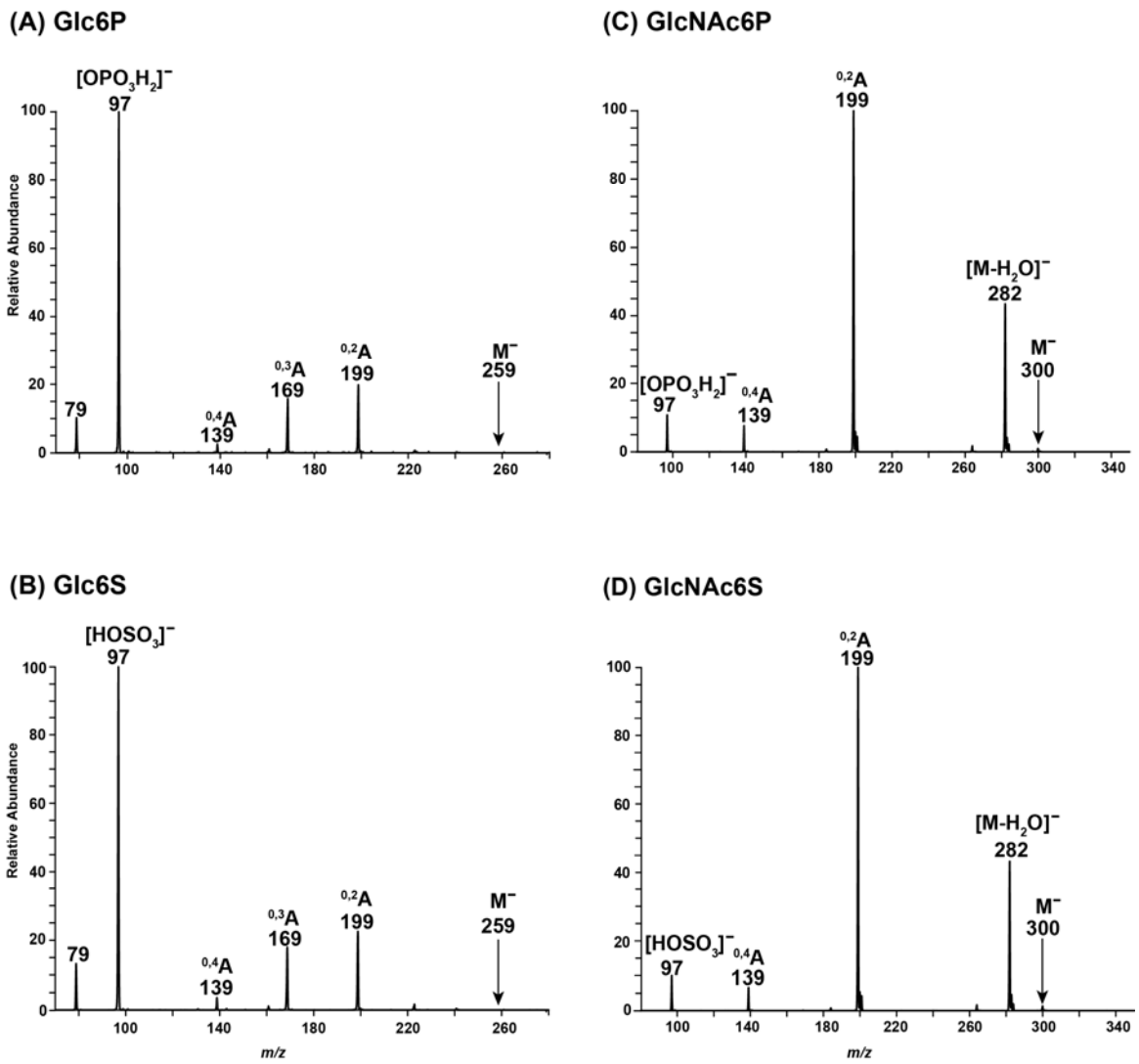

Figure 1. (-) ESI-MS/MS data for phosphorylated and sulfated carbohydrates. Isobaric pairs provide identical spectra. Each product ion is labeled: A) glucose-6-phosphate (Glc6P) B) glucose-6-sulfate (Glc6S) C) N-acetyl-glucosamine-6-phosphate (GlcNAc6P) and D) N-acetyl-glucosamine-6-sulfate (GlcNAc6S).

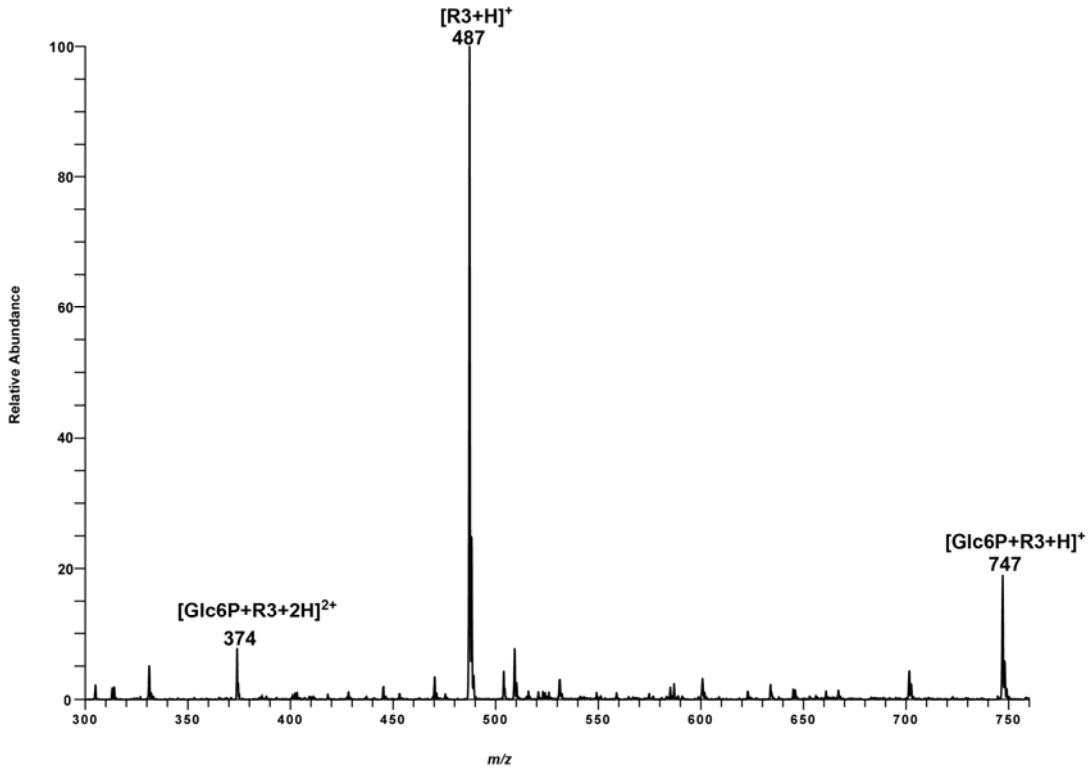

Figure 2. (+)ESI-MS data for the phosphorylated carbohydrate glucose-6-phosphate (Glc6P) after the addition of the ion-pairing reagent Arg-Arg-Arg (R3). The spectrum shows the two ion-pairs, $[Glc6P+R3+2H]^{2+}$ and $[Glc6P+R3+H]^{+}$.

in a charge-state independent fashion. The ion-pair complexes can have different charge states (singly and doubly charge) in ESI. Thus, it would be beneficial if this method could be used to discriminate the ion-pairs in both charge states. In addition, being able to differentiate the isobars using two different charge states is useful because it provides two methods of confirming the functional groups' assignment. To better understand *why* these isobaric complexes have different MS/MS data, the spectra for the phosphorylated and sulfated ion-pairs are compared.

Table 1: MS/MS data of singly charged complexes with different peptides

	Glc6P			Glc6S			GlcNac6P				GlcNac6S			
	Parent ions [*m/z*]	H_2O loss	Peptide	Parent ions [*m/z*]	H_2O loss	Peptide	Parent ions [*m/z*]	H_2O loss	Peptide	Other peaks [*m/z*]	Parent ions [*m/z*]	H_2O loss	Peptide	Other peaks [*m/z*]
P1	1219	+	+	1219	+	+	1260	+	+	-	1260	+	+	-
P2	1263	+	+	N/A	N/A	N/A	N/A	N/A	N/A	N/A	1305	+	-	1203
P3	1089	+	+	1089	+	+	1130	+	+	-	1130	+	+	1209
R3	**747**	**-**	**+**	**747**	**+**	**+**	**788**	**+**	**+**	**-**	**788**	**+**	**+**	**687**
K4	791	+	+	791	+	-	N/A	N/A	N/A	N/A	832	+	-	796
K3	**661**	**+**	**+**	**663**	**+**	**-**	**704**	**+**	**+**	**-**	**704**	**+**	**-**	**-**
KYK	**698**	**+**	**+**	**698**	**-**	**-**	**739**	**+**	**+**	**-**	**739**	**-**	**-**	**-**
K2	535	+	+	535	+	+	576	+	+	-	576	+	+	-
RGK	620	+	+	620	+	+	661	+	+	-	661	+	+	-
RSK	650	-	+	650	+	+	691	+	+	-	691	+	+	-

N/A: the precursor ions or product ions are not detected. +: peak detected in MS/MS. -: peak absent in MS/MS.

Peptides were ruled out based on the following criteria: (1) Data are identical for each set of the isobars. (2) The peptide cannot form a complex with at least one carbohydrate, so the complexes are not apparent on spectra. Bolded peptides are good for discriminating the isobars.

Table 2: MS/MS data of doubly charged complexes with different peptides

	Glc6P				Glc6S				GlcNAc6P				GlcNAc6S			
	Parent ions [*m/z*]	H_2O loss	Peptide	Other peaks [*m/z*]	Parent ions [*m/z*]	H_2O loss	Peptide	Other peaks [*m/z*]	Parent ions [*m/z*]	H_2O loss	Peptide	Other peaks [*m/z*]	Parent ions [*m/z*]	H_2O loss	Peptide	Other peaks [*m/z*]
P1	**610**	**+**	**+**	**-**	**610**	**+**	**-**	**-**	**631**	**+**	**+**	**-**	**631**	**+**	**-**	**-**
P2	**633**	**-**	**+**	**-**	**633**	**+**	**+**	**-**	**653**	**+**	**+**	**542**	**653**	**+**	**+**	**602**
P3	**545**	**+**	**+**	**-**	**545**	**+**	**-**	**-**	**566**	**+**	**+**	**-**	**566**	**+**	**-**	**-**
R3	374	-	+	-	374	-	+	-	395	-	+	-	395	+	+	-
K4	396	+	-	-	396	+	-	-	417	+	-	531/302	417	+	-	-
K3	**332**	**+**	**+**	**403 261/243**	**332**	**+**	**-**	**242**	**353**	**-**	**-**	**302/403**	**353**	**+**	**-**	**403/302 284/222**
KYK	350	+	+	483 261/243	350	+	+	309	N/A	N/A	N/A	N/A	370	+	-	438/302 222
K2	N/A	N/A	N/A	N/A	N/A	N/A	N/A	N/A	289	-	-	271/161	289	N/A	N/A	271/161
RGK	311	-	+	360 261/243	N/A	N/A	N/A	N/A	N/A	N/A	N/A	N/A	N/A	N/A	N/A	N/A
RSK	326	-	+	390 261/243	326	+	+	285 276/236	346	+	-	390/302	346	+	-	390/302

N/A: the precursor ions or product ions are not detected. +: peak detected in MS/MS. -: peak absent in MS/MS.

Peptides were rule out based on the following criteria: (1) Data are identical for each set of the isobars. (2) The peptide cannot form a complex with at least one carbohydrate, so the complexes are not apparent on spectra. Bolded peptides are good for discriminating the isobars.

Comparison of the MS/MS data: Doubly charged complexes with K3

The MS/MS data of the doubly charged ion-pairs of glucose-6-phosphate $[Glc6P+K3+2H]^{2+}$ and glucose-6-sulfate $[Glc6S+K3+2H]^{2+}$ are in Figure 3A and 3B. The product ions of the ion-pair complex, $[Glc6P+K3+2H]^{2+}$, in Figure 3A include the singly charged K3 at *m/z* 403, the doubly charged K3 at *m/z* 202, and two ions corresponding to the water loss from the ion-pair complex, labeled as $[M-H_2O+2H]^{2+}$ and $[M-2H_2O+2H]^{2+}$, respectively. Water loss is generally expected in the MS/MS data of carbohydrates due to the presence of many hydroxyl groups in the carbohydrate's structure [25,26]. Two other singly charged ions at *m/z* 261 and 243 corresponding to the product ion, $[Glc6P+H]^+$, and water loss from phosphorylated monosaccharide, respectively, were also observed.

In Figure 3A, an ion corresponding to the protonated monosaccharide ($[Glc6P+H]^+$) appears in the spectrum of the phosphorylated complex, $[Glc6P+K3+2H]^{2+}$. This ion forms when the doubly charged complex dissociates to two singly charged ions, $[K3+H]^+$ at *m/z* 403 and $[Glc6P+H]^+$ at *m/z* 261. Doubly charged product ions dominate the spectrum of the sulfated complex, $[Glc6S+K3+2H]^{2+}$. This indicates that the distribution of charges on the phosphorylated complex is different from that of the sulfated complex. The two protons on the phosphorylated complex are not exclusively located on the basic residue of the peptide. One of them can be transferred to the phosphate group of the carbohydrate. The difference in the charge distribution of the doubly charged sulfated and phosphorylated ion-pairs can be explained in terms of the proton affinities of the two functional groups. From the known pKa values of the sulfate (pKa=1.89) and the phosphate group (pKa=2.13) [27], it can be deduced that

the functional group with higher pKa has stronger proton affinity. Thus the proton transfer from basic residue to the mono-phosphorylated residue is more facile, compared to the mono-sulfated carbohydrates. Another difference in the dissociation between the sulfated and phosphorylated complexes is the product ion $[K3+SO_3+2H]^{2+}$ at *m/z* 242, which appears in Figure 3B, but not 3A. This ion formed by bond cleavage between the carbohydrate and the SO_3 group. The formation of this ion is likely due to stronger non-covalent interactions between the peptide and the sulfate group. Since the sulfate group has lower pKa than the phosphate group, it most likely complexes to the basic peptide residue more strongly. As a result, the covalent oxygen-sulfur bond cleaves, and the SO_3 remains complexed to the ion-pairing reagent during CID. In contrast, the covalent phosphorus-oxygen bond does not cleave during CID. Because of the differences in chemical reactivity, the complexes have different fragmentation patterns when they undergo the same CID conditions.

Figure 3C and 3D show MS/MS data for the two other isobaric species, GlcNAc6P and GlcNAc6S, complexed with K3. These two ion-pair complexes can also be distinguished, based on their MS/MS data. In Figure 3C, two singly charged complementary ions $[GlcNAc6P+H]^+$ and $[K3+H]^+$ (*m/z* 302 and 403, respectively) originate from the precursor ion. These ions correspond to the ligand dissociation of the ion-pair complex. Only one other small product ion corresponding to the loss of water from the carbohydrate was observed, indicating that the interaction between phosphate and basic peptide is weaker than the covalent bonds in the phosphorylated monosaccharide. In addition to the two complementary ions observed in Fig 3C, other product ions appear in the spectrum containing GlcNAc6S

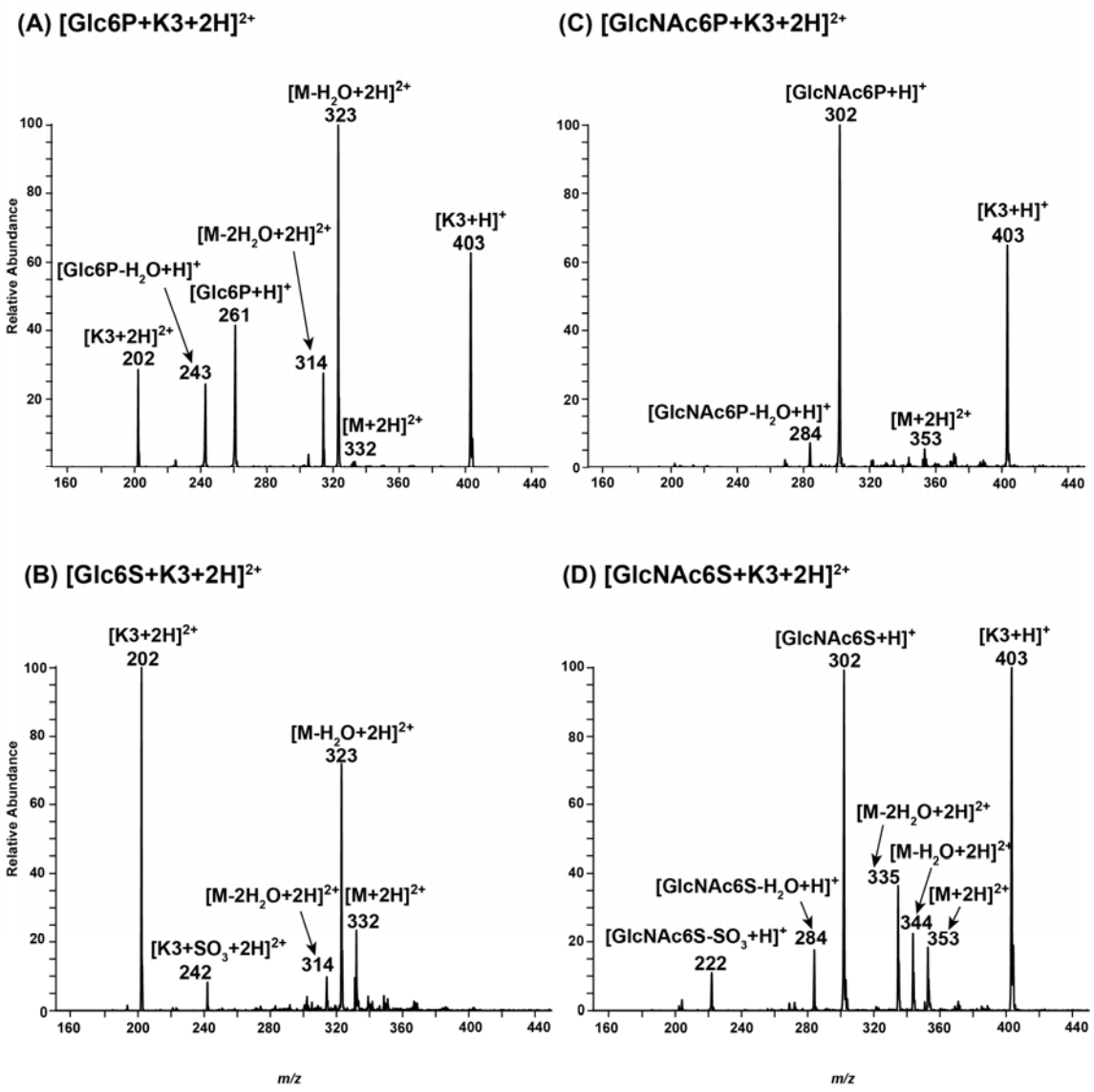

Figure 3. (+)ESI-MS/MS data for the doubly charged ion-pairs with Lys-Lys-Lys (K3): A) phosphorylated complex $[Glc6P+K3+2H]^{2+}$ B) sulfated complex $[Glc6S+K3+2H]^{2+}$ C) phosphorylated complex $[GlcNAc6P+K3+2H]^{2+}$ and D) sulfated complex $[GlcNAc6S+K3+2H]^{2+}$. 3B and 3D both show characteristic ions resulting from oxygen-sulfur bond cleavage.

and K3 in Figure 3D. These ions include water loss ions (*m/z* 344, 335, and 284) and the product ion at *m/z* 222, which corresponds to cleaving the oxygen-sulfur bond in the carbohydrate. Note that this covalent bond cleavage is only observed in

the MS/MS data of the sulfated carbohydrates (Figure 3B and 3D).

Another interesting observation in the MS/MS data in Figure 3C and 3D is that only the precursor and the product ions corresponding to the loss of H_2O (*m/z* 344 and 335, respectively) are doubly charged. All of the other product ions are singly charged. This fragmentation behavior is different than the MS/MS data of the ion-pair complexes shown in Figure 3A and 3B. This must be due to the type of carbohydrate complexed with the peptide. Hence, in addition to proton affinities, the type of carbohydrate is another important factor that can influence the ions formed in the CID spectra of phosphorylated and sulfated ion-pair complexes.

Singly charged complexes with K3

As discussed above, the MS data of the carbohydrate:peptide ion pairs show the formation of ion-pair complexes with different charge states: singly and doubly charge state complexes. MS/MS experiments were performed on the singly charged complexes, and the sulfated and phosphorylated monosaccharides can also be distinguished using these CID spectra (Figure 4). Three important ions were observed in the spectra: The molecular ions (MH^+), the ions corresponding to water loss ($[M-H_2O+H]^+$), and the singly charged peptides ($[K3+H]^+$). When identical collision conditions are used, the protonated peptide K3 at m/z 403 in Figure 4 is observed upon CID in the MS/MS data of the phosphorylated complex, but not in that of the sulfated complex. The presence of these singly charged peptide product ions $[K3+H]^+$ provides additional evidence that phosphorylated ion-pair complexes are weaker than the sulfated ion-pair complexes, because the sulfated complexes undergo the covalent cleavage only (loss of H_2O), while the phosphorylated complexes undergo cleavage of the non-covalent interaction. This method of

differentiating the isobars is dependent on the collision energy used. At higher collision energies, the sulfated complexes also undergo ligand dissociation.

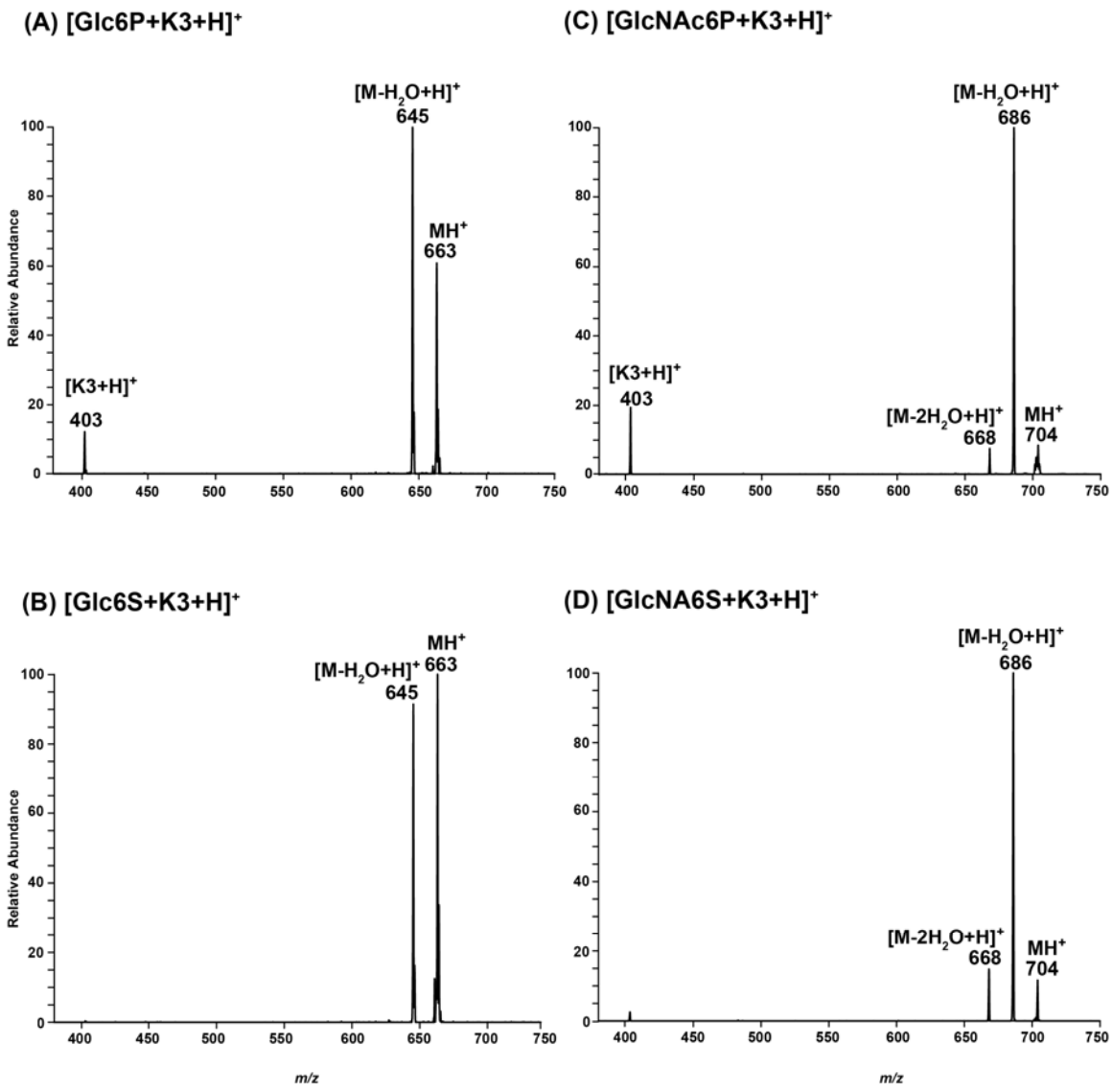

Figure 4. (+)ESI-MS/MS data for singly charged complexes with Lys-Lys-Lys (K3) to identify the difference in chemical reactivity between phosphate and sulfate of the following carbohydrate:peptide complexes: A) phosphorylated ion-pair complex $[Glc6P+K3+H]^+$, B) sulfated ion-pair complex $[Glc6S+K3+H]^+$, C) phosphorylated ion-pair complex $[GlcNAc6P+K3+H]^+$, and D) sulfated ion-pair complex $[GlcNAc6S+K3+H]^+$.

Application to other phosphorylated and sulfated monosaccharides

The ion-pairs with different charge states have different fragmentation characteristics based on the observations discussed above. Doubly charged sulfated compounds produce ions that correspond to cleavage of the oxygen-sulfur bond, resulting in losses of SO_3 in the MS/MS data, while phosphorylated compounds are more likely to undergo ligand dissociation to produce the protonated carbohydrates, instead of covalent bond cleavages. When singly charged ion-pair complexes undergo CID, the dissociation of the non-covalent complex occurs more readily for the phosphorylated compounds. This results in formation of the product ions $[K3+H]^+$ in the CID data of the phosphorylated complexes. To test whether the chemical reactivity trends observed for the four isobaric monosaccharides are conserved when slight changes in the monosaccharides occur, the ion pairing MS/MS experiments were applied to other commercially available phosphorylated and sulfated monosaccharides.

The structures of the monosaccharides shown in Scheme 2 include N-acetyl-glucosamine-1-phosphate (GlcNAc1P), N-acetyl-galactosamine-4-sulfate (GalNAc4S), glucose-3-sulfate (Glc3S) and isomers α-glucose-1-phosphate (αGlc1P), β-glucose-1-phosphate (βGlc1P). MS/MS data of the doubly charged ion-pair complexes of the sulfated and phosphorylated carbohydrates complexed with K3 are shown in Figure 5. Figure 5A and 5B are two phosphorylated isomers α-Glc1P and β-Glc1P complexed with K3, while the two N-acetylhexosamine:peptide ion pairs $[GlcNAc1P+K3+2H]^{2+}$ and $[GalNAc4S+K3+2H]^{2+}$ are shown in Figure 5D and 5E.

The two N-acetylhexosamines are readily distinguished in this experiment. Two complementary ions: protonated hexosamine $[GlcNAc1P+H]^+$ (*m/z* 302) and peptide ion $[K3+H]^+$ (*m/z* 403) are shown in Figure 5D, which is consistent with the trends of dissociation of phosphorylated ion pairs upon CID. The ion (*m/z* 204) is

most likely a secondary product resulting from the fragmentation of the ion at *m/z* 302. In Figure 5E the product ion corresponding to the cleavage of the oxygen-sulfur bond is labeled at *m/z* 222 which corresponds to $[GalNAc4S\text{-}SO_3+H]^+$. This ion clearly indicates that the monosaccharide is sulfated and not phosphorylated.

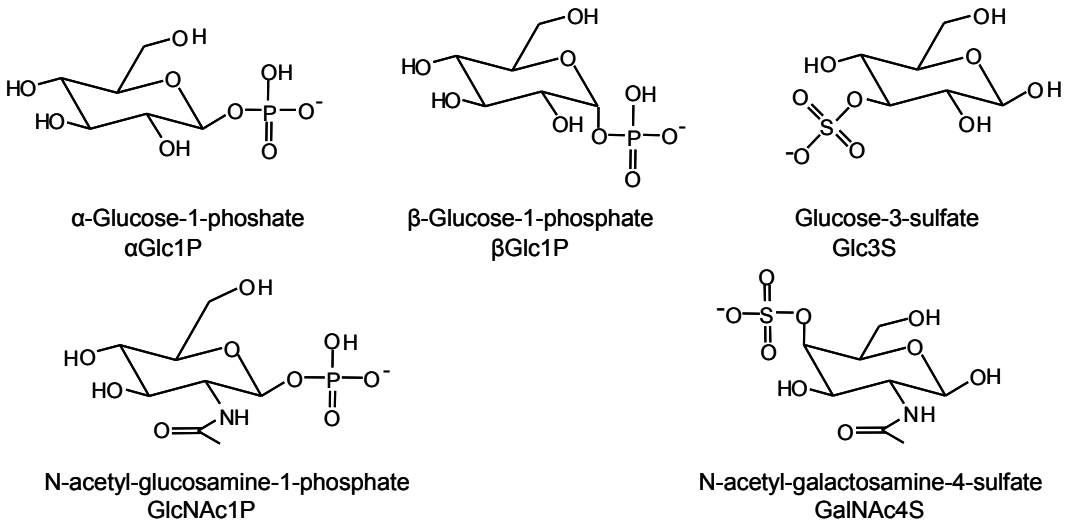

Scheme 2. Structures of other phosphorylated and sulfated monosaccharides used for the ion-pairing experiments.

The data for the hexose monosaccharides is also consistent with the trends established for the CID spectra of the isobaric monosaccharides in Figure 3. Two product ions (*m/z* 261 and *m/z* 403) originating from the ligand dissociation are apparent in the spectra of phosphorylated complexes $[\alpha Glc1P+K3+2H]^{2+}$, Figure 5A and $[\beta Glc1P+K3+2H]^{2+}$, Figure 5B. The product ion at *m/z* 242 corresponding to the oxygen-sulfur bond cleavage appears in Figure 5C. However, these three characteristic product ions that are useful to discriminate the hexoses are not present in abundance. To further verify the different fragmentation characteristics of both phosphorylated and sulfated hexoses:peptide ion-pair complexes upon collisional

activation, peptide KYK was introduced in the analysis.

Figure 6 shows the MS/MS data of the doubly charged hexoses:peptide ion-pairs. The observed difference between the MS/MS data of the ion-pair complexes in Figure 6A and 6B, which are model isobaric molecules, are consistent with the trends discussed above. Two complementary product ions at *m/z* 260.9 and *m/z* 438.3 are originating from the ligand dissociation in Figure 6A. While an ion corresponding to oxygen-sulfur bond cleavage appears in Figure 6B, along with many other product ions resulting from the covalent bond cleavages. This demonstrates that peptide KYK is useful to distinguish doubly charged hexoses:peptide ion pairs. From the other spectra in Figure 6, the relative abundance of the ions corresponding to the non-covalent cleavage in phosphorylated complexes (ions at *m/z* 260.9 and *m/z* 438.1 in Fig. 6C and 6D) and oxygen-sulfur cleavage in sulfated complexes (ion at *m/z* 309.4 in Fig. 6E) are enhanced when KYK is used as the ion-pairing reagent, instead of K3. This peptide provides the complementary information to confirm the fragmentation characteristics of hexoses:peptide ion pairs. To summarize, the peptide K3 was useful at distinguishing the monosaccharides, but the important, discriminating ions were in low abundance. The identity of each of the monosaccharides could be further supported using another peptide that discriminated the hexoses, KYK.

Aside from the doubly charged ion pairs, the CID data of the singly charged ion pairs are summarized in Table 3. Upon collisional activation, the singly charged phosphorylated ion-pair complexes dissociate to produce the abundant peptide $[K3+H]^+$. This ion is useful to distinguish phosphorylated and sulfated complexes. These results are consistent with the MS/MS data for the original four isobaric

monosaccharides, in Figure 4.Using the singly charged complexes to differentiate the hexose monosaccharides represents a third successful approach to identifying the chemical composition of these monosaccharides. Clearly, the ion pairing strategy is robust in that it is useful under many conditions, for various types of monosaccharides, various charge states, and various ion-pairing reagents. These data also demonstrate that the rules developed to describe the dissociation of the isobaric monosaccharides could be applied to any other sulfated or phosphorylated monosaccharide. Since these rules appear to be functional group specific, and not compound specific, it is quite plausible that these principles could be extended to larger oligosaccharides or glycopeptides. Overall, the comparison of the MS/MS data of both abundant ion-pairs demonstrates that ion-pairing reagents, K3 and KYK, can be used to effectively distinguish phosphorylated and sulfated compounds in terms of their fragmentation characteristics in the CID spectra.

While differentiating positional isomers is not the subject of this investigation, ion-pairing may also be useful for identifying the location of the phosphate on the monosaccharides. A unique product ion is present in Figures 5 and 6 for the monosaccharides phosphorylated at the anomeric carbon. This product ion corresponds to cleavage of H_3PO_4 from the monosaccharides. When the phosphate is at the C6 position, a loss of H_2O is observed instead. A possible explanation for this behavior is that the water loss from Glc6P and GlcNAc6P is coming from the hydroxyl group of C1. Once the hydroxyl group is replaced by the phosphate group, a carbohydrate/phosphate cleavage occurs instead. This hypothesis is also supported by the observation that the complexes produced from Glc1P or GlcNAc1P do not have water loss product ions in their CID spectra.

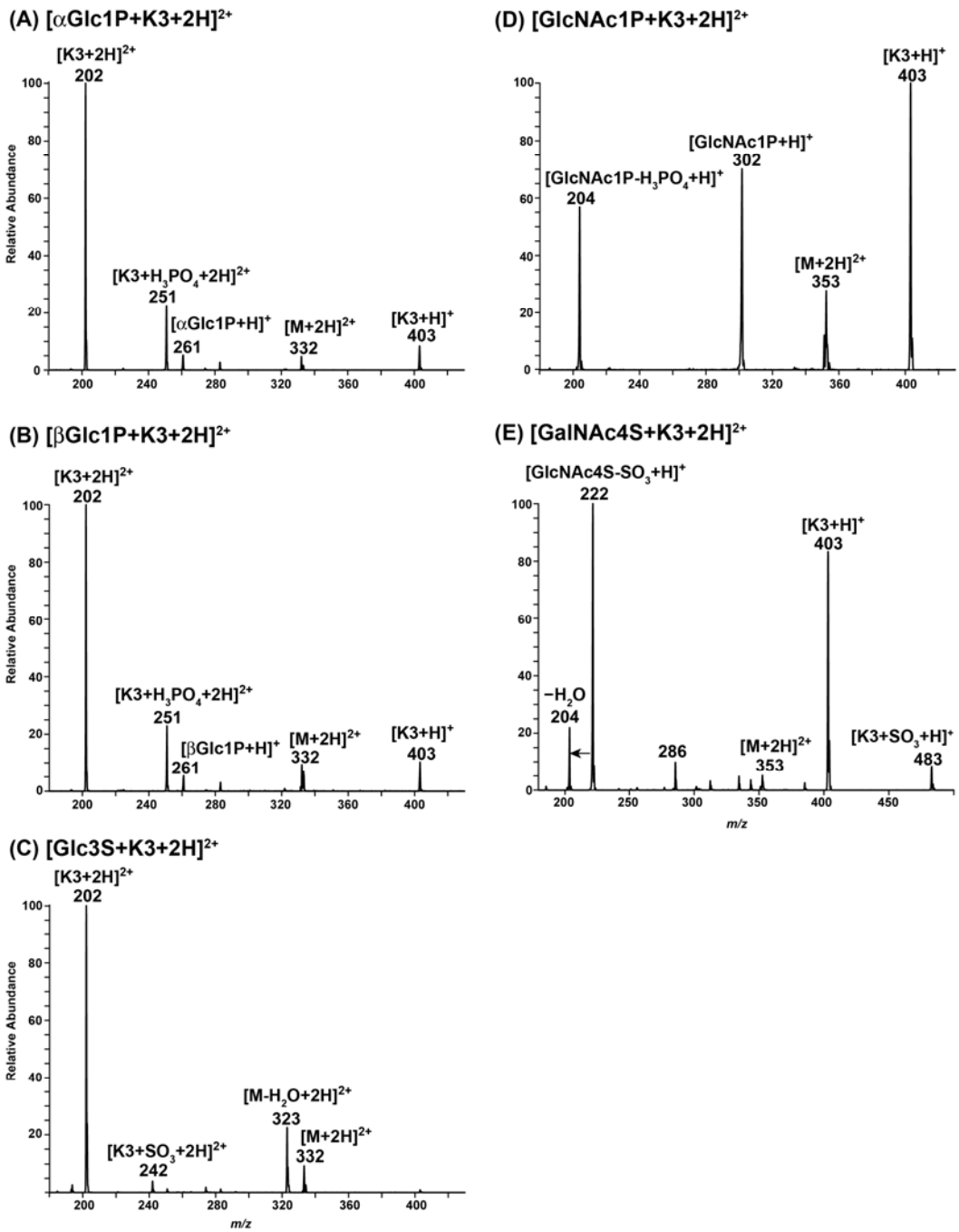

Figure 5. (+)ESI-MS/MS data for the doubly charged ion-pair complexes with the tripeptide Lys-Lys-Lys (K3) verifying which species were sulfated or phosphorylated of the following carbohydrate:peptide complexes: A) phosphorylated complex $[\alpha Glc1P+K3+2H]^{2+}$, B) phosphorylated complex $[\beta Glc1P+K3+2H]^{2+}$, C) sulfated complex $[Glc3S+K3+2H]^{2+}$, D) phosphorylated complex $[GlcNAc1P+K3+2H]^{2+}$, and E) sulfated complex $[GalNAc4S+K3+2H]^{2+}$. 5C and 5E both show characteristic ions resulting from oxygen-sulfur bond cleavage.

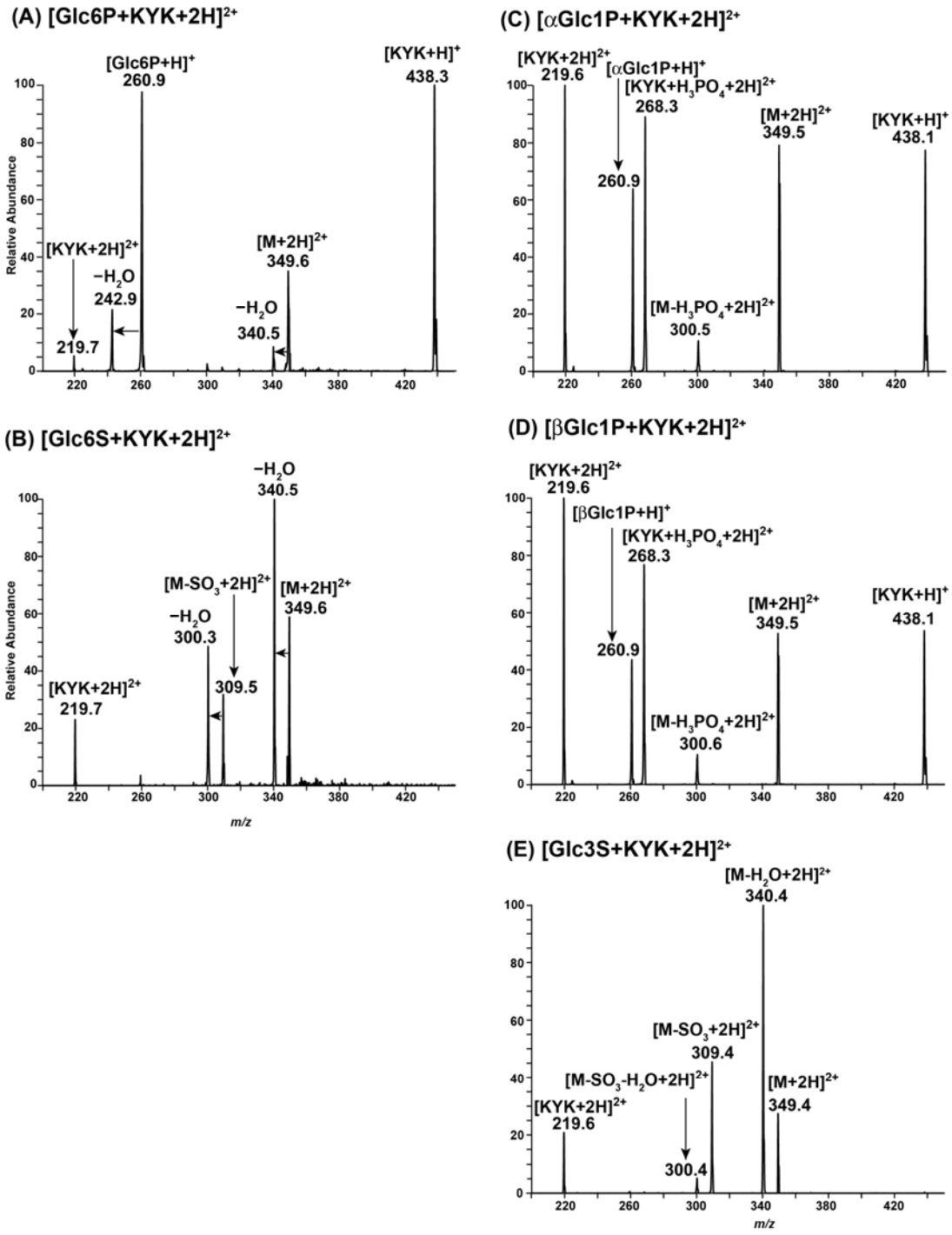

Figure 6. (+)ESI-MS/MS data for the doubly charged ion-pair complexes with Lys-Tyr-Lys (KYK) A) phosphorylated complex $[Glc6P+KYK+2H]^{2+}$ and B) sulfated complex $[Glc6S+KYK+2H]^{2+}$ C) phosphorylated complex $[\alpha Glc1P+KYK+2H]^{2+}$, D) phosphorylated complex $[\beta Glc1P+KYK+2H]^{2+}$, and E) sulfated complex $[Glc3S+KYK+2H]^{2+}$.

Table 3: MS/MS data of singly charged complexes with K3

$[HexNAcs+K3]^+$			$[Hexoses+K3]^+$		
HexNAcs	Parent Ions *m/z*	$[K3+H]^+$ *m/z* 403 (Abundance %)	Hexoses	Parent Ions *m/z*	$[K3+H]^+$ *m/z* 403 (Abundance %)
GlcNAc6P	704	18	Glc6P	663	15
GlcNAc1P	704	100	αGlc1P	663	10
GlcNAc6S	704	N/A	βGlc1P	663	10
GlcNAc4S	704	N/A	Glc6S	663	N/A
			Glc3S	663	N/A

N/A: The product ions are not detected.

Potential application to biological samples

Phosphorylation and sulfation of glycoprotein and glycopeptides are involved in a variety of significant biological functions. Differentiation between these species is crucial in the characterization of structure/function relationship of modified glycoprotein or glycopeptides. As discussed above, the peptides, K3 and KYK, are effective ion-pairing reagents to distinguish phosphorylated and sulfated carbohydrates. Since KYK cannot readily form the complexes with some monosaccharides, K3 is a potential ion-pairing reagent that can be used to distinguish sulfate and phosphate biological systems. In a previous study, K3 has been utilized to complex with mono- and di-sulfated glycopeptides to enhance the signal in the positive ion mode of ESI-MS and provide structural information about the sulfated glycopeptides [20]. Also, the results presented herein indicate that the

phosphorylated carbohydrates can also complex with the ion-pairing reagents in good abundance in ESI-MS. This implies that K3 can potentially be applied to distinguish between phosphorylated and sulfated glycopeptides. A full investigation of the utility of ion-pairing for differentiation analysis of phosphorylated and sulfated glycopeptides is ongoing and will be presented separately.

2.4 Conclusions

In this manuscript all the commercially available sulfated and phosphorylated monosaccharides are differentiated using ion pairing and MS/MS. Furthermore, this method is robust because it is effective regardless of the charge state of the ion-pair. The fragmentation characteristics in the CID spectra for both abundant ion-pairs were summarized. For doubly charged complexes, sulfated compounds are likely to undergo sulfur-oxygen bond cleavage, while phosphorylated compounds tend to dissociate by discrupting noncovalent interactions. The type of monosaccharide also affects the MS data of the ion pairs, but it does not affect the characteristic product ions that are useful at discriminating between sulfate and phosphate.

MS/MS data of singly charged ion pairs also support the hypothesis that phosphorylated ion-pair complexes are weaker than the sulfated ion-pair complexes, because the sulfated complexes undergo covalent cleavage only, while the phosphorylated complexes undergo cleavage of the non-covalent interaction.

This is the first example of using ion-pairing on phosphorylated compounds and the first use of ion-pairing reagents to discriminate the presence of sulfates and phosphates. Since we have recently demonstrated that the ion-pairing method enhances the mass spectral signal of sulfated glycopeptides that are minor components (<5%) of glycopeptide

mixtures [20], this is the *only* method that can simultaneously facilitate the MS detection of acidic species in complex mixtures *and* discriminate the acidic groups, sulfate and phosphate.

Acknowledgements

The authors acknowledge the National Institutes of Health for funding (project number 1 P20 RR17708-01).

2.5 References

1. Petzold, C.J.; Leavell, M.D.; Leary, J.A. Screening and identification of acidic carbohydrates in bovine colostrums by using ion/molecule reactions and Fourier transform ion cyclotron resonance mass spectrometry: specificity toward phosphorylated complexes. *Anal. Chem.* **2004,** *76,* 203-210.

2. Bossio, R.E.; Marshall, A.G. Baseline resolution of isobaric phosphorylated and sulfated peptides and nucleotides by electrospray ionization FTICR MS: another step toward mass spectrometry-based proteomics. *Anal. Chem*. **2002**, *74,* 1674-1679.

3. Mann, M.; Ong, S.; Grønborg, M.; Steen, H.; Jensen, O.N.; Pandey, A. Analysis of protein phosphorylation using mass spectrometry: deciphering the phosphoproteome. *Trends Biotechnol.* **2002,** *20,* 261-268.

4. Mclachlin, D.; Chait, B.T. Analysis of phosphorylated proteins and peptides by mass spectrometry. *Curr Opin Chem Biol.* **2001,** *5,* 591-602.

5. Nelson, D.L.; Cox, M.M. Biosignaling. In *Principles of Biochemistry.* W.H.Freeman and Company, Inc: New York, 2004; pp 428-429.

6. Zhou, H.; Watts, J.D.; Aebersold, R. A systematic approach to the analysis of protein phosphorylation. Nat. Biotechnol. **2001,** *19,* 375-378.

7. Gao, H.; Petzold, C.J.; Leavell, M.D.; Leary, J.A.; Investigation of ion/molecule reactions as a quantification method for phosphorylated positional isomers: an FT-ICR approach. *J.Am.Soc.Mass. Spectrom.* **2003,** *14,* 916-924.

8. Nelson, D.L.; Cox, M.M. Biosignaling. In *Principles of Biochemistry.* W.H.Freeman and Company, Inc: New York, 2004; pp 421-422.

9. Siegel, M.M.; Tabei, K.; Kagan, M.Z.; Vlahov, I.R.; Hileman, R.E.; Linhardt, R.J.

Polysulfated carbonhydrates analyzed as Ion-paired complexes with basic peptides and proteins using electrospray negative ionization mass spectrometry. *J Mass Spectrom.* **1997,** *32,* 760-772.

10. Witczak, Z.J.; Nieforth, K.A. Carohydrates as new and old targets for future drug design. In *Carbohydrates in drug design.* Marcel Dekker, Inc.: New York, 1997; pp 1-39.

11. Delcommenne, M.; Kannagi, R.; Johnson, P. TNF-α increases the carbohydrate sulfation of CD44: induction of 6-sulfo N-acetyl lactosamine on N- and O-linked glycans. *Glycobiology.* **2002,** *12,* 613-622.

12. Bowman, K.G.; Cook, B.N.; de Graffenried, C.L.; Bertozzi, C.R.; Biosynthesis of L-selectin ligands: sulfation of sialyl lewis x-related oligosaccharides by a family of GlcNAc-6-sulfotransferases. *Biochemistry.* **2001,** *40,* 5382-5391.

13. Green E.D.; Baenziger, J.U. Asparagine-linked oligosaccharides on lutropin, follitropin, and tryrotropin. *J.Biol.Chem.* **1988,** *263,* 36-44.

14. Bai, X.; Brown, J.R.; Varki, A.; Esko, J.D.; Enhanced 3-O-sulfation of galactose in Asn-linked glycans and Maackia amurenesis lectin binding in a new Chinese hamster ovary cell line. *Glycobiology,* **2001,** *11,* 621-632.

15. Chen, S.L.; Huddleston, M.J.; Shou, W.; Deshaies, R.J.; Annan, R.S.; Carr, S.A. Mass spectrometry-based methods for phosphorylation site mapping of hyperphosphorylated proteins applied to Net1, a regulator of exit from mitosis in yeast. *Mol. Cell. Proteomics.* **2002,** 186-187.

16. Tuytten, R.; Lemiere, F.; Dongen, W.V.; Esmans, E.L.; Slegers, H. Short capillary ion-pair high performance liquid chromatography coupled to electrospray (tandem) mass spectrometry for the simultaneous analysis of nucleoside mono, di- and triphosphates. *Rapid. Commun. Mass Spectrom.* **2002,** *16,* 1205-1215.

17. Ruse, C.I. Willard, B.; Jin, J.P.; Hass, T.; Kinter, M.; Bond, M. Quantitative dynamics of site-specific protein phosphorylation determination using liquid chromatography electrospray ionization mass spectrometry. *Anal. Chem.* **2002,** *74,* 1658-1664.

18. Watkins, M.A.; Price, J.M.; Winger, B.E.; Kenttamaa, H.I. Ion-molecule reactions for mass spectrometric identification of functional groups in protonated oxygen-containing monofunctional compounds. *Anal. Chem.* **2004,** *76,* 964-976.

19. Juhasz, P.; Biemann, K. Mass spectrometric molecular-weight determination of highly acidic compounds of biological significance via their complexes with basic polypeptides. *Proc. Natl. Acad. Sci. USA.* **1994**, *91,* 4333-4337.

20. Jiang, H; Irungu, J; Desaire, H. “Enhanced Detection of Sulfated Glycosylation Sites in Glycoproteins.” *J. Am. Soc. Mass Spectrom*. In press.

21. Juhasz, P.; Biemann, K. Utility of non-covalent complexes in the matrix- assisted laser desorption ionization mass spectrometry of heparin-derived oligosaccharides. *Carbohyr Res.* **1995,** *270,* 131-147.

22. Fromm, J.R.; Hileman, R.E.; Caldwell, E.E; Weiler, J.M.; Linhardt, R.J. Differences in the interaction of heparin with arginine and lysine and the importance of these basic amino acids in the binding of heparin to acidic fibrolast growth factor. *Arch. Biochem. Biophys.* **1995,** *323,* 279-287.

23. Svoboda, M.; Meister, W.; Kitas, E.A; Vetter, W. The influence of strongly acidic groups on the protonation of peptides in electrospray MS. *J. Mass. Spectrom.* **1997,** *32,* 1117-1123.

24. Harvey, D.J.; Bousfield, G.R. Differentiatin between sulphated and phosphated carbohydrates in low-resolution matrix-assisted laser desorption/ionization mass spectra. *Rapid. Commun. Mass Spectrom.* **2005,** *19,* 287-288.

25. Desaire, H.; Leary, J.A. The effects of coordination number and ligand size on the gas phase dissociation and sterochemical differentiation of co-coordinated monosacchrides. *Int. J. Mass spectrum.* **2001,** *209,* 171-184.

26. Desaire, H.; Leavell, M.D.; Leary, J.A. Solvent effects in tandem mass spectrometry: Mechanistic studies indicating how a change in solvent conditions and pH can dramatically alter CID spectra. *J. Org. Chem.* **2002,** *67,* 3693-3699.

27. Chang, R. Acids and Bases In *Chemistry.* McGraw-Hill, Inc.: New York, 2005; pp 626-675.

Chapter III

Distinguishing phosphorylation and sulfation in carbohydrates and glycoproteins using ion-pairing and mass spectrometry

3.1 Introduction

Phosphorylation and sulfation are significant biological modifications that affect the functions of numerous species ─ carbohydrates,[1] proteins,[2-5] and glycoproteins.[6-15] For example, tyrosine phosphorylation of proteins in the cytoplasm plays an essential role in intracellular signaling transduction,[2,3] cell cycle control,[4] transcription of gene expression,[4] cytoskeletal regulation, and apoptosis.[3,4] Tyrosine sulfation results in different functions, including modulation of intracellular protein transportation, regulation of proteolytic process of proteins, and the alteration of biological activity of proteins.[3, 5-7] Phosphorylation and sulfation present on carbohydrate moieties of glycoproteins also causes different biological responses. Changes in sulfation on the glycoproteins have been related to various diseases, such as diabetes, arthritis, Alzheimer's disease, and cystic fibrosis etc.[8] In addition, alterations in phosphorylation of carbohydrate moieties on glycoproteins are also linked to diverse types of diseases including the neuronal ceroid lipofuscinoses (NCLs) which are hereditary neurodegenerative diseases affecting human beings.[9] Moreover, phosphorylated glycoproteins, such as mannose-6-phosphorylated glycoprotein, can be used as prognostic markers for breast cancer, ovarian cancer, and prostate cancer, etc.[10] Since phosphorylation and sulfation have been

associated with significantly different biological functions, developing efficient and sensitive methods to discriminate these structures is essential for understanding their roles in protein functions and in diseases.

Traditionally, phosphorylation and sulfation of carbohydrates or proteins are detected by radiolabeling using ^{32}P or ^{35}S [2,6,7,14-17] isotopes, separation using gel-filtration chromatography,[11-13] high performance liquid chromatography (HPLC),[11-13,16-17] two-dimensional thin-layer chromatography (TLC),[7,16] and the detection of these isotopes in scintillation counting or autoradiography.[16] While radiolabeling is effective at identifying the presence of phosphorylation or sulfation, the detection step must be followed by additional characterization steps, since determining the presence of the radioisotopes does not provide any information about the structure of the compound that was labeled.

In recent years, mass spectrometry has become a powerful analytical tool in the identification and characterization of biological molecules and their posttranslational modifications. It is highly sensitive and selective, and provides rapid means to analyze samples, obviating the need for radiolabeling.[16,18] A MS-based method to discriminate between phosphorylation and sulfation involves reacting suspected phosphorylated compounds with alkaline phosphatase.[16] MS analysis is applied before and after treatment with the enzyme to detect the loss of phosphate in the products.[16] Although this type of enzymatic assay is effective in differentiation between phosphorylation and sulfation, its application is limited when analyzing complex mixtures, which imparts a significant barrier in many biological applications, especially when the compounds are phosphorylated or sulfated at low levels.[16]

High resolution MS methods, such as Fourier transform ion cyclotron

resonance mass spectrometry (FTICR-MS), have been used to distinguish between phosphorylated and sulfated compounds based on their slight difference in mass[19] or by their ability to react differently in ion-molecule reactions.[20] Other MS methods, such as matrix-assisted laser desorption/ionization (MALDI) [21] and electrospray ionization (ESI),[22] have been recently reported to distinguish phosphorylation and sulfation. In MALDI analysis, sulfated and phosphorylated products ionize somewhat differently, and these differences could potentially be used to distinguish phosphate and sulfate in an unknown compound.[21] In ESI analysis, ion-pairing reagents have been utilized to complex with singly phosphorylated or sulfated monosaccharides.[22] The isobaric ion-pairing complexes can be differentiated in MS/MS experiments because of their different chemical reactivities. The fundamental study indicates that this approach is only functional group dependent,[22] thus, it could potentially be effective in discriminating the phosphorylation and sulfation in larger biologically relevant molecules. If the ion-pairing method, which distinguishes phosphorylated and sulfated monosaccharides, could be adapted to larger macromolecules, like oligosaccharides and glycoproteins, this approach would afford a unique and effective way to distinguish phosphorylation from sulfation. Using ion-pairing to discriminate these groups is advantageous to other methods because this approach provides significant advantages that are not related to phosphate/sulfate discrimination: The ion-pairing method has already been demonstrated to enhance the signal of sulfated glycopeptides,[23] and to facilitate structural elucidation of the glycan moiety present in glycoproteins.[24] Thus, sulfate/phosphate determination could be accomplished in a synergistic analysis that also enhances sensitivity and provides additional structural information about glycoproteins.

In the work presented here, the ion-pairing approach described previously to discriminate monosaccharides[22] is utilized to identify the phosphorylation and sulfation present in disaccharides and glycopeptides generated from a proteolytic digest of oLHα (ovine luteinizing hormone, α-subunit). Difference in chemical reactivities between these two acidic functional groups observed in the monosaccharides[22] can be preserved when this approach is applied to complex biomolecules. This is the first study to use the ion-pairing technique in conjunction with MS/MS to differentiate phosphorylation and sulfation on disaccharides and glycopeptides. In addition to discriminating the isobaric compounds, this approach can also simultaneously enhance the mass spectral signal of acidic groups in complex mixtures by enhancing the ionization efficiency of these functional groups.[23]

3.2 Materials and Methods

Materials

Phosphorylated or sulfated monosaccharides, disaccharides, and the peptide Lys-Lys-Lys were purchased from Sigma-Aldrich (St. Louis, MO) and were used without further purification. Glycopeptides from ovine luteinizing hormone, α-subunit, (oLHα) were produced in the laboratory of Dr. George Bousfield, Wichita State University, as described elsewhere.[23,25]

Ion-pairing experiments

Ion-pair complexes were formed by combining equal volumes of basic peptide, Lys-Lys-Lys, (henceforth referred to as K3), with solutions of monosaccharides or disaccharides. Phosphorylated or sulfated carbohydrates and K3 were dissolved in a minimal amount of HPLC grade water, respectively.

Carbohydrate solutions were further diluted with a methanol:water (MeOH:H_2O) mixture (1:1) containing 0.5% acetic acid, to the final concentration of 1 mM. The peptide, K3, was diluted to 2 mM. Ion-pair complexes were generated by mixing 5 μL of carbohydrate solution with 5 μL of peptide solution, vortexing and injecting 2 μL of this mixture into the mass spectrometer. The ion-pair complexes of glycopeptides with K3 were formed by dissolving 1 μg of the glycopeptide mixture in 3 μL of a 1.25 mM solution of K3. 1-3 μL of this sample were injected into the mass spectrometer.

Mass spectrometry

All the ion-pair complexes were monitored on a Thermo Finnigan LCQ Advantage quadrupole ion trap mass spectrometer (Thermo, San Jose, CA). A surveyor MS-pump (Thermo, San Jose, CA) was used to deliver the mobile phase ─ MeOH:H_2O mixture (1:1) containing 0.5% acetic acid at a flow rate of 20 □L/min. Ion-pair complexes were directly introduced to the mass spectrometer, and all the mass spectra were acquired in the positive ion mode. Electrospray ionization was achieved by using a spray voltage of 4.0 KV. Nitrogen was used as nebulizing gas, at a pressure of 20 psi. The capillary temperature was maintained at 230 °C.

Collision-induced dissociation (CID) was performed to obtain structural information about the ion-pairs. Specifically, for the phosphorylated or sulfated mono- and disaccharide ion-pair complexes, doubly charged precursor ions were activated for 30 ms with 20% normalized collision energy. A q_z value of 0.25 and an isolation width of 3 Da were used. For the ion-pairing complexes containing glycopeptides released from oLHα and the peptide K3, doubly charged precursor ions were activated with 19% normalized collision energy. All the data were acquired and analyzed using Xcalibur 1.3 software (Thermo, San Jose, CA).

3.3 Results and Discussion

Ion pairing complexes readily form when the ion-pairing reagent is mixed with sulfated/phosphorylated carbohydrates. An example of the resulting MS data is shown in Figure 1. Recently, we demonstrated that phosphorylated and sulfated monosaccharides can be differentiated based on the different characteristic product ions of singly or doubly charged ion-pairing complexes; see Table 1.[22] For doubly charged complexes, sulfated monosaccharides undergo sulfur-oxygen bond cleavage while phosphorylated monosaccharides dissociate by disrupting the noncovalent interaction between the carbohydrate and the ion-pairing reagent. Since HexNAc's contain an amide group in their structure, the ligand dissociation can also be observed for the doubly charged, sulfated ion-pairs. For singly charged complexes, sulfated complexes undergo covalent cleavage, resulting in the losses of water, while the phosphorylated complexes undergo cleavage of noncovalent interactions, resulting in the presence of the singly charged peptide ion $[K3+H]^+$.[22] The differences in the fragmentation pattern of these two modifications are induced by different chemical reactivities resulting from the slightly different pKa values of these two acidic groups. Since the ion-pairing MS/MS method has been demonstrated to be functional group specific, it should be useful in identifying phosphorylation and sulfation in more complex carbohydrates and glycopeptides.

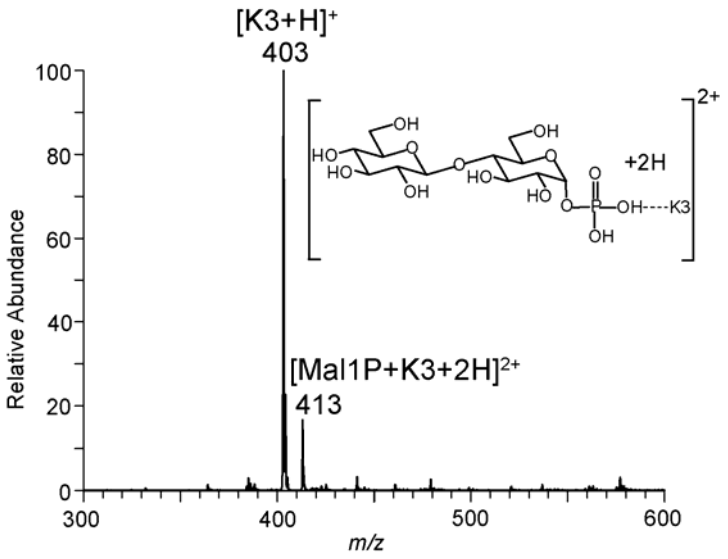

Figure 1. (+) ESI-MS data for the phosphorylated disaccharide maltose-1-phosphate (Mal1P) after the addition of the ion-pairing reagent Lys-Lys-Lys (K3). The spectrum shows two ions, $[K3+H]^+$ and $[Mal1P+K3+2H]^{2+}$.

MS/MS of doubly charged monosaccharide:K3 ion pairs

Owing to the successful application of ion-pairing technique in discriminating mono- phosphorylated and sulfated carbohydrates, we extend its utility in discriminating biologically relevant molecules. To this end, several diphosphorylated and disulfated monosaccharides, along with sulfated and phosphorylated disaccharides were selected (Figure 2). An initial set of experiments was performed to establish whether the characteristic product ions in Table 1 are preserved for diphosphorylated and disulfated monosaccharides, D-glucose-1,6-diphosphate (Glc1,6P) and *N*-acetyl-glucosamine 3,6-disulfate (GlcNAc 3,6S). MS/MS data (Figure 3) show that the mass of doubly charged precursor ions at *m/z* 372 and *m/z* 393 are consistent with the expected mass of the ion pairs $[Glc1,6P+K3+2H]^{2+}$ and $[GlcNAc3,6S+K3+2H]^{2+}$, respectively. Two complementary ions $[Glc1,6P+H]^+$ at *m/z* 341 and $[K3+H]^+$ at *m/z* 403 correspond to the dissociation of the noncovalent

interaction between the carbohydrate and the ion-pairing reagent, K3, in Figure 3A. This ligand dissociation is much more abundant for the phosphorylated complex, compared to the sulfated complex, because the phosphate-peptide

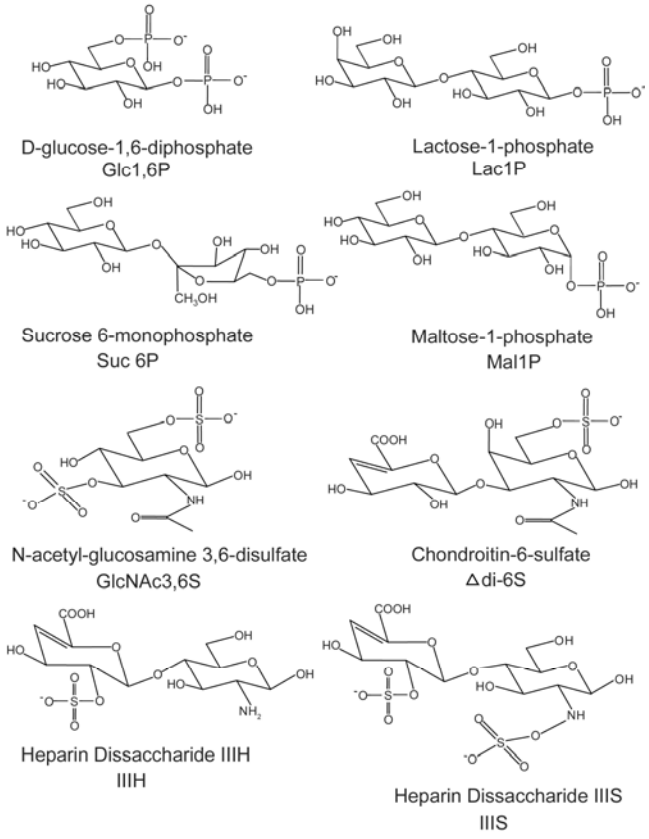

Figure 2. Structures of phosphorylated and sulfated carbohydrates used for the ion-pairing experiments.

interaction is weaker than the sulfate-peptide interaction.[22] As expected, ligand dissociation is the most favorable fragmentation pathway in phosphorylated ion pairs.

In Figure 3B, the ion at *m/z* 353, which originates from oxygen-sulfur bond cleavage, is observed as the base peak. Since sulfated monosaccharide:peptide complex is more stable than the phosphorylated ion pairs, the covalent bond dissociates preferentially compared to the noncovalent bonds.[26] In addition, two

small product ions at *m/z* 384 and *m/z* 403 correspond to the ligand dissociation from the precursor ion. This is due to the presence of the amide group on the sulfated HexNAc (Table 1), facilitating the proton transfer.[22] As a result, the observed abundant characteristic product ions in Figure 3 indicate that ion-pairing is useful in discriminating diphosphorylated and disulfated monosaccharides.

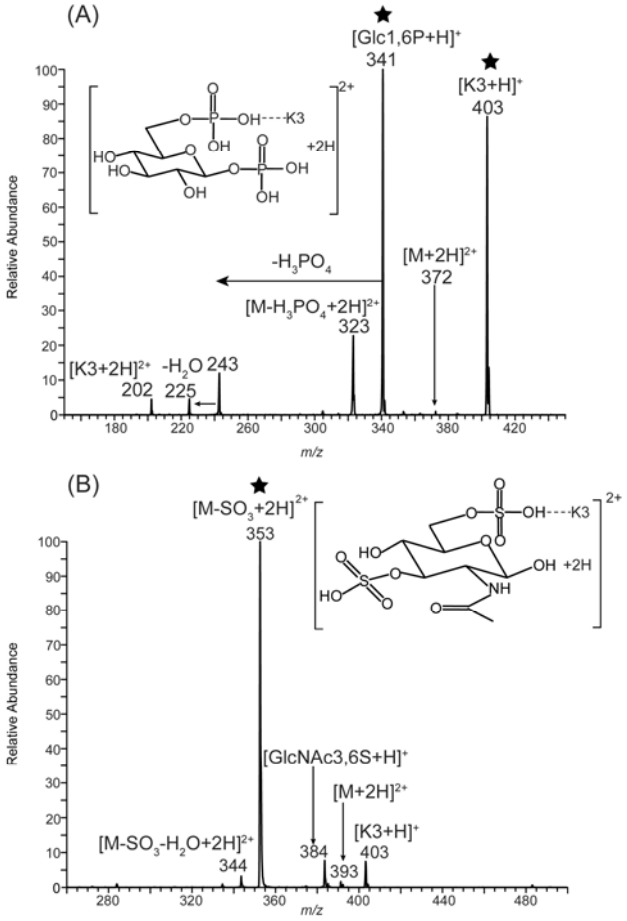

Figure 3. (+) ESI-MS/MS data for the doubly charged diphosphorylated or disulfated ion pairs with Lys-Lys-Lys (K3): A) diphosphorylated monosaccharide complex $[Glc1,6P+K3+2H]^{2+}$ B) disulfated monosaccharide complex $[GlcNAc3,6S+K3+2H]^{2+}$. In (A), the precursor ion underwent the ligand dissociation upon CID, while (B) shows characteristic ions resulting from oxygen-sulfur bond cleavage. Characteristic ions are marked with a star.

MS/MS of doubly charged disaccharide:K3 ion pairs

Aside from the monosaccharides, the ion-pairing approach is also applied to

the structurally more complex disaccharides that are phosphorylated or sulfated. Three phosphorylated disaccharides, maltose-1-phosphate (Mal1P), lactose-1-phosphate (Lac1P), sucrose 6-monophosphate (Suc6P) and three sulfated disaccharides, heparin disaccharide IIIH (IIIH), heparin disaccharide IIIS (IIIS), chondroitin-6-sulfate (∆di-6S) (Figure 2) were complexed with the peptide, K3. MS/MS data of two isomeric phosphorylated disaccharide:peptide ion-pairs (maltose-1-phosphate:K3 and lactose-1-phosphate:K3) in Figure 4 demonstrate that the fragmentation pattern of these two

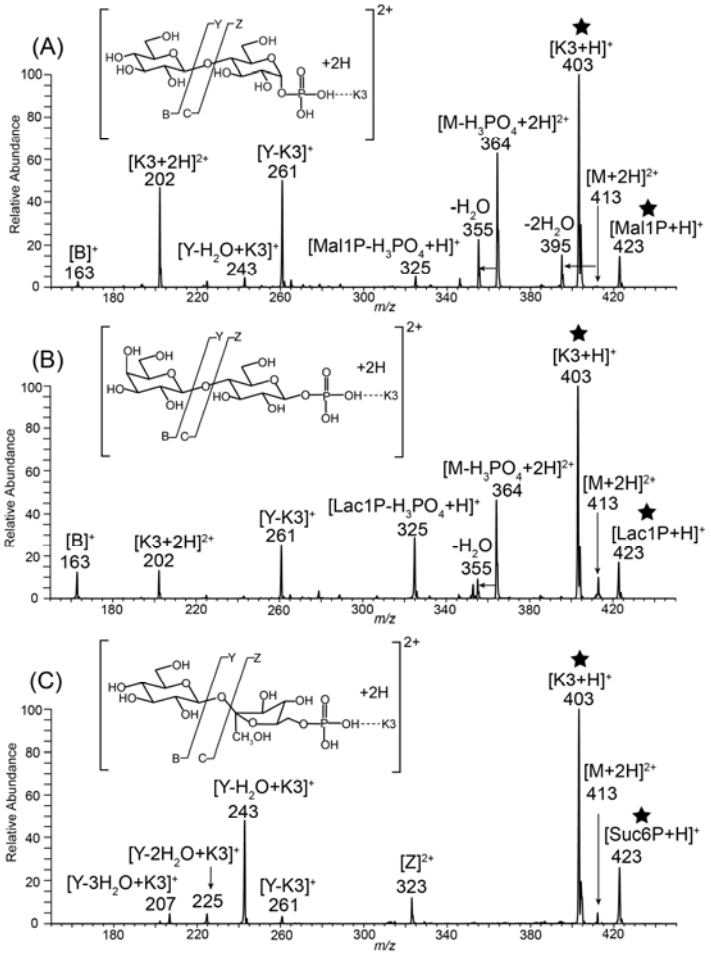

Figure 4. (+) ESI-MS/MS data for the doubly charged phosphorylated ion pairs with Lys-Lys-Lys (K3): A) $[Mal1P+K3+2H]^{2+}$ B) $[Lac1P+K3+2H]^{2+}$ C) $[Suc6P+K3+2H]^{2+}$. As expected, abundant ligand dissociation ions are observed in the CID data, which

are characteristic for phosphorylated carbohydrates. These ions are marked with a star.

structures is similar when the complexes are subjected to CID. In both spectra (Figure 4A and B), the precursor ions at *m/z* 413 correspond to the doubly charged ions, $[Mal1P+K3+2H]^{2+}$ and $[Lac1P+K3+2H]^{2+}$, respectively. Two complementary ions, $[Mal1P+H]^{+}$ (Figure 4A) or $[Lac1P+H]^{+}$ (Figure 4B) at *m/z* 423 and the peptide K3 ion at *m/z* 403, originate from ligand dissociation. Both characteristic ions are consistent with the expected fragmentation trends described in Table 1. Two interesting ions at *m/z* 364 and *m/z* 325 in Figure 4A and B correspond to the loss of H_3PO_4. The loss of H_3PO_4 only occurs when the carbohydrates are phosphorylated at the anomeric carbon.[22] Thus, the loss of H_3PO_4 (98 Da) can be used to identify the position of the phosphate on the structure.[22]

Figure 4C shows the MS/MS data of the doubly charged phosphorylated complex $[Suc6P+K3+2H]^{2+}$. In this spectrum, the parent ion at *m/z* 413 dissociates into two singly charged characteristic ions, the peptide ion (K3, *m/z* 403) and the protonated disaccharide ion (*m/z* 423). All the other product ions are related to the dissociation of the glycosidic bonds and the loss of water. In summary, all the phosphorylated disaccharide complexes dissociated according to the fragmentation trends that were established based on the dissociations of phosphorylated monosaccharide/ion-pair complexes.

The fragmentation of the sulfated disaccharide:peptide ion-pairs was also investigated, employing the same collisional dissociation (Figure 5). For the doubly charged complex $[IIIH+K3+2H]^{2+}$ in Figure 5A, the singly charged ion at *m/z* 338 corresponds to the characteristic ion resulting from oxygen-sulfur bond cleavage. Due to the presence of the amine group in the structure of IIIH, two complementary

ions, the singly charged peptide ion at *m/z* 403 and the protonated disaccharide ion at *m/z* 418, were observed (Table 1).

Figure 5B shows the MS/MS data of the doubly charged ion-pair complex $[IIIS+K3+2H]^{2+}$, at *m/z* 450.4. Four characteristic ions at *m/z* 338.0, 417.8, 483.0, and the base peak ion at *m/z* 410.6 originate from oxygen-sulfur bond cleavage. With an amine group present in the carbohydrate portion of the ion-pair complex, the complementary ions, singly charged peptide $[K3+H]^+$ and protonated disaccharide $[IIIS+H]^+$, should be observed. The peptide ion is observed at *m/z* 403.2, but an ion corresponding to $[IIIS+H]^+$ is not present in the spectrum. Since the peptide ion is observed, the dissociation reaction obviously occurs, but the ion corresponding to $[IIIS+H]^+$ probably dissociates by undergoing loss of SO_3, producing the secondary ion at *m/z* 417.8.

In the MS/MS data of the ion pair complex $[\Delta di\text{-}6S +K3+2H]^{2+}$ in Figure 5C, the observed characteristic ion is *m/z* 380, which originates from oxygen-sulfur bond cleavage. Also, the expected singly charged ions, protonated sulfated disaccharide $[\Delta di\text{-}6S +H]^+$ (*m/z* 460) and the singly charged peptide ion $[K3+H]^+$ (*m/z* 403), are present. Thus, from these results it is apparent that the ion-pairing approach in combination with MS/MS experiments can be used to identify the phosphorylation and sulfation on doubly charged mono-and disaccharides. The characteristic product ions are useful in characterizing the acidic functional groups present on carbohydrates.

Table 1. Characteristic product ions used to differentiate phosphate and sulfate in monosaccharides

	Doubly charged ion pairs				Singly charged ion pairs
	$[Hexose+K3+2H]^{2+}$		$[HexNAc+K3+2H]^{2+}$		$[Carbohydrates+K3+H]^{+}$
Observed Reaction Pathways	Oxygen-sulfur (or oxygen-phosphorus) bond cleavage	Ligand dissociation	Oxygen-sulfur (or oxygen-phosphorous) bond cleavage	Ligand dissociation	Ligand dissociation
Sulfate	yes	no	yes	yes*	no
Phosphate	no	yes	no	yes	yes

*: Ligand dissociation in sulfated HexNAcs is caused by the amine group on the carbohydrate.

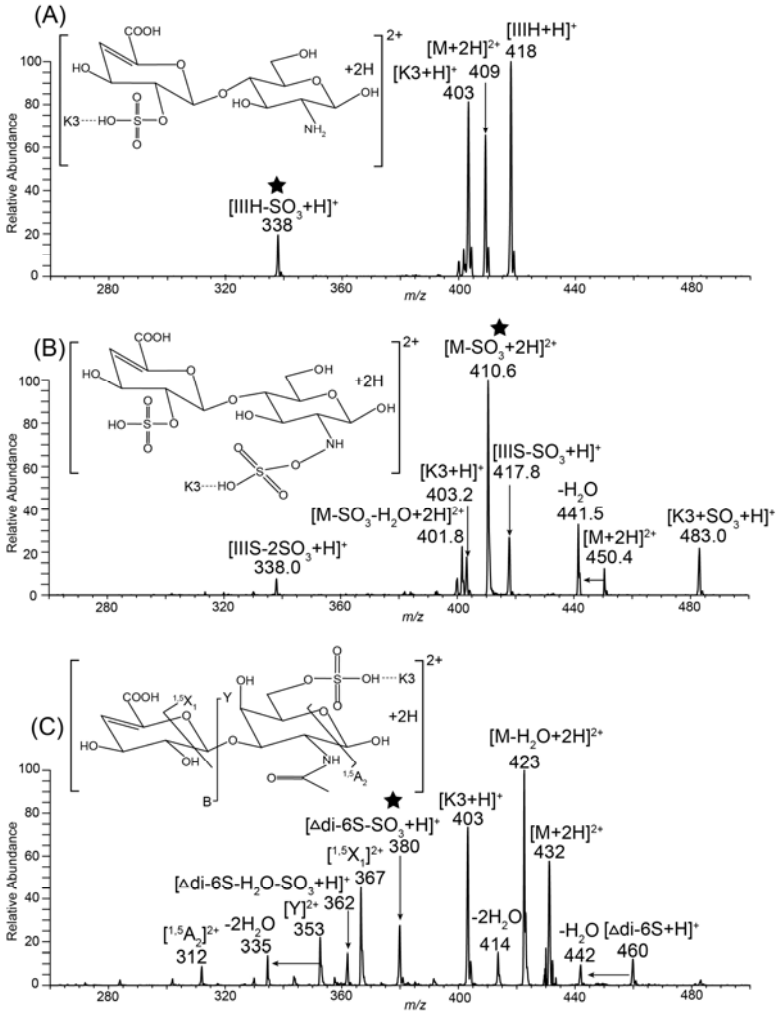

Figure 5. (+) ESI-MS/MS data for the doubly charged sulfated ion pairs with Lys-Lys-Lys (K3): A) $[IIIH+K3+2H]^{2+}$ B) $[IIIS+K3+2H]^{2+}$ C) $[\Delta di\text{-}6S+K3+2H]^{2+}$ As expected, the spectrum shows characteristic ions resulting from oxygen-sulfur bond cleavage. These ions are marked with a star.

Biological application

To test the efficacy of using the ion-pairing approach in identifying functional groups on larger biomolecules, a highly sulfated glycoprotein hormone oLHα (ovine luteinizing hormone, alpha subunit) was used as a test case. In a previous study, the ion pairing approach was used to enhance the signal of mono-, di-sulfated glycopeptides from this protein.[23] Sulfated ion pairs can be readily observed in the

ESI-MS analysis when adding the peptide K3 to the complex mixture.[23] This is because the peptide K3 suppresses the signal of neutral glycopeptides to facilitate the detection of sulfated glycoforms.[23] In this study, these glycopeptides are complexed with the peptide, K3, to demonstrate that the presence of sulfation on the structure can be confirmed by the ion-pairing method.

Four sulfated glycopeptides, which are present in the glycoprotein and contain different types of glycans, were selectively ion-paired with K3, and they formed abundant ion-pairing complexes at *m/z* 1065.4, *m/z* 1165.7, *m/z* 1227.3, and *m/z* 1146.3. The structures of the glycopeptides appear in Figure 6. To confirm that these glycopeptides contain sulfate and not phosphate, the ion-pairing complexes were subjected to CID experiments. MS/MS data of one of the precursor ions at *m/z* 1065.4 is shown in Figure 6A. The base peak (*m/z* 1645.5) is an ion originating from oxygen-sulfur bond cleavage; this peak confirms that this glycopeptide is sulfated. Also, the ion at *m/z* 483.3 corresponding to $[K3+SO_3+H]^+$ provides the additional evidence for the functional group's assignment. The complementary ions, singly charged K3 (*m/z* 403.3) and $[M+H-K3]^+$ (*m/z* 1725.73), are also expected. These ions correspond to dissociation of the noncovalent complex, and they are expected for sulfated HexNAc's.[22]

The other three glycopeptides (Figure 6B, 6C, and 6D) also dissociated to produce the product ions that correspond to oxygen-sulfur bond cleavage. These ions are at *m/z* 1848.2 (Figure 6B), *m/z* 1969.3 (Figure 6C), and *m/z* 1807.4 (Figure 6D). This implies that all of these glycopeptides are sulfated, which is consistent with the results obtained from radiolabelling.[14,15] The ion at *m/z* 403, corresponding to the peptide ion $[K3+H]^+$, is apparent on the spectrum of these glycopeptides. This ion

indicates that the ion pairing complexes also undergo ligand dissociation, which is expected for sulfated HexNAc's. Hence, the ion-pairing approach is useful to identify the modifications in complex biomolecules.

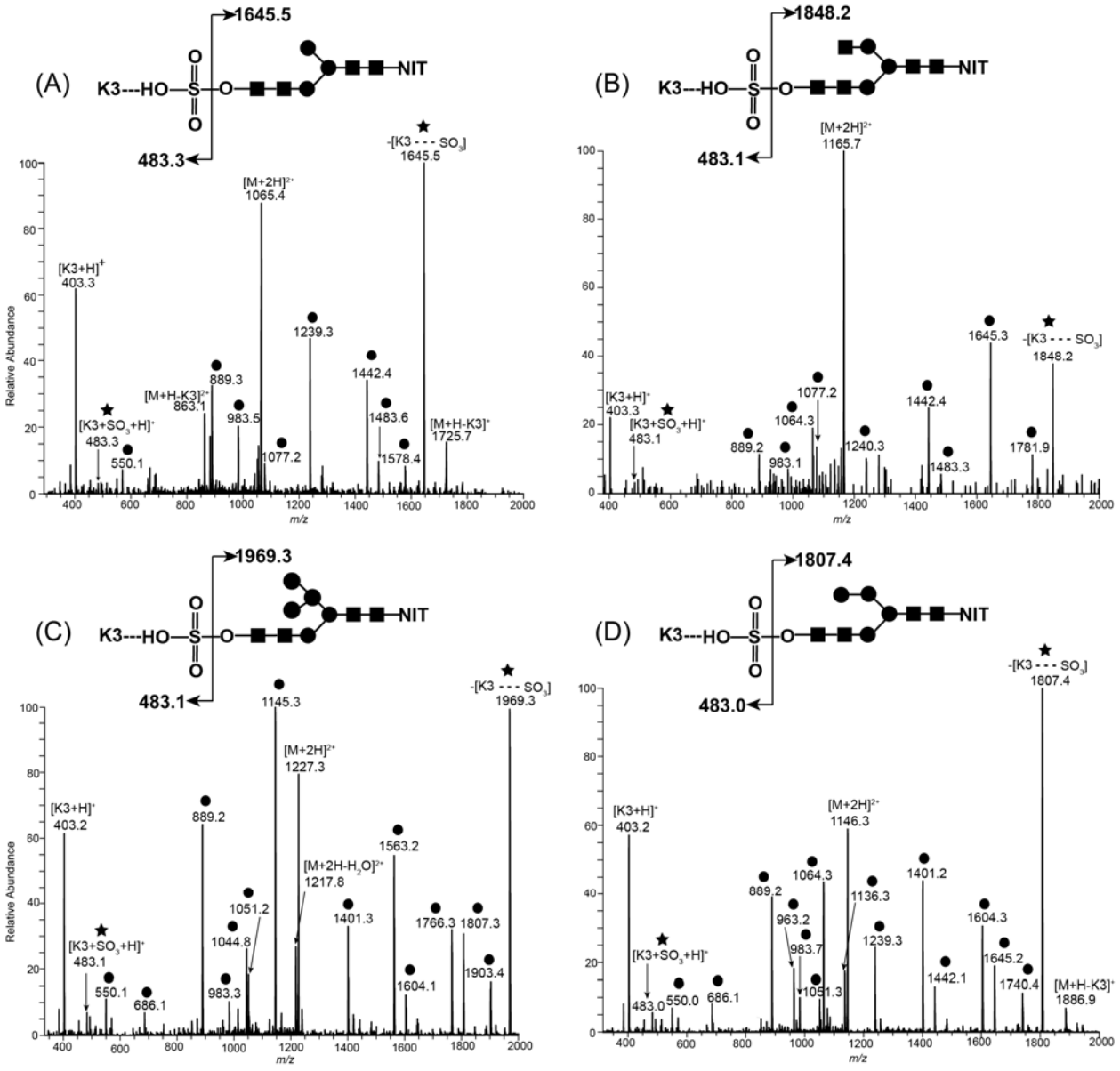

Figure 6. (+) ESI-MS/MS data for the doubly charged ion-pair complexes of glycopeptides from oLHα with Lys-Lys-Lys (K3): The characteristic ions marked with a star confirm that the glycopeptides are sulfated. The ions marked with a circle represent the ions that originated from glycosidic bond cleavage.

3.4 Conclusions

The differentiation between phosphorylation and sulfation on monosaccharides, disaccharides, and glycopeptides is accomplished using ion-pairing in combination with MS/MS experiments. The characteristic product ions of ion-pairing complexes are applicable in identifying the modification of larger biomolecules, such as glycopeptide mixtures obtained from ovine luteinizing hormone proteolytic digest. This is the first example of applying ion-pairing in discriminating the presence of phosphates and sulfates in complex biomolecules. This approach also has the added advantages of enhancing the signal of acidic functional groups in complex biological mixtures [23] as well as elucidating the structure of carbohydrate moiety of glycopeptides.[24] Therefore, this sulfate/phosphate discrimination strategy can be successfully incorporated into a single synergistic approach that can be used to structurally characterize phosphorylated or sulfated glycoproteins, without any separation or enrichment of the samples prior to analysis.

Acknowledgements

The authors acknowledge the NIH for funding (project number 1 P20 RR17708-01 and RO1GM077266)

3.5 References

1. Siegel, M.M.; Tabei, K.; Kagan, M.Z.; Vlahov, I.R.; Hileman, R.E.; Linhardt, R.J. Polysulfated carbohydrates analyzed as ion-paired complexes with basic peptides and proteins using electrospray negative ionization mass spectrometry. *J Mass Spectrom.* **1997,** *32,* 760-772.

2. Mann, M.; Ong, S.; Gronborg, M.; Steen, H.; Jensen, O.N.; Pandey, A. Analysis of protein phosphorylation using mass spectrometry: deciphering the phosphoproteome. *Trends Biotechnol.* **2002,** *20,* 261-268.

3. Rappsilber, J.; Steen, H.; Mann, M. Labile sulfogroup allows differentiation of sulfotyrosine and phosphortyrosin in peptides. *J. Mass. Spectrom.* **2001,** *36,* 832-833.

4. Hunter, T. The croonian lecture 1997. The phosphorylation of proteins on tyrosine: its role in cell growth and disease*. Phil. Trans. R. Lond. B.* **1998,** *353,* 583-605.

5. Huttner, W.B. Protein tyrosine sulfation. *Trends Biochem. Sci.* **1987,** *12,* 361-363.

6. Delcommenne, M.; Kannagi, R.; Johnson, P. TNF-α increases the carbohydrate sulfation of CD44: induction of 6-sulfo N-acetyl lactosamine on N- and O-linked glycans. *Glycobiology* **2002,** *12,* 613-622.

7. Bai, X.; Brown, J.R.; Varki, A.; Esko, J.D. Enhanced 3-O-sulfation of galactose in Asn-linked glycans and Macckia amurenesis lectin binding in a new Chinese hamster ovary cell line. *Glycobiology* **2001,** *11,* 621-632.

8. Xiong, L.; Andrews,D.; Regnier, F. Comparative proteomics of glycoproteins based on lectin selection and isotope coding. *J. Proteome Res.* **2003,** *2,* 618-625.

9. Sleat, D.E.; Sohar, I.; Pullarkat, P.S.; Lobel, P.; Pullarkat, R.K. Specific alterations in levels of mannose-6-phosphorylated glycoprotiens in different neuronal ceroid lipofuscinoses. *Biochem. J.* **1998**, *334,* 547-551.

10. Lobel, P.; Karel, R. Assay for glycoproteins containing mannose-6-phosphate. PCT Int. Appl. **1997,** 60pp.

11. Harvey, D.J. Structural determination of N-linked glycans by matrix-assisted laser desorption/ionization and electrospray ionization mass spectrometry*. Proteomics.* **2005,** *5,* 1774-1786.

12. Harvey, D.J. Fragmentation of negative ions from carbohydrates: part 1. use of nitrate and other anionic adducts for the production of negative ion electrospray spectra from N-linked carbohydrates. *J. Am. Soc. Mass Spectrom.* **2005,** *16,* 622-630.

13. Wheeler, S.F.; Harvey, D.J. Extension of the in-gel release method for structural analysis of neutral and sialylated N-linked glycans to the analysis of sulfated glycans: application to the glycans from bovine thyroid-stimulating hormone. *Anal. Biochem.* **2001,** *296,* 92-100.

14. Green, E.D.; Baenziger, J.U. Asparagine-linked oligosaccharides on lutropin, follitropin, and tyrotropin. I. Structure elucidation of the sulfated and sialylated

oligosaccharides on bovine, ovine, and human pituitary glycoprotein hormones. *J. Biol. Chem.* **1988,** *263,* 25-35.

15. Green, E.D.; Baenziger, J.U. Asparagine-linked oligosaccharides on lutropin, follitropin, and tryrotropin. II. Distributions of sulfated and sialylated oligosaccharides on bovine, ovine, and human pituitary glycoprotein hormones. *J. Biol. Chem.* **1988,** *263,* 36-44.

16. Chen, S.L.; Huddleston, M.J.; Shou, W.; Deshaies, R.J.; Annan, R.S.; Carr, S.A. Mass spectrometry-based methods for phosphorylation site mapping of hyperphosphorylated proteins applied to Net1, a regulator of exit from mitosis in yeast. *Mol. Cell Proteomics.* **2002,** *1,* 186-196.

17. Annan, R.S.; Carr, S.A. Phosphopeptide analysis by matrix-assisted laser desorption time-of-flight mass spectrometry. *Anal.Chem.* **1996,** *68,* 3413-3421.

18. Oda, Y.; Nagasu, T.; Chait, B.T. Enrichment analysis of phosphorylated proteins as a tool for probing the phosphoproteome. *Nat. Biotechnol.* **2001,** *19,* 379-382.

19. Bossio, R.E.; Marshall, A.G. Baseline resolution of isobaric phosphorylated and sulfated peptides and nucleotides by electrospray ionization FTICR MS: another step toward mass spectrometry-based proteomics. *Anal. Chem.* **2002,** *74,* 1647-1679.

20. Petzold, C.J.; Leavell, M.D.; Leary, J.A. Sreening and identification of acidic carbohydrates in bovine colostrum by using ion/molecule reactions and Fourier transform ion cyclotron resonance mass spectrometry: specific toward phosphorylated complexes. *Anal. Chem.* **2004,** *76,* 203-210.

21. Harvey, D.J.; Bousfield, G.R. Differentiation between sulphated and phosphated carbohydrates in low-resolution matrix-assisted laser desorption/ionization mass spectra. *Rapid Commun. Mass Spectrom.* **2005,** *19,* 287-288.

22. Zhang, Y.; Go, E.P.; Jiang, H.; Desaire, H. A novel mass spectrometric method to distinguish isobaric monosaccharides that are phosphorylated or sulfated using ion-pairing reagents. *J. Am. Soc. Mass Spectrom.* **2005,** *16,* 1827-1839.

23. Jiang, H.; Irungu, J.; Desaire, H. Enhanced detection of sulfated glycosylation sites in glycoproteins. *J. Am. Soc. Mass Spectrom.* **2005,** *16,* 340-348.

24. Irungu, J.; Dalpathado, D.S.; Go, E.P.; Jiang, H.; Ha, H.; Bousfield, G.R.; Desaire, H. Method for characterizing sulfated glycoproteins in a glycosylation site-specific fashion, using ion pairing and tandem mass spectrometry. *Anal. Chem.* **2006,** *78,*1181-1190.

25. Jiang, H.; Butnev, V.Y.; Bousfield, G.R.; Desaire, H. Glycoprotein profiling by electrospray mass spectrometry. *J. Am. Soc. Mass Spectrom.* **2004,** *15,* 750-758.

26. Loo, J.A. Studying noncovalent protein complexes by electrospray ionization mass spectrometry. *Mass Spectrom. Rev.* **1997,** *16,* 1-23.

Chapter IV

Maximizing coverage of glycosylation heterogeneity in MALDI-MS analysis of glycoproteins with up to 27 glycosylation sites

"Maximizing coverage of glycosylation heterogeneity in MALDI-MS analysis of glycoproteins with up to 27 glycosylation sites" by Zhang, Y.; Go, E.P.; Desaire, H. Submitted to Analytical Chemistry.

4.1 Introduction

Protein glycosylation is one of the essential post-translational modifications (PTMs), and it is involved in various biological processes.[34-37, 39, 46, 58] Glycosylation can modify protein properties such as stability, solubility,[34-38, 45] the protein's binding affinity to the other biomolecules,[34-38] and it can also affect inter-, intra-cell signaling.[34-38, 59] Studying glycosylation is important because most proteins secreted from tissues are glycosylated and many plasma protein biomarkers are also glycosylated.[45, 60, 61] Alteration in the glycan structures or pattern on glycoproteins has been implicated in several disease states, such as cancer,[46, 58, 61] Alzheimer's disease,[48] rheumatoid arthritis,[50] and chronic obstructive pulmonary disease,[62] etc. Therefore, characterizing the glycans and monitoring the changes of glycan profiles are important to elucidate their biological significance and discern their roles in the disease process. However, the global mapping and comprehensive analysis of glycosylation remains a challenging task due to heterogeneous populations of glycans present on glycoproteins.[54] As a result, maximizing the coverage of glycosylation heterogeneity on glycoproteins is important, especially for the biological variants that typically occur at low abundance.[54]

There are two basic approaches to analyzing glycosylation on proteins, either cleaving the glycans or analyzing glycopeptides. For glycan analysis, several analytical methodologies have been employed, such as high performance anion-

exchange chromatography (HPAEC),[63] capillary electrophoresis (CE),[64] ^{1}H nuclear magnetic resonance spectroscopy (^{1}H NMR)[63], microarray construction,[65] and mass spectrometry[34, 38, 39, 66-68]. These techniques involve enzymatic or chemical release of glycans from glycoproteins, followed by a separation method then detection. Although these approaches have advantages to distinguish between isomeric structures, glycosylation site-specific information is lost, unless the glycosylation sites are separated prior to glycan release.[69]

Mass spectrometry can also provide glycosylation site-specific information by conducting glycopeptide-based analysis,[46, 49, 58, 61, 70-74] wherein the glycan and its attachment site to the protein can be elucidated in the same experiment.[74] This glycosylation site-specific information is useful in elucidating functional properties of glycoprotein.[74] Typically, glycopeptide-based MS analysis entails enzymatic cleavage of glycoproteins with an endoprotease, followed by a separation technique and mass analysis. Due to the high degree of heterogeneity of glycans on glycopeptides, the mass spectral signals of glycopeptides are suppressed by the strongly ionizing peptides, when both species co-exist in the complex mixture.[39, 45, 51, 58] As a result, separation and/or enrichment approaches are usually employed to isolate and detect glycopeptides in proteolytic digests.

At present, several chromatographic and/or enrichment methods have been used for glycopeptide-based MS analysis, including reverse-phase HPLC fractionation,[75, 76] lectin-based affinity chromatography,[70, 71] and hydrophilic affinity methods that use porous graphitized carbon [45], carbohydrate-based resins, [46, 74] and hydrophilic interaction liquid chromatography,[72, 77] etc. Among these methods, reverse phase HPLC coupled with electrospray ionization (ESI) mass spectrometry

has been widely used.[75, 76] Lectin–based affinity chromatography is another prevalent approach to isolate and detect the glycopeptides. This method relies on the binding specificity of glycan structures,[74, 78, 79] hence, the glycopeptide profile of the enriched fraction is dictated by the type of lectin column used for the enrichment.[74] The recent introduction of hydrophilic affinity methods have provided a promising approach to isolate glycopeptides by taking advantage of the hydrophilic interactions between the glycans and resin materials,[77] thereby, revealing the glycan profiles on glycoproteins. Although all of these separation and/or enrichment approaches have been utilized to improve the glycopeptide detection in the complex digest mixtures, there is no consensus in the field as to which sample separation/enrichment approaches best maximize coverage of glycosylation heterogeneity.

Herein, we present an in-depth study of maximizing glycosylation coverage in terms of the number of glycosylation sites detected and their corresponding glycoforms, by optimizing all the experimental steps in the glycopeptide-based analysis, including sample preparative approaches, mass spectral techniques, and data analysis strategies. Specifically, for sample preparation, a comparative analysis has been performed on several approaches, such as reverse phase HPLC fractionation, lectin-based affinity enrichment, and hydrophilic affinity method using carbohydrate-based resin beads – Sepharose®. All preparation methods are performed in combination with MALDI-TOF/TOF mass spectrometry, to determine an efficient approach for maximizing glycosylation coverage in glycan profiling. MALDI mass spectrometry was the chosen detection method due to its simplicity, speed, high sensitivity, and selectivity.[34, 38, 67, 68]

Three well-characterized glycoproteins that include immunoglobulin G (IgG),

transferrin, and α1-acid glycoprotein (AGP) were used as model glycoproteins in this study. These glycoproteins vary in terms of the number of glycosylation sites (from one to five) and the diversity in their glycan profiles, from mainly neutral glycans (IgG) to highly sialylated glycans (transferrin, AGP). Based on comparative analysis of sample preparation approaches, the efficacy of each sample preparative method is evaluated and the pros and cons for each method are described.

In addition to addressing the issue of which sample preparation method best enhances glycosylation coverage, several other approaches are implemented in our comprehensive strategy of increasing glycosylation coverage. To optimize mass spectral signal of the glycopeptides, MALDI analysis was performed in both positive and negative ion mode to obtain the maximum glycan profiles for each glycoprotein. To increase the number of assigned peaks in the mass spectra, methods were implemented that identify glycopeptides that contain modifications on peptide moieties ─ such as conversion of an N-terminal glutamine into pyroglutamic acid, and deamination of alkylated cysteines on N-terminus. This was accomplished by enhancing the functionality of GlycoPep DB,[80] a publicly available data analysis tool, built and administered by our research group, and used for all the data analysis completed in this study.

Finally, PNGase F was used to cleave off the glycans in order to enhance glycosylation site coverage. Upon releasing the glycans from glycopeptides, the peptide moiety bearing the glycosylation site can be detected. This is useful because sometimes the presence of weakly ionizing glycopeptides cannot be detected when they co-elute with more strongly ionizing species; so cleaving the glycans off allows for the detection of the peptides that were glycosylated. While the glycan moieties

themselves are not identified in this technique, data about glycosylation site occupancy is obtained, which is another important aspect of maximizing glycosylation coverage on glycoproteins.

As a demonstration of the effectiveness of the comprehensive approach we developed, the strategies were applied to the very heavily glycosylated HIV envelope protein — JR-FL gp140 ΔCF, which contains 27 potential glycosylation sites.[81] By optimizing each experimental step in glycopeptide-based analysis, over 85% glycosylation coverage was achieved on JR-FL. This study demonstrates that our strategies significantly improve the glycopeptide detection and maximize coverage of glycosylation heterogeneity on glycoproteins.

4.2 Experimental Section

Materials and reagents

Human serum glycoproteins (IgG, transferrin, AGP), PNGase F from *Elizabethkingia meningosepticum*, urea, dithiothreitol (DTT), iodoacetamide (IAA), acetonitrile, sodium phosphate, sodium chloride, formic acid, trifluoroacetic acid (TFA), Trizma hydrochloride, Trizma base, ammonium bicarbonate, *N*-acetyl-D-glucosamine, 2,5-dihydroxybenzoic acid (DHB), α-cyano-4-hydroxycinnamic acid (CHCA), and Sepharose® CL-4B were all purchased from Sigma (St. Louis, MO). The HIV envelope glycoprotein JR-FL gp140 ΔCF was expressed and purified in the laboratory of Dr. Barton F. Haynes, Duke Human Vaccine Research Institute (Durham, NC), using the method described in liturature[81]. Concanavilin A (ConA) TopTips® and hypercarb NuTips® were purchased from Glygen Corp (Columbia, MD). Proteomics grade trypsin was obtained from Promega (Madison, WI). Milli-Q

water was obtained from a Millipore filtration system (Billerica, MA).

Glycoprotein digestion

Glycoproteins (100 µg-1mg) were dissolved in 100 µL of 100 mM Tris-HCl buffer with 6M urea, pH 8.0. Protein samples were reduced with 15 mM DTT and alkylated with 25 mM IAA in dark for 1 hour at ambient temperature, respectively. Excess IAA was removed with the addition of DTT. Prior to adding trypsin, the solution was diluted to less than 1M urea. Typsin was added at an enzyme-to-substrate ratio of 1:30 (w/w). The solution was incubated overnight at 37 °C and was stopped by the addition of 1 µL concentrated acetic acid.

Hydrophilic affinity method for glycopeptide enrichment

This method follows a literature protocol[3, 27] with slight modification, which optimizes glycopeptide detection. About 200 µg of the digest was added to a microcentrifuge tube packed with 20 µL Sepharose®. Then 1 mL of organic solvent mixture containing butanol:ethanol:water (5:1:1 by volume) was added to the digest: Sepharose® mixture. The resulting mixture was gently mixed for 45 min and then centrifuged for 5 min. The supernatant was removed and the pellet was washed twice with the same organic solvent. The glycopeptides were extracted by incubating the pellet in 1 mL ethanol:water (1:1 v/v) for 45 min. The samples were vortexed then centrifuged and the supernatant was transferred to another microcentrifuge tube. The same extraction procedure was repeated twice. The combined supernatant was completely dried in the Labconco centrivap cold trap (Kansas City, MO) and reconstituted with 100 µL of deionized water prior to MALDI analysis or HPLC fractionation.

Lectin affinity method for glycopeptide enrichment

Con A packed TopTips® and hypercarb NuTips® were utilized according to the protocol recommended by the manufacturer. Briefly, Con A packed TopTips® were conditioned by adding 50 µL of loading buffer, 100 mM Na_3PO_4, 0.2M NaCl, pH 7.0. Approximately 50 µL of digest mixture was loaded on the Con A packed bed. The eluate was reloaded 5 times. The packed bed was washed with 50 µL of washing buffer, 50 mM Na_3PO_4, 0.2M NaCl pH 7.0, for 2-3 times. The sample was eluted by the addition of elution buffer, 0.3M *N*-acetyl-D-glucosamine in 50 mM Na_3PO_4, 0.2M NaCl, pH 7.0. The same sample releasing procedure was repeated 3 times. The combined eluates were concentrated to 20 µL in the Labconco centrivap cold trap (Kansas City, MO) and desalted using hypercarb NuTips®.

Desalting by hypercarb NuTips®

Before loading the sample, the hypercarb NuTips® were conditioned by aspirating 20 µL of the releasing solution, 40% acetonitrile with 0.05% TFA, followed by the binding solution, water with 0.05% TFA. The concentrated eluate from Con A packed TopTips® were loaded on the hypercarb NuTips® by aspirating 50 times to allow the maximum absorption. Then the hypercarb NuTips® were washed with 20 µL binding solution ~10 times, and the samples were eluted by expelling the releasing solution ~50 times. The same releasing procedure was repeated 3 times. Then the combined eluate was evaporated to 10 µL prior to MALDI analysis.

Reverse phase HPLC fractionation

The tryptic digest mixtures were desalted and separated on a Shimadzu HPLC system. The mobile phase A was water with 0.1% formic acid. Mobile phase B was acetonitrile with 0.1% formic acid. About 20 µL of the sample was injected and separated on a C18 column (150×4.6mm, 5 µM, Alltech, Deerfield, IL) with flow rate

1mL/min at 40 °C. The fractions were collected every minute manually. Since each glycoprotein has different glycan structures and peptide sequences, different gradients were used to optimize the separation. Human IgG: initial conditions were 5% B for 3 min, followed by a linear gradient to 40% B by 15 min, maintaining 40% B for another 15 min, then ramped to 85% B by 60 min. Human transferrin and JR-FL gp140 ΔCF: the gradient was started with 1% B and a linear gradient to 40% B was achieved in 50 min, then ramped to 90% B in 60 min.[82] Human AGP: the column was equilibrated at 5% B for 3 min. A linear gradient to 20% B in 10 min were achieved, followed by 40% B in 60 min, then up to 100% B in 64 min.[58] The collected fractions were dried on centrivap and reconstituted with 10 µL water, prior to MALDI analysis.

Deglycosylation of tryptic glycopeptides by PNGase F

PNGase F enzyme solution (≥ 500 units/mL) was prepared by adding 100 µL water into the sample vial of 50 units. Each glycopeptide fraction collected from HPLC fractionation was reconstituted with 25 µL of 20 mM ammonium bicarbonate buffer, pH 8.0, and treated with 2 – 4 µL of PNGase F for 3 hours at 37 °C. The reaction was stopped by heating to 100 °C for 10 minutes and the sample was directly spotted on the MALDI target plate.

MALDI-TOF analysis and data interpretation

The matrix used in MALDI analysis was the combination of DHB and CHCA. DHB and CHCA were initially dissolved in 70% ACN/ H_2O to the final concentration of 20 mg/mL, respectively. The matrix was prepared by mixing DHB and CHCA (1:1 V/V). The sample was mixed with the matrix solution (1:1 V/V) and 1.5 µL was spotted on a stainless steel MALDI target plate (Applied Biosystems, Foster City, CA) and air-dried. MS and MS/MS spectra were acquired on an Applied Biosystems

4700 proteomics analyzer. The samples were irradiated by a 355 nm Nd-YAG laser at 200 Hz. The acceleration voltage was 25 kV. Each mass spectrum was generated by averaging 3000 laser shots. In the positive ion mode, the instrument was operated in the reflectron mode. In the negative ion mode, the spectra were obtained in the linear mode. All the data were processed in Data Explorer version 4.5 (Applied Biosystems).

The glycopeptide composition was assigned by using a glycopeptide web-based tool (Glycopep DB).[80] The primary sequence of two glycoproteins human IgG (accession number AAA02914) and transferrin (accession number NP_001054) were obtained from National Center for Biotechnology Information (NCBI). The peptide sequence of human AGP (accession number P02763) and JRFL gp 140 ΔCF was obtained from Swiss-Prot and the literature,[81] respectively. Theoretical tryptic digest peptide sequences containing glycosylation sites were determined from a home-built glycopeptide database (Glycopep ID) by inputting primary sequence of the glycoproteins.[83] MALDI-MS/MS data were used to confirm both peptide and glycan compositions of glycopeptides from the tryptic digest. Specifically, peptide composition was identified by two characteristic ions in the MALDI-MS/MS spectrum, $^{0,2}X$ ([peptide+83+H]$^+$) and $Y_{1\alpha}$ ([peptide+HexNAc+H]$^+$)[71], corresponding to a cross-ring cleavage and a glycosidic cleavage, respectively. The peptide composition was also confirmed by internal ions observed on MS/MS spectra and deglycosylation of glycopeptide HPLC fractions using PNGase F. Glycan composition was initially assigned by using the glycopeptide web-based tool (GlycoPep DB)[80] and further confirmed with MALDI-MS/MS data.

4.3 Results and Discussion

Overview of the analytical protocols

Aiming to determine the best strategy in maximizing glycosylation coverage on the glycoproteins, and subsequently, heavily glycosylated proteins like the HIV glycoprotein *env*, all the aspects of the glycopeptide-based analysis, such as sample preparation, mass spectral techniques and data analysis, have been optimized for each glycoprotein used in this study. Specifically, for optimizing the sample preparation approaches, a systematic comparison was conducted on reverse phase HPLC fractionation, lectin-based affinity, and hydrophilic affinity methods. Each method was evaluated in terms of the number of glycosylation sites detected and the glycopeptide coverage on three model glycoproteins. Figure 1 provides the experimental template used in this study. Model glycoproteins were first subjected to proteolytic digestion followed by either HPLC fractionation or/and enrichment methods prior to MALDI-MS analysis. To facilitate the data analysis, model glycoproteins were digested with trypsin. All three methods were initially applied to IgG, which contains one glycosylation site and a corresponding N-linked glycosylation profile consisting of mainly neutral glycans. Since no sialylated glycopeptides were detected on human IgG in the negative ion mode, the MALDI-MS data presented only includes analysis in the positive mode for this protein. After assessing the differences between glycopeptide enrichment methods using IgG, the applicability of each method was determined for acidic glycoproteins with two (transferrin) and five (AGP) glycosylation sites.

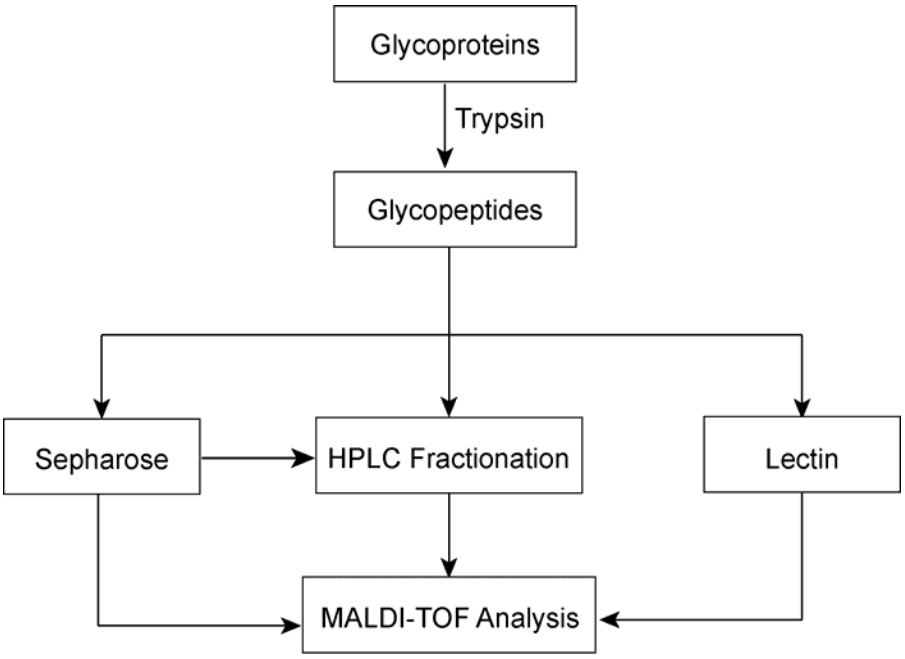

Figure 1. Analytical protocols used to separate or/and enrich glycopeptides of model glycoproteins.

Comparison of three sample preparation methods on human IgG

a) Hydrophilic affinity method using Sepharose®

The hydrophilic affinity enrichment approach used to separate glycopeptides from proteolytic digest relies on the hydrogen bonding interaction between the glycans of glycopeptides and the carbohydrates on the resin material – Sepharose®.[46, 74] This interaction is sufficient to bind glycopeptides allowing facile extraction of glycopeptides from the complex digest mixture. (+) MALDI-MS analysis of the glycopeptide enriched sample of IgG with Sepharose® in Figure 2A shows the glycopeptide profile of glycosylation site (Asn^{326}) on the C_H^2 region of heavy chain. Seven glycan structures were observed and mainly consist of core fucosylated biantennary complex structures with or without a bisecting *N*-acetylglucosamine, consistent with the structures reported

in literature.[84] In addition to heterogeneity in the glycosylation, heterogeneity in the peptide portion was also observed. Two peptide sequences encompassing the same glycosylation site, corresponding to EEQYNSTYR and EEQFNSTFR, were detected.

b) Lectin affinity isolation using Concanavalin A (Con A) TopTips®

Lectins are plant proteins with binding specificities for specific glycan structures.[71, 85] Among the ten known types of lectins, Con A is one of the commonly used lectins for glycoprotein enrichment.[71, 85] Con A selectively binds to N-linked hybrid, high-mannose, or biantennary complex type glycans.[71, 86] In this experiment, Con A TopTips® were used for the selective enrichment of IgG glycopeptides; see Figure 2B. Glycopeptides observed in (+) MALDI-MS measurement of the lectin enriched samples contain glycans with biantennary complex type and high mannose structures. Particularly, the glycopeptide peak observed at *m/z* 2892.0605 corresponds to the high mannose glycan structure. Compared with the (+) MALDI-MS data in Figure 2A, only a small portion of glycopeptides with a bisecting *N*-acetyl-glucosamine were observed in Figure 2B because these glycopeptides have low affinity for Con A.[46] Specifically, four glycopeptide peaks at *m/z* 2805, 2837, 2967, and 2999 observed in Figure 2A are corresponding to the glycopeptides with a bisecting *N*-acetyl-glucosamine. While only two peaks at *m/z* 2805, and 2967 arising from glycopeptides with a bisecting *N*-acetyl-glucosamine are present in Figure 2B. Using this sample preparation method, MALDI-MS measurement generated glycopeptides with six glycan structures consisting of fucosylated and non-fucosylated biantennary complex type with or without a bisecting *N*-acetyl-glucosamine and one high mannose glycan structure. Since Con A binds to glycoproteins with specific glycan structures, the selective enrichment of

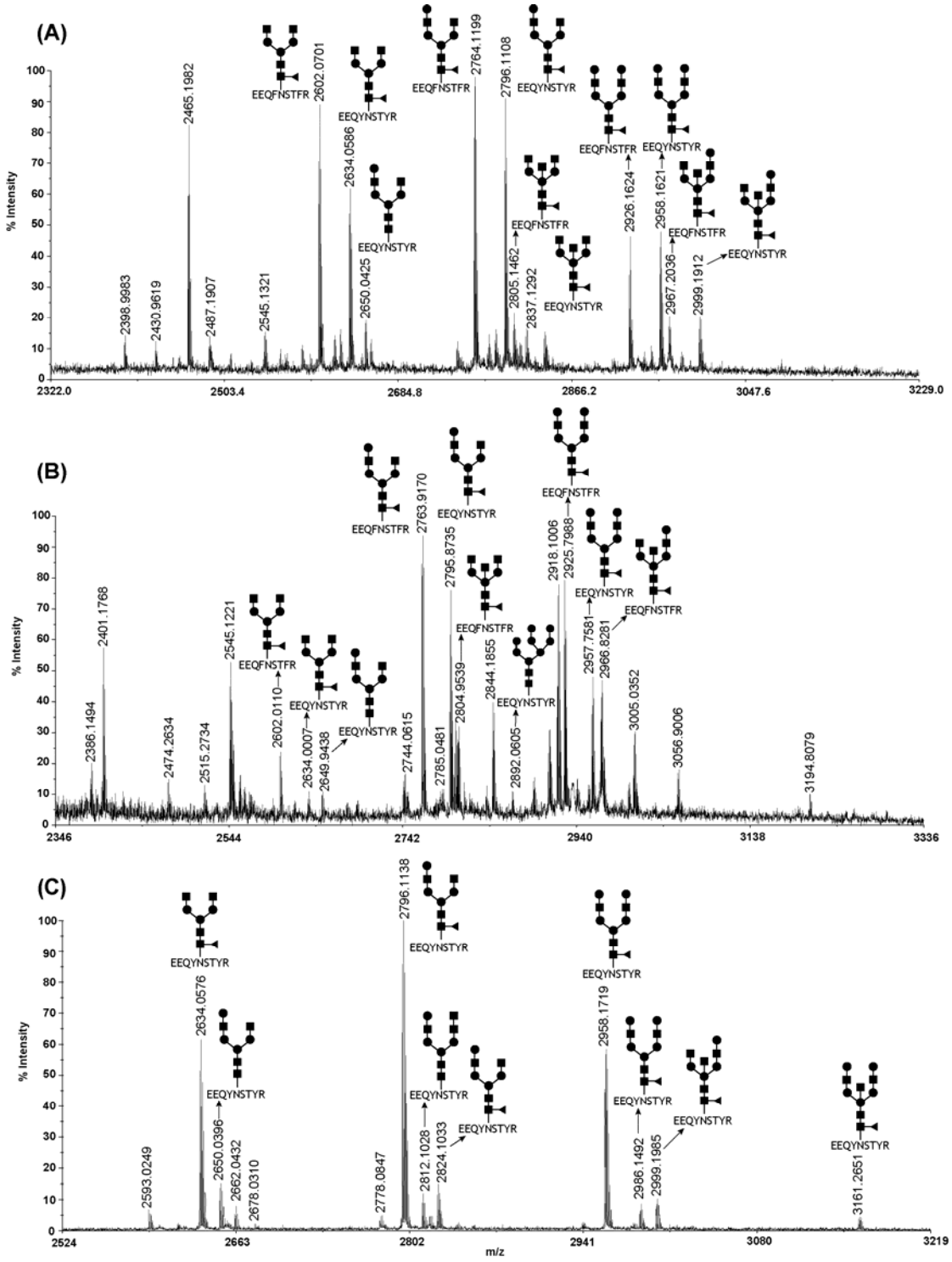

Figure 2. (+) MALDI-TOF data of glycopeptides from human IgG separated or/and

enriched by different approaches: (A) hydrophilic affinity method with Sepharose®, (B) Con A TopTips®; (C) reverse phase HPLC fractionation. 2C shows the best quality data (i.e. S/N ratio). Postulated glycopeptide structures are shown. These are based on compositional data and biological precedence; other isomeric structures would also be possible.

glycopeptides bearing glycans that have strong affinity to Con A was observed. Because this method is effective in selectively enriching this subset of glycopeptides, the lectin enrichment method using Con A is not suitable when the goal of the analysis is to detect the complete glycosylation profile of the protein. One obvious disadvantage of single lectin-based purification methods is that they bias the results towards whatever carbohydrate structures they have strongest affinity for, as observed in Figure 2. In addition, we found that the Con A TopTips® suffered from very poor run-to-run reproducibility, while reproducible profiles were much easier to obtain using the other methods.

c) Reverse phase HPLC fractionation

In RP-HPLC fractionation, proteolytic digests were subjected to a chromatographic separation using a C18 column to resolve glycopeptides in the digest into fractions. Each collected fraction was dried and reconstituted with H_2O prior to analysis. Glycopeptides from the IgG tryptic digest were eluted at 6, 7, 9, and 10 min. Figure 2C represents the (+) MALDI-MS data of the glycopeptide fraction eluting at 6 min. Compared to the (+) MALDI-MS data obtained from the two enrichment methods in Figure 2A and 2B, MALDI-MS data from HPLC fractionation was far superior with respect to the quality of the data (i.e, better signal-to-noise (S/N) ratio) and the total number of glycopeptides observed. A summary of the glycan compositions for all glycopeptide fractions is shown in Table 1. Overall, thirteen glycan structures were observed from HPLC fractionation. In addition,

Table 1. (+) MALDI-MS data of human IgG purified by different methods

Methods	Experimental *m/z*	Theoretical *m/z*	Peptide Sequence*	Glycan	Mod *
Sepharose®	2602.0701	2602.0560	EEQFNSTFR	[Hex]3[HexNAc]4[Fuc]1	
	2634.0586	2634.0458	EEQYNSTYR	[Hex]3[HexNAc]4[Fuc]1	
	2650.0425	2650.0408	EEQYNSTYR	[Hex]4[HexNAc]4	
	2764.1199	2764.1089	EEQFNSTFR	[Hex]4[HexNAc]4[Fuc]1	
	2796.1108	2796.0987	EEQYNSTYR	[Hex]4[HexNAc]4[Fuc]1	
	2805.1462	2805.1354	EEQFNSTFR	[Hex]3[HexNAc]5[Fuc]1	
	2837.1292	2837.1252	EEQYNSTYR	[Hex]3[HexNAc]5[Fuc]1	
	2926.1624	2926.1617	EEQFNSTFR	[Hex]5[HexNAc]4[Fuc]1	
	2958.1621	2958.1515	EEQYNSTYR	[Hex]5[HexNAc]4[Fuc]1	
	2967.2036	2967.1882	EEQFNSTFR	[Hex]4[HexNAc]5[Fuc]1	
	2999.1912	2999.1780	EEQYNSTYR	[Hex]4[HexNAc]5[Fuc]1	
Lectin	2602.0110	2602.0560	EEQFNSTFR	[Hex]3[HexNAc]4[Fuc]1	
	2634.0007	2634.0458	EEQYNSTYR	[Hex]3[HexNAc]4[Fuc]1	
	2649.9438	2650.0408	EEQYNSTYR	[Hex]4[HexNAc]4	
	2763.9170	2764.1089	EEQFNSTFR	[Hex]4[HexNAc]4[Fuc]1	
	2795.8735	2796.0987	EEQYNSTYR	[Hex]4[HexNAc]4[Fuc]1	
	2804.9539	2805.1354	EEQFNSTFR	[Hex]3[HexNAc]5[Fuc]1	
	2892.0605	2892.0933	EEQYNSTYR	[Hex]8[HexNAc]2	
	2925.7988	2926.1617	EEQFNSTFR	[Hex]5[HexNAc]4[Fuc]1	
	2957.7581	2958.1515	EEQYNSTYR	[Hex]5[HexNAc]4[Fuc]1	
	2966.8281	2967.1882	EEQFNSTFR	[Hex]4[HexNAc]5[Fuc]1	
HPLC F6 *	2488.0723	2487.9879	EEQYNSTYR	[Hex]3[HexNAc]4	
	2634.0576	2634.0458	EEQYNSTYR	[Hex]3[HexNAc]4[Fuc]1	
	2650.0396	2650.0408	EEQYNSTYR	[Hex]4[HexNAc]4	
	2796.1138	2796.0987	EEQYNSTYR	[Hex]4[HexNAc]4[Fuc]1	
	2812.1028	2812.0936	EEQYNSTYR	[Hex]5[HexNAc]4	
	2824.1033	2824.0936	EEQYNSTYR	[Hex]4[HexNAc]4[Fuc]1	For *
	2958.1719	2958.1515	EEQYNSTYR	[Hex]5[HexNAc]4[Fuc]1	
	2986.1492	2986.1464	EEQYNSTYR	[Hex]5[HexNAc]4[Fuc]1	For
	2999.1985	2999.1780	EEQYNSTYR	[Hex]4[HexNAc]5[Fuc]1	
	3161.2651	3161.2309	EEQYNSTYR	[Hex]5[HexNAc]5[Fuc]1	
HPLC F7	2430.9497	2430.9664	EEQYNSTYR	[Hex]3[HexNAc]3[Fuc]1	
	2487.9900	2487.9879	EEQYNSTYR	[Hex]3[HexNAc]4	
	2634.0430	2634.0458	EEQYNSTYR	[Hex]3[HexNAc]4[Fuc]1	
	2650.0437	2650.0408	EEQYNSTYR	[Hex]4[HexNAc]4	
	2662.0315	2662.0407	EEQYNSTYR	[Hex]3[HexNAc]4[Fuc]1	For
	2691.0566	2691.0673	EEQYNSTYR	[Hex]3[HexNAc]5	
	2796.0884	2796.0987	EEQYNSTYR	[Hex]4[HexNAc]4[Fuc]1	
	2837.1194	2837.1252	EEQYNSTYR	[Hex]3[HexNAc]5[Fuc]1	
	2853.0918	2853.1201	EEQYNSTYR	[Hex]4[HexNAc]5	
	2865.1138	2865.1201	EEQYNSTYR	[Hex]3[HexNAc]5[Fuc]1	For
	2958.1357	2958.1515	EEQYNSTYR	[Hex]5[HexNAc]4[Fuc]1	
	2999.1692	2999.1780	EEQYNSTYR	[Hex]4[HexNAc]5[Fuc]1	
	3027.1580	3027.1729	EEQYNSTYR	[Hex]4[HexNAc]5[Fuc]1	For
	3161.2034	3161.2309	EEQYNSTYR	[Hex]5[HexNAc]5[Fuc]1	
HPLC F9	2618.0376	2618.0510	EEQFNSTFR	[Hex]4[HexNAc]4	
	2780.0857	2780.1038	EEQFNSTFR	[Hex]5[HexNAc]4	
	2821.1301	2821.1303	EEQFNSTFR	[Hex]4[HexNAc]5	
	2983.1633	2983.1832	EEQFNSTFR	[Hex]5[HexNAc]5	
HPLC F10	2455.9993	2455.9981	EEQFNSTFR	[Hex]3[HexNAc]4	
	2602.0762	2602.0560	EEQFNSTFR	[Hex]3[HexNAc]4[Fuc]1	
	2618.0388	2618.0510	EEQFNSTFR	[Hex]4[HexNAc]4	
	2630.0620	2630.0509	EEQFNSTFR	[Hex]3[HexNAc]4[Fuc]1	For
	2764.1260	2764.1089	EEQFNSTFR	[Hex]4[HexNAc]4[Fuc]1	
	2792.1216	2792.1038	EEQFNSTFR	[Hex]4[HexNAc]4[Fuc]1	For
	2805.1550	2805.1354	EEQFNSTFR	[Hex]3[HexNAc]5[Fuc]1	
	2833.1384	2833.1303	EEQFNSTFR	[Hex]3[HexNAc]5[Fuc]1	For
	2926.1790	2926.1617	EEQFNSTFR	[Hex]5[HexNAc]4[Fuc]1	
	2954.1675	2954.1566	EEQFNSTFR	[Hex]5[HexNAc]4[Fuc]1	For
	2967.1997	2967.1882	EEQFNSTFR	[Hex]4[HexNAc]5[Fuc]1	

*Peptide sequence (positions 322-330) with no miscleavages; Mod: modification on peptide moieties; For: Formylation; F6: HPLC fraction 6

glycopeptide with peptide sequences, EEQYNSTYR and EEQFNSTFR, are better resolved in the HPLC experiment, and formylation occurs on these peptide moieties during fractionation. This modification is discussed in a later section of the manuscript. Based on these results, MALDI-MS analysis of the HPLC fractionated IgG glycopeptides yielded a more comprehensive glycan profile, compared to Sepharose® and Con A enrichment schemes; see Table 1. Thus, reverse phase HPLC fractionation was proven to be an efficient approach for maximizing coverage of glycosylation heterogeneity of glycoproteins using MALDI analysis.

Sample preparation methods for human transferrin

Having demonstrated the strength and weaknesses of each method on a glycoprotein with one glycosylation site, the applicability of these methods was tested on two glycoproteins with more than one glycosylation site, transferrin and AGP. Human transferrin contains two glycosylation sites with highly sialylated biantennary complex-type glycans.[87] Compared with human IgG, identifying glycan structures of transferrin in MALDI-MS analysis is more challenging because it is sialylated. Sialic acids are labile and ionize less efficiently than neutral glycans, in the positive ion mode.[88] To detect the sialic acids on transferrin, MALDI data was acquired mainly in negative ion mode. From the information obtained with IgG, the sample preparation approach employed for transferrin were hydrophilic affinity method using Sepharose® and reverse phase HPLC fractionation. Because the glycopeptide coverage of lectin-based affinity enrichment largely depends on the lectin-glycan binding specificity, the application of this approach to profiling glycosylation on transferrin was not successful.

a) Hydrophilic affinity method using Sepharose®

Glycopeptides generated from the tryptic digest of transferrin were subjected to hydrophilic affinity enrichment followed by (-) MALDI-MS analysis and the data is shown in Figure 3A. Two glycosylation sites (Asn^{413} and Asn^{611}) are detected, which contain sialylated glycans and peptide compositions, QQQHLFGSN^{611}VTDCSGNFCLFR and CGLVPVLAENYN^{413}K. Both of these peptides were modified during the proteolytic digestion. In the case of tryptic peptide, QQQHLFGSN^{611}VTDCSGNFCLFR, the modification arises from the formation of pyroglutamic acid on N-terminus. For the tryptic peptide composition, CGLVPVLAENYN^{413}K, the alkylated cysteine residue was deaminated to form 5-oxo-thiomorpholine-3-carboxylic acid.[73, 89] These modifications are previously documented in the literature.[73, 89] Two major glycan structures observed in Figure 3A were bi- and mono-sialylated complex-types, illustrating that this enrichment method is a practical approach in the identification of sialylated glycopeptides. In positive ion mode, no new glycopeptides were detected (data not shown). Some of the sialylated glycopeptides were observed; however, the signal was stronger in negative ion mode, as expected.

b) Reverse phase HPLC fractionation

For comparison, reverse phase HPLC fractionation was also evaluated in the analysis of glycopeptides generated from transferrin. MALDI-MS analysis of the glycopeptide fractions eluting at 25 and 28 min in Figure 3B and 3C show two glycosylation sites (Asn^{413} and Asn^{611}) with peptide compositions, QQQHLFGSN^{611}VTDCSGNFCLFR and CGLVPVLAENYN^{413}K. The modifications on these peptides comprise deamination of glutamine, alkylated cysteine on the N-terminus,[73, 89] and formylation. The peptide sequences and modifications were

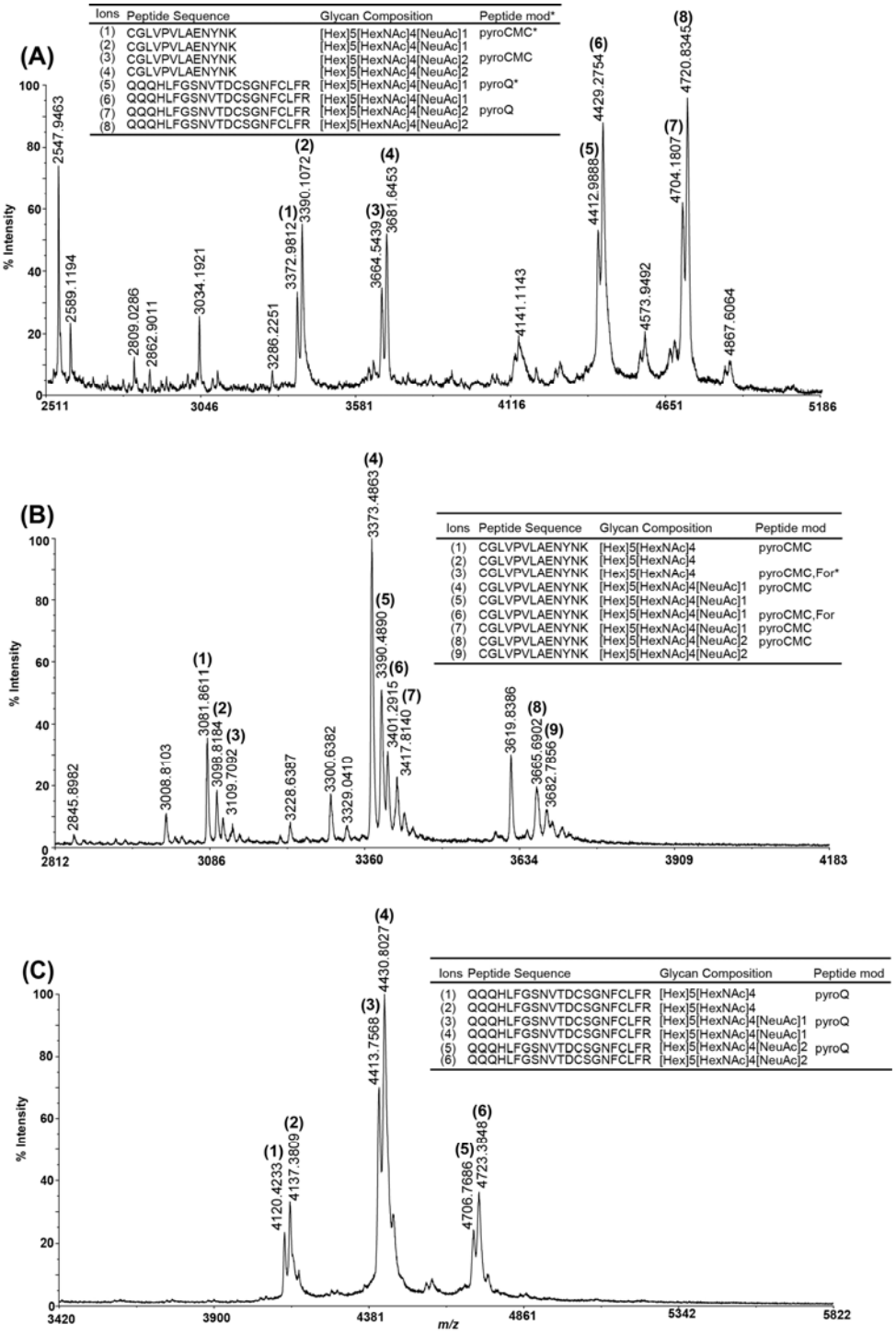

Figure 3. (-)MALDI-TOF data of glycopeptides from human transferrin separated or/and enriched by two methods: (A) hydrophilic affinity method with Sepharose®, (B)

reverse phase HPLC fraction eluting at 25 min (C) reverse phase HPLC fraction eluting at 28 min. Several modifications are present on peptide portion of the glycopeptides. *Peptide mod: modification on the peptide moieties. PyroCMC: deamination of alkylated cysteine of N-terminus; PyroQ: pyroglutamic acid of N-terminus of peptide. For: formylation of amino groups of the peptide.

confirmed using several approaches, including identifying peptide-based ions in MS/MS data and deglycosylation of glycopeptide HPLC fractions using PNGase F, which is discussed in a later section of this manuscript. In addition to glycopeptides with sialylated glycans present in the spectra, neutral glycans are also observed. Specifically, glycopeptide peaks observed at *m/z* 3081, 3098, and 3109 in Figure 3B and glycopeptide peaks observed at *m/z* 4120, and 4137 in Figure 3C correspond to glycopeptides with neutral glycans. Compared to Figure 3A, the relative abundance of di-sialylated glycopeptides decrease dramatically in HPLC fractionation and neutral glycopeptides are present on the spectra; see Figure 3B and 3C. According to the glycan structures of human transferrin reported in literature,[87] over 90% glycans are di-sialylated biantennary complex type. Therefore, the neutral glycopeptides observed on Figure 3B and 3C could arise from the decomposition of the glycopeptides bearing di-sialic acids in the acidic HPLC fractionation, in which the sialic acids are hydrolyzed, and non-sialylated glycopeptides are formed. Although more glycopeptide peaks are observed in the HPLC fractionation for human transferrin, decomposition of sialylated glycopeptides were also present in the experiment. In addition, since glycopeptides can be better resolved in the HPLC fractionation, spectra with better S/N ratio were obtained in HPLC experiments, compared with the Sepharose® enrichment method.

Sample preparation methods for human α1-acid glycoprotein

From the results obtained from IgG and transferrin, all three methods were

able to detect all the glycosylation sites. While this is beneficial in obtaining glycosylation site-specific information, the glycopeptide coverage obtained from each method was not the same. HPLC fractionation provided better glycopeptide coverage. Accordingly, HPLC fractionation was used to characterize the glycosylation on AGP. AGP is a structurally complex glycoprotein with five glycosylation sites (Asn^{15}, Asn^{38}, Asn^{54}, Asn^{75} and Asn^{85}). The glycan profile on the glycosylation sites consist of highly sialylated bi-, tri- and tetra-antennary complex-type structures.[90, 91]

For (+) MALDI-MS analysis of the HPLC fractions of AGP glycopeptides, see Table 2A; only a few glycopeptide fractions are observed, and out of these fractions, only two glycosylation sites (Asn^{15} and Asn^{75}), eluting between 12 –18 mins, are identified. The tryptic peptide sequence bearing glycosylation site Asn^{15} is CANLVPVPITN^{15}ATLDR. Two tryptic peptides, QDQCIYN^{75}TTYLNVQR and QNQCFYN^{75}SSYLNVQR, represent the same glycosylation site (Asn^{75}) and their difference in sequence is due to the peptide heterogeneity.[58] The modifications on these peptide moieties include deamination of alkylated cysteine, glutamine on N-terminus, carbamylation and formylation.[73, 89] These modifications were verified with deglycosylation of glycopeptide fractions using PNGase F. Eleven glycan structures containing fucosylated and non-fucosylated complex-type with or without sialic acids were observed, as summarized in Table 2A. Table 2B contains data from the negative ion mode, and it is discussed in more detail later.

Because of the relatively poor glycopeptide coverage and few glycosylation sites detected, we employed a two-step sample preparation approach using hydrophilic affinity method with Sepharose® followed by HPLC fractionation.[46, 74] The

results (Table 3) show four glycosylation sites (Asn^{15}, Asn^{54}, Asn^{75} and Asn^{85}) are observed, and thirty-three unique glycopeptide ions are identified from MALDI analysis of the HPLC fractions. A comparison of the data in Table 2A with those in Table 3 shows a marked improvement in the glycopeptide coverage and the number of glycosylation sites detected using the two-step sample preparation approach. In addition to increasing the number of glycopeptide ions detected, an additional benefit of improving the glycopeptide signal in the mass spectra is that MALDI-MS/MS data can be acquired on the ions of sufficient abundance. This is critical for confirming the peptide assignment of the glycopeptides. Representative MALDI-MS and MS/MS data of the glycopeptide fraction eluting at 27 min (fraction 27 in Table 3) is shown in Figure 4A and 4B, respectively. The precursor ion in Figure 4B is the base peak at *m/z* 4192 in Figure 4A. Abundant glycopeptide peaks observed at *m/z* 2594, 3283, and 3811 on Figure 4B were used to confirm the glycan composition. Glycopeptide peaks observed at *m/z* 2271 and 2391 correspond to $^{0,2}X$ ($[peptide+83+H]^+$) and $Y_{1\alpha}$ ($[peptide+HexNAc+H]^+$) ions, respectively, identifying the peptide composition of the glycopeptides. Peptide peaks observed at *m/z* 112, 175, 403, 497, 575, 893, and 1179, were used to verify the peptide sequence.

Among five glycosylation sites, the signal of the glycopeptides from site Asn^{38} (NEEYNK) was not detected in MALDI-MS analysis. It has been observed previously that these glycopeptides co-elute with the glycopeptides from site Asn^{85} (ENGTISR).[90, 91] Since the peptide portion of the glycopeptides generated from Asn^{85} ends with arginine (R), these glycopeptides ionize better than the glycopeptides from site Asn^{38}, which ends in lysine (K).[92] Hence, the mass spectral signal of glycopeptides from site Asn^{38} were most likely suppressed by the signal of the

Table 2A. (+)MALDI-MS data of human AGP purified by reverse phase HPLC

F#	Experimental *m/z*	Theoretical *m/z*	Peptide Sequence*	Glycan	Mod*	Position
F12*	3908.6648	3908.5794	QNQCFYNSSYLNVQR	[Hex]6[HexNAc]5		[69-83]
	4270.8794	4271.6959	QNQCFYNSSYLNVQR	[Hex]5[HexNAc]4[Fuc]1[NeuNAc]2		[69-83]
F15	2832.2952	2832.2964	CANLVPVPITNATLDR	[Hex]3[HexNAc]3	PyroCMC*	[5-24]
	2849.3416	2849.3230	CANLVPVPITNATLDR	[Hex]3[HexNAc]3		[5-24]
	3224.4536	3224.4394	CANLVPVPITNATLDR	[Hex]3[HexNAc]4[Fuc]1	PyroCMC,U*	[5-24]
	3359.4902	3359.4814	CANLVPVPITNATLDR	[Hex]5[HexNAc]4	PyroCMC	[5-24]
	3417.1836	3417.5345	CANLVPVPITNATLDR	[Hex]4[HexNAc]5		[5-24]
	3724.6660	3724.6136	CANLVPVPITNATLDR	[Hex]6[HexNAc]5	PyroCMC	[5-24]
	3741.6431	3741.6402	CANLVPVPITNATLDR	[Hex]6[HexNAc]5		[5-24]
	3751.9329	3751.6245	CANLVPVPITNATLDR	[Hex]5[HexNAc]5[Fuc]1	PyroCMC,U	[5-24]
	3769.6492	3769.6351	CANLVPVPITNATLDR	[Hex]6[HexNAc]5	For*	[5-24]
	3784.3374	3784.6460	CANLVPVPITNATLDR	[Hex]6[HexNAc]5	U	[5-24]
	4000.0461	3999.7141	CANLVPVPITNATLDR	[Hex]5[HexNAc]5[Fuc]1[NeuNAc]1	PyroCMC	[5-24]
	4001.8379	4001.7046	CANLVPVPITNATLDR	[Hex]5[HexNAc]4[NeuNAc]2	U	[5-24]
	4016.8613	4016.7407	CANLVPVPITNATLDR	[Hex]5[HexNAc]5[Fuc]1[NeuNAc]1		[5-24]
F17	4269.1821	4268.7427	QDQCIYNTTYLNVQR	[Hex]7[HexNAc]6	PyroQ*	[69-83]
F18	4265.6187	4265.7066	QDQCIYNTTYLNVQR	[Hex]6 [HexNAc]5 [NeuNAc]1	PyroQ	[69-83]

*Peptide sequence with no miscleavages; Mod: modification on peptide moieties; PyroCMC: Deamination of alkylated cysteine; PyroQ: pryoglutamic acid; U: Carbamylation; For: Formylation; F12: HPLC fraction 12

Table 2B. (-) MALDI-MS data of human AGP purified by reverse phase HPLC

F#	Experimental *m/z*	Theoretical *m/z*	Peptide Sequence*	Glycan	Mod*	Position
F12 *	4182.5767	4183.1234	QNQCFYNSSYLNVQR	[Hex]6[HexNAc]5[NeuNAc]1	PyroQ*	[69-83]
	4199.3818	4200.1540	QNQCFYNSSYLNVQR	[Hex]6[HexNAc]5[NeuNAc]1		[69-83]
	4474.4048	4474.3813	QNQCFYNSSYLNVQR	[Hex]6[HexNAc]5[NeuNAc]2	PyroQ	[69-83]
	4491.7310	4491.4119	QNQCFYNSSYLNVQR	[Hex]6[HexNAc]5[NeuNAc]2		[69-83]
	4548.2524	4548.4608	QNQCFYNSSYLNVQR	[Hex]7[HexNAc]6[NeuNAc]1	PyroQ	[69-83]
	4565.2778	4565.4914	QNQCFYNSSYLNVQR	[Hex]7[HexNAc]6[NeuNAc]1		[69-83]
	4841.1680	4840.7468	QNQCFYNSSYLNVQR	[Hex]7[HexNAc]6[Fuc]2[NeuNAc]1	PyroQ	[69-83]
	4857.7441	4857.7774	QNQCFYNSSYLNVQR	[Hex]7[HexNAc]6[Fuc]2[NeuNAc]1		[69-83]
F15	3650.1174	3650.7463	CANLVPVPITNATLDR	[Hex]5[HexNAc]4[NeuNAc]1	PyroCMC*	[5-24]
	3666.8960	3667.7769	CANLVPVPITNATLDR	[Hex]5[HexNAc]4[NeuNAc]1		[5-24]
	4015.4675	4016.0837	CANLVPVPITNATLDR	[Hex]6[HexNAc]5[NeuNAc]1	PyroCMC	[5-24]
	4032.4404	4033.1143	CANLVPVPITNATLDR	[Hex]6[HexNAc]5[NeuNAc]1		[5-24]
	4059.9331	4061.1247	CANLVPVPITNATLDR	[Hex]6[HexNAc]5[NeuNAc]1	For*	[5-24]
	4307.6665	4307.3416	CANLVPVPITNATLDR	[Hex]6[HexNAc]5[NeuNAc]2	PyroCMC	[5-24]
	4324.5693	4324.3722	CANLVPVPITNATLDR	[Hex]6[HexNAc]5[NeuNAc]2		[5-24]
	4352.2925	4352.3826	CANLVPVPITNATLDR	[Hex]6[HexNAc]5[NeuNAc]2	For	[5-24]
	4616.7363	4616.6582	CANLVPVPITNATLDR	[Hex]6[HexNAc]5[Fuc]2[NeuNAc]2		[5-24]
F17	4542.4535	4541.8923	QDQCIYNTTYLNVQR	[Hex]7[HexNAc]6[NeuNAc]1	PyroQ	[69-83]
	4832.5283	4831.8923	QDQCIYNTTYLNVQR	[Hex]7[HexNAc]6[NeuNAc]2	PyroQ	[69-83]

*Peptide sequence with no miscleavages; Mod: modification on peptide moieties; PyroCMC: Deamination of alkylated cysteine; PyroQ: pryoglutamic acid; For: Formylation; F12 neg: HPLC fraction 12 in negative ion mode

glycopeptides from Asn^{85}. Due to the relatively low glycopeptide intensities obtained from this fraction compared to the other fractions, the glycans were cleaved with PNGase F to confirm the presence of the tryptic peptides (NEEYNK and ENGTISR). MALDI-MS analysis of the deglycosylated fraction indeed confirmed the presence of NEEYNK and ENGTISR (data not shown). Although the glycoforms could not be observed on site Asn^{38}, the PNGase F experiment confirms that this site is occupied with glycans, therefore, increasing the number of detected glycosylation sites on this protein. As demonstrated here, the use of PNGase F to identify the glycosylation site occupancy on the weakly ionized glycopeptides is one more strategy that can be implemented to maximize glycosylation coverage, when the goal is to determine which glycosylation sites are occupied.

Note that MALDI-MS analysis of AGP discussed so far were performed in the positive ion mode. Mass analysis of the AGP glycopeptide fractions in the negative ion mode revealed the presence of sialylated species. Table 2B shows the sialylated glycans when the same fractions in Table 2A were analyzed in the negative ion mode. Six glycan structures were observed in (-) MALDI-MS analysis. Combining the glycan structures detected in both modes, a total of seventeen glycans containing fucosylated and non-fucosylated complex-type with or without sialic acids were observed.

Representative MALDI data acquired both in the positive and negative ion mode of AGP glycopeptide fraction eluting at 15 min (F15 in Table 2A and 2B) in Figure 5 show glycopeptides with neutral glycans were mainly observed in the positive ion mode (Figure 5A), while sialylated species were mainly observed in the negative ion mode (Figure 5B). This capability to observe sialylated species in the negative mode improves the glycopeptide coverage.

Table 3. (+) MALDI-MS data of human AGP purified by Sepharose®- RP HPLC

F#	Experimental *m/z*	Theoretical *m/z*	Peptide Sequence	Glycan	Mod *	Position	MC*
F4*	2764.1667	2764.1036	ENGTISR	[Hex]6[HexNAc]5		[84-90]	0
	2776.0334	2776.1036	ENGTISR	[Hex]5[HexNAc]5[Fuc]1	For*	[84-90]	0
	2792.2368	2792.0985	ENGTISR	[Hex]6[HexNAc]5	For	[84-90]	0
F7	2748.1545	2748.1087	ENGTISR	[Hex]5[HexNAc]5[Fuc]1		[84-90]	0
	3127.1633	3127.2201	ENGTISR	[Hex]5[HexNAc]4[Fuc]1[NeuNAc]2		[84-90]	0
F12	3538.4541	3538.4783	QDQCIYNTTYLNVQR	[Hex]5[HexNAc]4		[69-83]	0
	3903.6887	3903.6105	QDQCIYNTTYLNVQR	[Hex]6[HexNAc]5		[69-83]	0
	4268.9014	4268.7427	QDQCIYNTTYLNVQR	[Hex]7[HexNAc]6		[69-83]	0
	4414.3745	4414.8006	QDQCIYNTTYLNVQR	[Hex]7[HexNAc]6[Fuc]1		[69-83]	0
	4560.3794	4559.8381	QDQCIYNTTYLNVQR	[Hex]7[HexNAc]6[NeuNAc]1		[69-83]	0
F15	2849.4407	2849.3230	CANLVPVPITNATLDR	[Hex]3[HexNAc]3		[5-24]	0
	3376.6685	3376.5080	CANLVPVPITNATLDR	[Hex]5[HexNAc]4		[5-24]	0
	3388.5715	3388.5080	CANLVPVPITNATLDR	[Hex]4[HexNAc]4[Fuc]1	For	[5-24]	0
	3741.8220	3741.6402	CANLVPVPITNATLDR	[Hex]6[HexNAc]5		[5-24]	0
	3753.9043	3753.6402	CANLVPVPITNATLDR	[Hex]5[HexNAc]5[Fuc]1	For	[5-24]	0
	3769.7837	3769.6351	CANLVPVPITNATLDR	[Hex]6[HexNAc]5	For	[5-24]	0
	4001.5813	4001.7046	CANLVPVPITNATLDR	[Hex]5[HexNAc]4[NeuNAc]2	U*	[5-24]	0
	4132.9878	4132.7516	CANLVPVPITNATLDR	[Hex]5[HexNAc]4[Fuc]1[NeuNAc]2	For	[5-24]	0
F19	2832.4209	2832.2964	CANLVPVPITNATLDR	[Hex]3[HexNAc]3	PyroCMC*	[5-24]	0
	3197.5012	3197.4286	CANLVPVPITNATLDR	[Hex]4[HexNAc]4	PyroCMC	[5-24]	0
	3359.6245	3359.4814	CANLVPVPITNATLDR	[Hex]5[HexNAc]4	PyroCMC	[5-24]	0
	3724.7466	3724.6136	CANLVPVPITNATLDR	[Hex]6[HexNAc]5	PyroCMC	[5-24]	0
	4016.8987	4016.7294	CANLVPVPITNATLDR	[Hex]6[HexNAc]5[Fuc]2	PyroCMC	[5-24]	0
F27	3283.7568	3283.5759	QIPLCANLVPVPITNATLDR	[Hex]3[HexNAc]3	PyroQ*	[1-20]	0
	3811.0088	3810.7609	QIPLCANLVPVPITNATLDR	[Hex]5[HexNAc]4	PyroQ	[1-20]	0
	4176.1411	4175.8931	QIPLCANLVPVPITNATLDR	[Hex]6[HexNAc]5	PyroQ	[1-20]	0
	4192.6221	4192.9197	QIPLCANLVPVPITNATLDR	[Hex]6[HexNAc]5		[1-20]	0
	4219.3154	4218.8989	QIPLCANLVPVPITNATLDR	[Hex]6[HexNAc]5	PyroQ,U	[1-20]	0
	4339.0093	4338.9776	QIPLCANLVPVPITNATLDR	[Hex]6[HexNAc]5[Fuc]1		[1-20]	0
F28	3810.9646	3810.7609	QIPLCANLVPVPITNATLDR	[Hex]5[HexNAc]4	PyroQ	[1-20]	0
	4177.1436	4176.9248	QIPLCANLVPVPITNATLDR	[Hex]5[HexNAc]5[Fuc]1	PyroQ	[1-20]	0
F29	4193.3369	4192.9197	QIPLCANLVPVPITNATLDR	[Hex]6 [HexNAc]5		[1-20]	0
F30	5261.9443	5262.2816	SVQEIQATFFYFTPNKTEDTIFLR	[Hex]6[HexNAc]4[NeuNAc]2		[40-63]	1
	5639.5239	5639.4138	SVQEIQATFFYFTPNKTEDTIFLR	[Hex]6[HexNAc]5[Fuc]1[NeuNAc]2	For	[40-63]	1
	5663.0205	5662.4774	SVQEIQATFFYFTPNKTEDTIFLR	[Hex]4[HexNAc]9[NeuNAc]1		[40-63]	1

*MC: trypsin miscleavage; Mod: modification on peptide moieties; PyroCMC: Deamination of alkylated cystein; PyroQ: pryoglutamic acid; U: Carbamylation; For: Formylation; F4: HPLC fraction 4

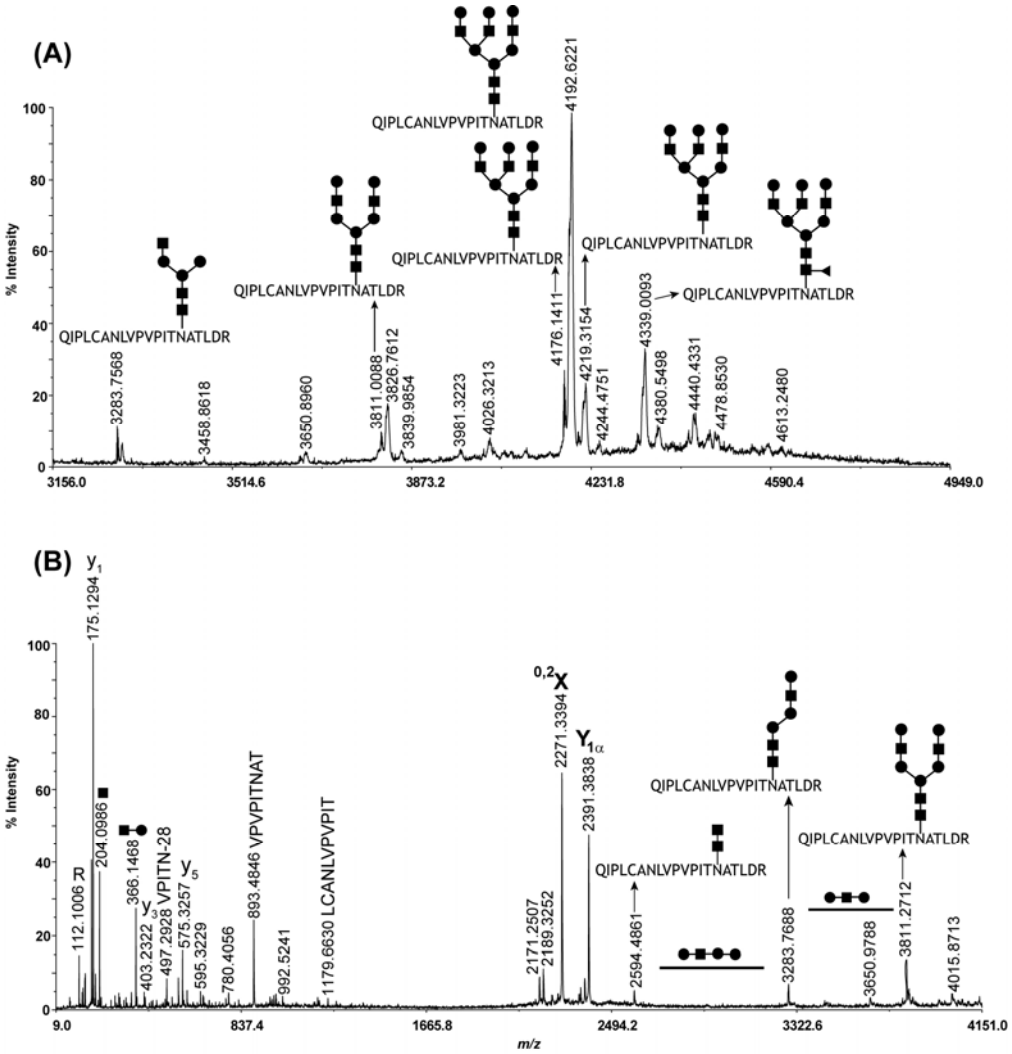

Figure 4. MALDI analysis of glycopeptides from human AGP separated with Sepharose® followed by reverse phase HPLC; fraction eluting at 27min (A) (+)MALDI-TOF data of HPLC fraction 27, (B) (+)MALDI-TOF/TOF data of base peak at *m/z* 4192.6221 in (A) to confirm the glycopeptide assignment. $^{0,2}X$ and $Y_{1\alpha}$ ions are used to identify the peptide moieties. Postulated glycopeptide structures are shown. These are based on compositional data and biological precedence; other isomeric structures would also be possible.

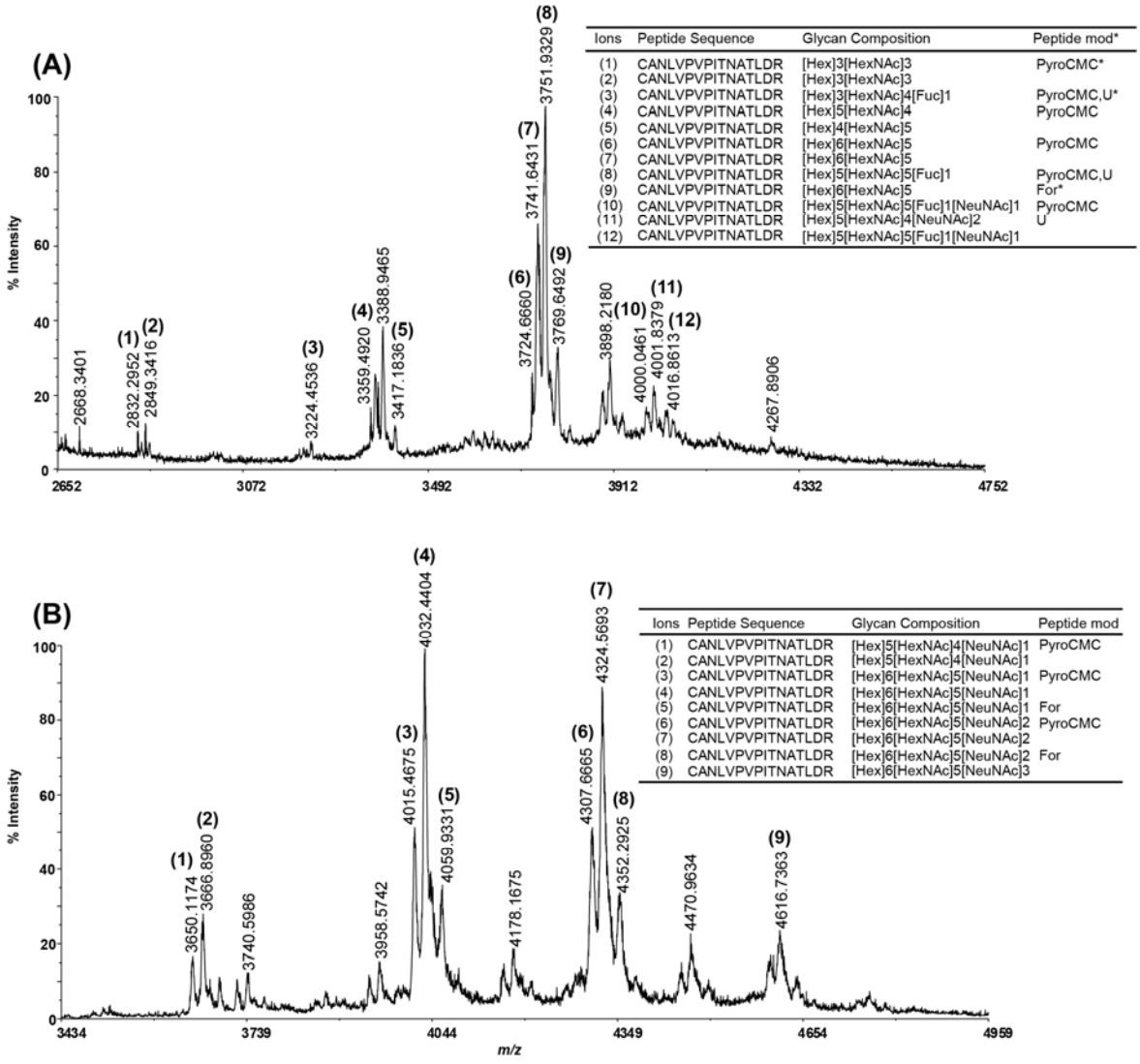

Figure 5. MALDI-TOF data of glycopeptides from human AGP separated by reverse phase HPLC; fraction eluting at 15 min (A) positive ion mode; mainly neutral glycans on glycopeptides are detected. (B) negative ion mode; sialylated glycopeptides are identified. Acquiring MS data in both positive and negative ion modes improves glycopeptide coverage for acidic glycoproteins. *Peptide mod: modification on the peptide moieties. PyroCMC: deamination of alkylated cysteine of N-terminus. For: formylation of amino groups of the peptide. U: carbamylation.

Modifications on peptide moieties of glycopeptides

In the glycopeptide-based analysis, we detected several modifications on the peptide moieties that have been previously observed in the proteolytic digests of

proteins. These include conversion of an N-terminal glutamine into pyroglutamic acid,[73, 89] deamination of alkylated cysteine on N-terminus when this residue was alkylated by iodoacetamide,[73, 89] carbamylation due to the presence of urea in protein denaturation, and formylation when the digest mixtures were separated in acidic HPLC conditions.

These modifications and their corresponding peptide sequences were confirmed by deglycosylation of glycopeptide HPLC fractions using PNGase F and assigning the MS and MS/MS data to the resulting peptides, which were generated during PNGase F hydrolysis. Representative MALDI-MS and MS/MS data of a deglycosylated glycopeptide fraction (eluting at 28 min) of human transferrin are shown in Figure 6. The tryptic peptide sequence bearing glycosylation site Asn^{611} was converted to QQQHLFGSD^{611}VTDCSGNFCLFR upon deglycosylation by PNGase F. The modification on this peptide moiety comprises conversion of glutamine into pyroglutamic acid on the N-terminus, which results in a mass shift of 17 Da. Two peaks at *m/z* 2498 and *m/z* 2515 in Figure 6A represent the modified and unmodified peptide moieties of glycopeptides from human transferrin, respectively. To further verify the presence of modification in this fraction and the corresponding peptide sequences, MALDI-MS/MS data were acquired and shown in Figure 6B and 6C. The characteristic ions at *m/z* 385, 635, and 782 in Figure 6B, originating from b_3, b_5 and b_6 ions are shifted 17 Da, compared to the same peaks (labeled in red) in Figure 6C. This demonstrates that the formation of pyroglutamic acid on N-terminus occurs when the glycoproteins undergo the proteolytic digestion. All the other peptide-based internal ions in Figure 6B and 6C were utilized to confirm the peptide sequences.

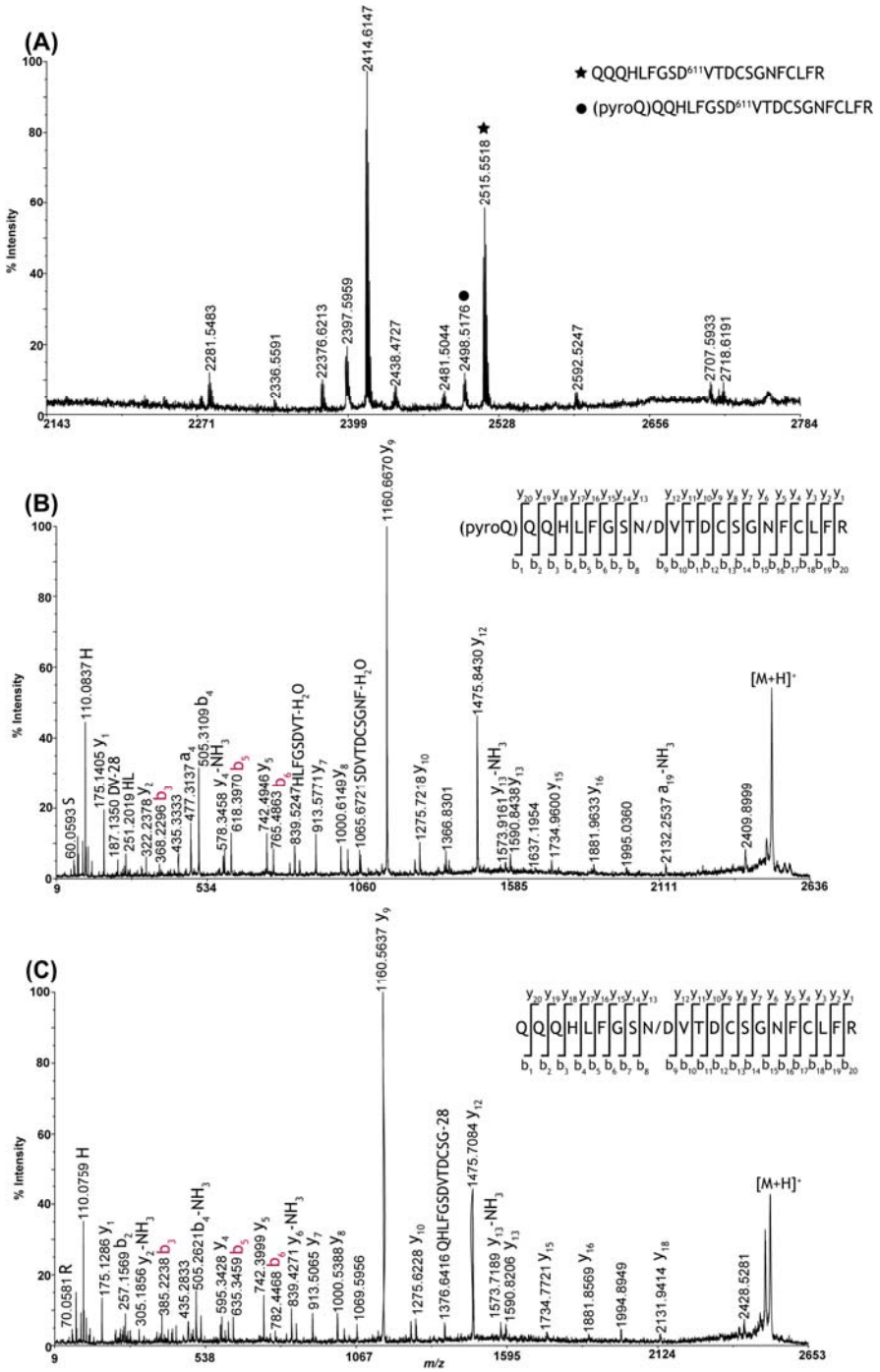

Figure 6. MALDI analysis of a deglycosylated glycopeptide fraction (eluting at 28 min) from human transferrin; (A) MALDI-TOF data of HPLC fraction 28; Asparagine converts to aspartic acid upon deglycosylation by PNGase F. The peak marked by a circle represents the modification on N-terminus of the peptide: the conversion of glutamine into pyroglutamic acid. The peak marked by a star represents the native peptide. (B) and (C) MALDI-TOF/TOF data of the modified and native peptide

moieties. The internal peptide ions confirm the peptide sequences and the peaks labeled in red are used to verify the modification on N-terminus by a mass shift of 17 Da, compared to the native peptide.

Due to the presence of these modifications in proteolytic digest of the proteins, incorporating the variable modifications into the database search is helpful in increasing the number of mass spectral assignments of glycopeptide peaks. For example, in the analysis of AGP purified by the two-step preparation approach, thirty-five glycopeptides were identified from all the fractions; see Table 3. However, out of thirty-five glycopeptide peaks, only sixteen glycopeptides were identified prior to applying the variable modifications into the database (GlycoPep DB) search. Therefore, considering these modifications in the assignment of glycopeptide compositions more than doubles the number of assignable peaks.

Summary of the strategies used in maximizing glycosylation coverage

As described above, each of the chromatographic or/and enrichment approaches was evaluated based on the number of glycosylation sites detected and glycopeptides identified in three model glycoproteins. The pros and cons for each preparative method are summarized in Table 4. In general, the hydrophilic and lectin-based affinity enrichment methods used in this study are straightforward, selective, show good reproducibility (in the case of Sepharose®), and deliver moderate throughput for

Table 4. Pros and cons of each sample preparation method

Methods		Pros	Cons
Instrumentation	RP-HPLC	Highest coverage Good reproducibility	Sialic acids are hydrolyzed in acidic conditions Low throughtput when coupled with MALDI analysis
Enrichment Methods	Sepharose®	Good reproducibility Moderate throughput	Low separation capacity
	ConA Toptips®	Selective Good for selecting specific glycans Moderate throughput	Low separation capacity Results biased towards certain glycan structures Poor run-to-run reproducibility

preparing several samples. While all glycosylation sites were detected in IgG and transferrin, the glycopeptide coverage is limited due to the lower separation capacities in the microcolumns, compared to HPLC fractionation. The glycan coverage of Con A packed lectin microcolumn tips is also limited by their glycan binding specificity. Although the glycan binding specificities can be improved by packing different lectins in one microcolumn tip, these tips are not commercially available. Additionally, the single lectin used in this study, Con A TopTips®, showed the poorest reproducibility of all the sample preparation methods.

Reverse phase HPLC fractionation gave the best glycopeptide coverage on the model glycoproteins. While this approach is beneficial in achieving good glycosylation coverage, the throughput is relatively low and the sample decomposition of sialylated glycopeptides is observable, due to the acidic conditions of the mobile phase. The recent development and implementation of automated LC-MALDI systems[93, 94] as well as the optimization of pH in mobile phase could help to mitigate these problems.[82] In the analysis of glycoproteins with more than two glycosylation sites, a two-step sample preparation method ─ Sepharose® followed by HPLC fractionation ─ is highly beneficial to optimize the glycosylation coverage because it depletes more peptides from digestion mixture, as illustrated in the analysis of AGP.

Finally, in addition to the sample preparation strategies compared here, the other important strategies, including the mass spectral techniques and data analysis strategies, were also implemented to enhance glycosylation coverage: First, profiling in both positive and negative ion mode in mass spectrometry is essential when neutral glycopeptides are intermixed with acidic ones, as is the case with AGP.

Second, the use of PNGase F was helpful in confirming the presence of a weakly ionizing glycopeptide that co-eluted with more strongly ionizing species, thus, increasing the number of glycosylation sites detected in glycopeptide-based analysis. Third, several modifications on the peptide portion commonly observed in proteolytic digestion, such as conversion of an N-terminal glutamine residue into pyroglutamic acid, and deamination of alkylated cysteine on N-terminus, can be incorporated into the database search (Glycopep DB)[80] to facilitate assigning more glycopeptide peaks in data analysis.

Application of maximizing glycosylation coverage strategies in HIV envelope glycoprotein

Owing to successfully optimizing glycosylation coverage on model glycoproteins (from one to five glycosylation sites), the same strategies were also tested on a very highly complex glycoprotein, the HIV envelope protein, JR-FL gp140 ΔCF, which contains 27 potential glycosylation sites. The proteolytic digests of JR-FL were subjected to RP-HPLC fractionation, with and without pre-treatment with Sepharose® affinity purification. Our study shows that over 300 glycoform were identified on 23 detected glycosylation sites from 36 HPLC fractions that contained glycopeptides of JR-FL in MALDI-MS analysis. Representative MALDI-MS and MS/MS data of a glycopeptide fraction of JR-FL eluting at 7 min (without Sepharose® pre-treatment) are shown in Figure 7. The two-step sample preparation method using Sepharose® followed by HPLC fractionation produced the same glycosylation coverage, compared to HPLC fractionation. In Figure 7, all the peaks marked with a star represent glycopeptides from glycosylation site Asn^{361} (LREQFEN^{361}K) on JR-FL gp140 ΔCF. This single spectrum shows a total 38 glycopeptide peaks detected, with

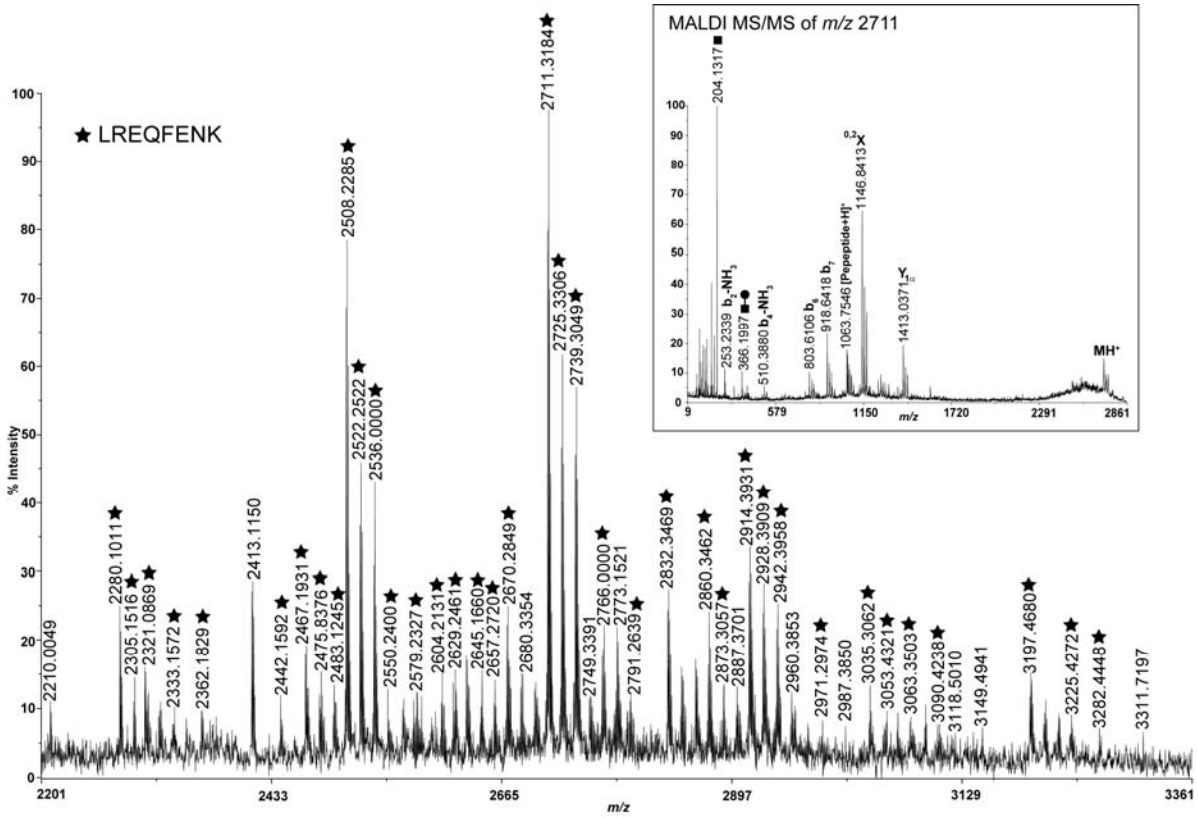

Figure 7. Representative MALDI-TOF data of glycopeptide fraction (eluting at 7 min) from tryptic digest of JR-FL gp140 ΔCF separated by reverse phase HPLC. All the identified glycopeptides are from glycosylation site Asn^{361} on JR-FL gp 140 ΔCF and marked by a star. Inset: MALDI-TOF/TOF data of the identified glycopeptide base peak at *m/z* 2711.3184. The peptide portion is $LREQFEN^{361}K$ and conformed by $^{0,2}X$ and $Y_{1\alpha}$ ions.

good S/N ratio. Out from 38 glycopeptide peaks, 26 unique glycan structures have been identified, which demonstrates that a highly heterogeneous population of glycans can be detected from this glycosylation site. This implies that our approach works not only for elucidation of overall glycan profiles on glycoproteins but also for the identification of glycan heterogeneity in each glycosylation site. The precursor ion in Figure 7 inset is the base peak at *m/z* 2711. Glycopeptide peaks observed at *m/z* 1147 and 1413 correspond to $^{0,2}X$ ($[peptide+83+H]^+$) and $Y_{1\alpha}$ ($[peptide+HexNAc+Fuc+H]^+$) ions, respectively, identifying the peptide

composition of the glycopeptides. Since the observed peptide mass is consistent with the calculated mass, no modification was found on the peptide portion of the base peak at *m/z* 2711. Peptide peaks observed at *m/z* 253, 510, 803, and 918, were used to verify the peptide sequence. The glycan compositions for each of the starred peaks in Figure 7 were determined using GlycoPep DB and are listed in Supplementary Table 1 online. A full discussion of this data, along with the glycan profiles at the other 22 glycosylation sites detected by MALDI-MS, is presented separately.

4.4 Conclusions

In order to design an experimental workflow that maximizes coverage of glycosylation heterogeneity on glycoproteins, we optimized all the features of glycopeptide-based MALDI-MS analysis, including sample preparation methods, mass spectral data acquisition, and data analysis. This is the first study aimed at independently determining the best strategies to maximize glycosylation coverage in glycopeptide-based analysis. These strategies are useful in obtaining complete glycan profiles on a variety of glycoproteins (from one to multiple glycosylation sites), thereby facilitating understanding how glycan structure affects the functions of glycoproteins. This investigation also provides beneficial information in the experimental design for glycan profiling on heavily glycosylated glycoproteins, such as HIV virus envelope protein ─ JR-FL gp 140 ΔCF, which contains 27 glycosylation sites.

Acknowledgments

The authors acknowledge the National Institutes of Health for funding (project number RO1GM077266), Dr. Barton F. Haynes, Dr. Hua-Xin Liao, and Laura L. Sutherland at Duke Human Vaccine Research Institute (Duke University, Durham, NC) for supplying the glycoprotein JR-FL gp140 ΔCF, and the KU proteomics facility for instrument time on the MALDI TOF/TOF.

Supplementary Table 1. Glycopeptide composition from site Asn^{361} of JRFL gp140 ΔCF in MALDI-MS analysis

Experimental *m/z*	Theoretical *m/z*	Peptide Sequence	Glycan	Mod*
2280.1011	2279.9760	LREQFENK	[Hex]5[HexNAc]2	
2305.1516	2305.0077	LREQFENK	[Hex]3[HexNAc]3[Fuc]1	
2321.0869	2321.0026	LREQFENK	[Hex]4[HexNAc]3	
2333.1572	2333.0026	LREQFENK	[Hex]3[HexNAc]3[Fuc]1	For*
2362.1829	2362.0291	LREQFENK	[Hex]3[HexNAc]4	
2442.1592	2442.0289	LREQFENK	[Hex]6 [HexNAc]2	
2467.1931	2467.0605	LREQFENK	[Hex]4[HexNAc]3[Fuc]1	
2483.1245	2483.0554	LREQFENK	[Hex]5 [HexNAc]3	
2508.2285	2508.0870	LREQFENK	[Hex]3[HexNAc]4[Fuc]1	
2522.2522	2522.1027	LREQFENK	[Hex]3[HexNAc]4[Fuc]1	Methyl*
2536.0000	2536.0819	LREQFENK	[Hex]3[HexNAc]4[Fuc]1	For
2550.2400	2550.0976	LREQFENK	[Hex]3[HexNAc]4[Fuc]1	Methyl, for
2579.2327	2579.1243	LREQFENK	[Hex]3[HexNAc]5	Methyl
2604.2131	2604.0817	LREQFENK	[Hex]7[HexNAc]2	
2629.2461	2629.1133	LREQFENK	[Hex]5[HexNAc]3[Fuc]1	
2645.1660	2645.1082	LREQFENK	[Hex]6[HexNAc]3	
2657.2720	2657.1082	LREQFENK	[Hex]5[HexNAc]3[Fuc]1	For
2670.2849	2670.1399	LREQFENK	[Hex]4[HexNAc]4[Fuc]1	
2711.3184	2711.1665	LREQFENK	[Hex]3[HexNAc]5[Fuc]1	
2725.3306	2725.1822	LREQFENK	[Hex]3[HexNAc]5[Fuc]1	Methyl
2739.3049	2739.1614	LREQFENK	[Hex]3[HexNAc]5[Fuc]1	For
2766.0000	2766.1345	LREQFENK	[Hex]8[HexNAc]2	
2791.2639	2791.1661	LREQFENK	[Hex]6[HexNAc]3[Fuc]1	
2832.3469	2832.1927	LREQFENK	[Hex]5[HexNAc]4[Fuc]1	
2860.3462	2860.1876	LREQFENK	[Hex]5[HexNAc]4[Fuc]1	For
2873.3057	2873.2192	LREQFENK	[Hex]4[HexNAc]5[Fuc]1	
2887.3701	2887.2349	LREQFENK	[Hex]4[HexNAc]5[Fuc]1	Methyl
2914.3931	2914.2459	LREQFENK	[Hex]3[HexNAc]6[Fuc]1	
2928.3909	2928.2616	LREQFENK	[Hex]3[HexNAc]6[Fuc]1	Methyl
2942.3958	2942.2030	LREQFENK	[Hex]9[HexNAc]2	Methyl
2971.2974	2971.1931	LREQFENK	[Hex]9[HexNAc]2	U*
3035.3062	3035.2721	LREQFENK	[Hex]5[HexNAc]5[Fuc]1	
3053.4321	3053.2462	LREQFENK	[Hex]7[HexNAc]4	U
3063.3503	3063.2670	LREQFENK	[Hex]5[HexNAc]5[Fuc]1	For
3090.4238	3090.2401	LREQFENK	[Hex]10[HexNAc]2	
3197.4680	3197.3249	LREQFENK	[Hex]6[HexNAc]5[Fuc]1	For
3225.4272	3225.3198	LREQFENK	[Hex]6[HexNAc]5[Fuc]1	
3282.4448	3282.3413	LREQFENK	[Hex]6[HexNAc]6	For

*Mod: modification on peptide moieties; For: Formylation; Methyl: methylation; U: Carbamylation;

4.5 References

1. Kameyama, A.; Kaneda, Y.; Yamanaka, H.; Yoshimine, H.; Narimatsu, H.; Shinohara, Y. Detection of oligosaccharides labeled with cyanine dyes using matrix-assisted laser desorption/ionization mass spectrometry. *Anal. Chem.* **2004,** *76,* 4537-4542.

2. Nilsson, B. Analysis of protein glycosylation by mass spectrometry. *Mol. Biotechnol.* **1994,** *2,* 243-280.

3. Wada, Y.; Tajiri, M.; Yoshida, S. Hydrophilic affinity isolation and MALDI multiple-stage tandem mass spectrometry of glycopeptides for glycoproteomics. *Anal. Chem.* **2004,** *76,* 6560-6565.

4. Imre, T.; Schlosser, G.; Pocsfalvi, G.; Siciliano, R.; Molnar-Szollosi, E.; Kremmer, T.; Malorni, A.; Vekey, K. Glycosylation site analysis of human alpha-1-acid glycoprotein (AGP) by capillary liquid chromatography - electrospray mass spectrometry. *J. Mass Spectrom.* **2005,** *40,* 1472-1483.

5. Kameyama, A.; Kikuchi, N.; Nakaya, S.; Ito, H.; Sato, T.; Shikanai, T.; Takahashi, Y.; Takahashi, K.; Narimatsu, H. A strategy for identification of oligosaccharide structures using observational multistage mass spectral library. *Anal. Chem.* **2005,** *77,* 4719-4725.

6. Palm, A. K.; Novotny, M. V. A monolithic PNGase F enzyme microreactor enabling glycan mass mapping of glycoproteins by mass spectrometry. *Rapid Commun. Mass Spectrom.* **2005,** *19,* 1730-1738.

7. Yu Y. Q.; Gilar, M.; Kaska, J.; Gebler J. C. A rapid sample preparation method for mass spectrometric characterization of N-linked glycans. *Rapid Commun. Mass Spectrom.* **2005,** *19,* 2331-2336.

8. Shinohara, Y.; Furukawa, J.; Niikura, K.; Miura, N.; Nishimura, S. Direct N-glycan profiling in the presence of tryptic peptides on MALDI-TOF by controlled ion enhancement and suppression upon glycan-selective derivatization. *Anal. Chem.* **2004,** *76,* 6989-6997.

9. Larsen, M. R.; Hojrup, P.; Roepstorff, P. Characterization of gel-separated glycoproteins using two-step proteolytic digestion combined with sequential microcolumns and mass spectrometry. *Mol. Cell Proteomics.* **2005,** *4,* 107-119.

10. Haslam, S. M.; North, S. J.; Dell, A. Mass spectrometric analysis of N- and O-glycosylation of tissues and cells. *Curr. Opin. Struct. Biol.* **2006,** *16,* 584-591.

11. Yang, Z.; Hancock, W. S.; Chew, T. R.; Bonilla, L. A study of glycoproteins in human serum and plasma reference standards (HUPO) using multilectin affinity chromatography coupled with RPLC-MS/MS. *Proteomics* **2005,** *5,* 3353-3366.

12. Wang, Y.; Wu, S.; Hancock, W. S. Approaches to the study of N-linked glycoproteins in human plasma using lectin affinity chromatography and nano-HPLC coupled to electrospray linear ion trap-Fourier transform mass spectrometry. *Glycobiology* **2006,** *16,* 514-523.

13. Van Rensburg, S. J.; Berman, P.; Potocnik, F.; MacGregor, P.; Hon, D.; De Villiers, N. 5- and 6-glycosylation of transferrin in patients with Alzheimer's disease. *Metab. Brain Dis.* **2004,** *19,* 89-96.

14. Fournier, T.; Medjoubi, N. N.; Porquet, D. Alpha-1-acid glycoprotein. *Biochim. Biophys. Acta.* **2000,** *1482,* 157-171.

15. Nihlen, U.; Montnemery, P.; Lindholm, L. H.; Loefdahl, C. G. Increased serum levels of carbohydrate-deficient transferrin in patients with chronic obstructive pulmonary disease. *Scand. J. Clin. Lab. Invest.* **2001,** *61,* 341-348.

16. Budnik, B. A. ; Lee, R. S. ; Steen, J. A. J. Global methods for protein glycosylation analysis by mass spectrometry. *Biochim. Biophys. Acta.* **2006,** *1764,* 1870-1880.

17. Haynes, P. A.; Batley, M.; Peach, R. J.; Brennan, S. O.; Redmond, J. W. Characterization of oligosaccharides from a glycoprotein variant of human serum albumin (albumin Casebrook) using high-performance anion-exchange chromatography and nuclear magnetic resonance spectroscopy. *J. Chromatogr.* **1992,** *581*, 187-193.

18. Mechref, Y.; Novotny, M. V. Miniaturized separation techniques in glycomic investigations. *J. Chromatogr. B Analyt. Technol. Biomed. Life Sci.* **2006,** *841*, 65-78.

19. Patwa, T. H.; Zhao, J.; Anderson, M. A.; Simeone, D. M.; Lubman, D. M. Screening of glycosylation patterns in serum using natural glycoprotein microarrays and multi-lectin fluorescence detection. *Anal. Chem.* **2006,** *78*, 6411-6421

20. Charlwood, J.; Birrell, H.; Camilleri, P. Carbohydrate release from picomole quantities of glycoprotein and characterization of glycans by high-performance liquid chromatography and mass spectrometry. *J. Chromatogr. B, Biomed. Sci. Appl.* **1999,** *734*, 169-174.

21. Kuester, B.; Naven, T. J. P.; Harvey, D. J., Rapid approach for sequencing neutral oligosaccharides by exoglycosidase digestion and matrix-assisted laser desorption/ionization time-of-flight mass spectrometry. *J. Mass Spectrom.* **1996,** *31,* 1131-1140.

22. Mechref, Y.; Novotny, M. V. Mass spectrometric mapping and sequencing of N-linked oligosaccharides derived from submicrogram amounts of glycoproteins. *Anal. Chem.* **1998,** *70,* 455-463.

23. Irungu, J.; Dalpathado, D. S.; Go, E. P.; Jiang, H.; Ha, H.; Bousfield, G. R.;

Desaire, H. Method for characterizing sulfated glycoproteins in a glycosylation site-specific fashion, using ion pairing and tandem mass spectrometry. *Anal. Chem.* **2006,** *78*, 1181-1190.

24. Bunkenborg, J.; Pilch, B. J.; Podteleinikov, A. V.; Wisniewski, J. R. Screening for N-glycosylated proteins by liquid chromatography mass spectrometry. *Proteomics* **2004,** *4,* 454-465.

25. Dage, J. L.; Ackermann, B. L.; Halsall, H. B. Site localization of sialyl LewisX antigen on α1-acid glycoprotein by high performance liquid chromatography-electrospray mass spectrometry. *Glycobiology* **1998,** *8,* 755-760.

26. Geng, M.; Zhang, X.; Bina, M.; Regnier, F. Proteomics of glycoproteins based on affinity selection of glycopeptides from tryptic digests. *J. Chromatogr. B Biomed. Sci. Appl.* **2001,** *752,* 293-306.

27. Haegglund, P.; Bunkenborg, J.; Elortza, F.; Jensen, O. N.; Roepstorff, P. A new strategy for identification of N-glycosylated proteins and unambiguous assignment of their glycosylation sites using HILIC enrichment and partial deglycosylation. *J. Proteome Res.* **2004,** *3,* 556-566.

28. Krokhin, O.; Ens, W.; Standing, K. G.; Wilkins, J.; Perreault, H. Site-specific N-glycosylation analysis: matrix-assisted laser desorption/ionization quadrupole-quadrupole time-of-flight tandem mass spectral signatures for recognition and identification of glycopeptides. *Rapid Commun. Mass Spectrom.* **2004,** *18,* 2020-2030.

29. Tajiri, M.; Yoshida, S.; Wada, Y. Differential analysis of site-specific glycans on plasma and cellular fibronectins: application of a hydrophilic affinity method for glycopeptide enrichment. *Glycobiology* **2005,** *15,* 1332-1340.

30. Nagy, K.; Vekey, K.; Imre, T.; Ludanyi, K.; Barrow, M. P.; Derrick, P. J. Electrospray ionization Fourier transform ion cyclotron resonance mass spectrometry of human α1-acid glycoprotein. *Anal. Chem.* **2004,** *76,* 4998-5005.

31. Carr, S. A.; Huddleston, M. J.; Bean, M. F. Selective identification and differentiation of N- and O-linked oligosaccharides in glycoproteins by liquid chromatography-mass spectrometry. *Protein Sci.* **1993,** *2,* 183-196.

32. Huddleston, M. J.; Bean, M. F.; Carr, S. A. Collisional fragmentation of glycopeptides by electrospray ionization LC/MS and LC/MS/MS: methods for selective detection of glycopeptides in protein digests. *Anal. Chem.* **1993,** *65,* 877-884.

33. Hemstroem, P.; Irgum, K. Hydrophilic interaction chromatography. *J. Sep. Sci.* **2006,** *29,* 1784-1821.

34. Atwood, J. A.; Minning, T.; Ludolf, F.; Nuccio, A.; Weatherly, D. B.; Alvarez-

Manilla, G.; Tarleton, R.; Orlando, R. Glycoproteomics of *trypanosoma cruzi* trypomastigotes using subcellular fractionation, lectin affinity, and stable isotope labeling. *J. Proteome Res.* **2006,** *5,* 3376-3384.

35. Alvarez-Manilla, G.; Atwood, J.; Guo, Y.; Warren, N. L.; Orlando, R.; Pierce, M. Tools for glycoproteomic analysis: Size exclusion chromatography facilitates identification of tryptic glycopeptides with N-linked glycosylation sites. *J. Proteome Res.* **2006,** *5,* 701-708.

36. Go, E. P.; Rebecchi, K. R.; Dalpathado, D. S.; Bandu, M. L.; Zhang, Y.; Desaire, H. GlycoPep DB: a tool for glycopeptide analysis using a "smart search". *Anal. Chem.* **2007,** *79,* 1708-1713.

37. Liao, H.; Sutherland, L.L.; Xia, S.; Brock, M. E.; Scearce, R. M.; Vanleeuwen, S.; Alam, S. M.; McAdams, M.; Weaver, E. A.; Camacho, Z. T.; Ma, B.; Li, Y.; Decker, J. M.; Nabel, G. J.; Montefiori, D. C.; Hahn, B. H.; Korber, B. T.; Gao, F.; Haynes, B. F. A group M consensus envelope glycoprotein induces antibodies that neutralize subsets of subtype B and C HIV-1 primary viruses. *Virology* **2006,** *353,* 268-282.

38. Zhu, X.; Borchers, C.; Bienstock, R. J.; Tomer, K. B. Mass spectrometric characterization of the glycosylation pattern of HIV-gp120 expressed in CHO cells. *Biochemistry* **2000,** *39*, 11194-11204.

39. Irungu, J.; Go. E. P.; Dalpathado, D. S.; Desaire, H. Simplification of mass spectral analysis of acidic glycopeptides using *GlycoPep ID. Anal. Chem.* **2007,** *79,* 3065-3074.

40. Butler, M.; Quelhas, D.; Critchley, A. J.; Carchon, H.; Hebestreit, H. F.; Hibbert, R. G.; Vilarinho, L.; Teles, E.; Matthijs, G.; Schollen, E.; Argibay, P.; Harvey, D. J.; Dwek, R. A.; Jaeken, J.; Rudd, P. M. Detailed glycan analysis of serum glycoproteins of patients with congenital disorders of glycosylation indicates the specific defective glycan processing step and provides an insight into pathogenesis. *Glycobiology* **2003**, *13,* 601-622.

41. Novotny, M. V.; Mechref, Y. New hyphenated methodologies in high-sensitivity glycoprotein analysis. *J. Sep. Sci.* **2005,** *28,* 1956-1968.

42. Qiu, R.; Regnier, F. E. Use of multidimensional lectin affinity chromatography in differential glycoproteomics. *Anal. Chem.* **2005,** *77,* 2802-2809.

43. Satomi, Y.; Shimonishi, Y.; Hase, T.; Takao, T., Site-specific carbohydrate profiling of human transferrin by nano-flow liquid chromatography/electrospray ionization mass spectrometry. *Rapid Commun. Mass Spectrom.* **2004,** *18,* 2983-2988.

44. Harvey, D. J., Structural determination of N-linked glycans by matrix-assisted laser desorption/ionization and electrospray ionization mass spectrometry.

Proteomics **2005,** *5,* 1774-1786.

45. Krokhin, O. V.; Ens, W.; Standing, K. G. Characterizing degradation products of peptides containing N-terminal Cys residues by (off-line high-performance liquid chromatography)/matrix-assisted laser desorption/ionization quadrupole time-of-flight measurements. *Rapid Commun. Mass Spectrom.* **2003,** *17,* 2528-2534.

46. Kremmer, T.; Szoelloesi, E.; Boldizsar, M.; Vincze, B.; Ludanyi, K.; Imre, T.; Schlosser, G.; Vekey, K., Liquid chromatographic and mass spectrometric analysis of human serum acid alpha-1-glycoprotein. *Biomed. Chromatogr.* **2004,** *18,* 323-329.

47. Szoellosi, E.; Kremmer, T.; Ludanyi, K.; Imre, T.; Schlosser, G.; Boldizsar, M.; Vincze, B.; Vekey, K. A novel method for the separation and purification of human serum acid alpha-1-glycoprotein: liquid chromatographic and mass spectrometric investigation of tryptic fragments. *Chromatographia* **2004,** *60,* S213-S219.

48. Brancia, F. L.; Oliver, S. G.; Gaskell, S. J. Improved matrix-assisted laser desorption/ionization mass spectrometric analysis of tryptic hydrolysates of proteins following guanidination of lysine-containing peptides. *Rapid Commun. Mass Spectrom.* **2000**, *14*, 2070-2073.

49. Connolly, J.; Openshaw, M.; Rasso, R.; Martin, R.; Ojima, N. Protein identification of complex mixtures using LC-MALDI on Axima-TOF2. *Shimadzu Hyoron* **2006,** *63,* 11-18.

50. Hattan, S. J.; Parker, K. C., Methodology utilizing MS signal intensity and LC retention time for quantitative analysis and precursor ion selection in proteomic LC-MALDI analyses. *Anal. Chem.* **2006,** *78,* 7986-7996.

Chapter V

Determination of disulfide bond arrangement of the oligomeric HIV envelope protein CON-S gp140 ΔCFI by LC/ESI-FTICR mass spectrometry

5.1 Introduction

Disulfide connectivity is one of the most essential protein modifications, and it plays a key role in stabilizing protein structures.[95-98] Disulfide bonds are usually formed between thiol groups of two cysteine residues that are proximal in three-dimensional structures in the secreted and non-cytoplasmic proteins.[2, 98] The formed disulfide bonds provide a significant reinforcement to the native folding state of the protein by decreasing the conformational entropy of the unfolded state, thus, stabilizing the protein.[98] Numerous studies have shown that the correct disulfide connectivity in proteins is important for protein folding and becomes an indispensable criterion to assess the quality of protein in recombinant DNA technology.[2, 97, 99, 100] Since disulfide linkages are essential in establishing and maintaining the proper protein folds, determination of disulfide bond arrangement is an important aspect to understanding protein chemical structures and defining the functional domains of proteins.[100-102]

If a x-ray crystal structure of a protein is available, the disulfide bonds can be determined from the protein structure directly.[103, 104] Likewise, if a protein structure has been assigned by nuclear magnetic resonance (NMR), the disulfide bonds are also determinable in a straightforward fashion.[105] However, if this level of structural data is not available *a priori,* other methods are more appropriate. For example, several analytical techniques, including high performance liquid chromatography (HPLC),[96, 106, 107] paper electrophoresis,[108] and Edman sequencing[96, 109] have been employed in the determination of disulfide bonds in proteins. These techniques were

used to originally characterize the disulfide bonding network in a monomeric HIV Env protein, from the IIIB isolate of HIV-1 generated in Chinese Hamster Ovary (CHO) cells.[96] Typically, the disulfide bond determination by these techniques entails the enzymatic cleavage of proteins, followed by a separation process and then the detection of disulfide-linked peptides.[100] Although Edman sequencing is a powerful tool to obtain the amino acid sequence of disulfide-linked peptides, it requires highly purified samples.[57, 100] As a result, this approach largely hinges on the ability to obtain highly purified peptides, when analyzing complex samples.[100] Mass spectrometry has emerged as an alternative analytical tool for Edman sequencing in determination of disulfide linkages in proteins, due to its ability to analyze peptide mixtures, along with its high sensitivity and throughput.

In addition to the analytical tools, disulfide mapping requires rigorous experimental controls, due to the possibility of disulfide rearrangement under certain circumstances. It has been previously observed that the disulfide bond scrambling could be triggered by the following conditions: (1) strong acid (e.g. 8.0 M sulfuric acid),[101, 102, 110] (2) the presence of a free thiol group on unpaired cysteine residues at neutral pH,[100-102, 110] and (3) the presence of a thiol group generated by hydrolytic cleavage of disulfide bonds during protein denaturation at neutral and alkaline pH. Thus, precautions must be taken when handling proteins to avoid disulfide bond rearrangement.

The focus of this paper is two-fold: to validate an efficient method of profiling disulfide bonds on proteins, using liquid chromatography electrospray ionization Fourier transform ion cyclotron resonance mass spectrometry (LC/ESI-FTICR-MS) and to use the validated approach to analyze the disulfide bond arrangement in an

oligomeric HIV Env CON-S gp140 ΔCFI. CON-S gp140 ΔCFI was developed as a potential HIV vaccine candidate. It is a synthetic form of Env representing a group M consensus envelope protein, and it induces neutralizing antibodies against type one and limited type two strains of the HIV-1 virus.[53] Compared to previously designed and synthesized immunogens, CON-S gp140 ΔCFI has marked improvement in its immunogenicity.[53]

To date, the disulfide bonding pattern of oligomeric Env proteins, such as CON-S gp140 ΔCFI has not been elucidated; however, the disulfide connectivity in several monomeric forms of HIV Env protein, gp120, have been described.[96, 111-114] These previous studies indicate a conserved disulfide bonding pattern is present in various monomeric forms of HIV Env proteins, where all cysteines are utilized for disulfide connectivity. While these prior studies provide useful insight into the connectivity of monomeric Env, this form of the protein is not the most relevant form for vaccine development, since it has been shown to perform inadequately as a vaccine candidate,[115, 116] and many believe a key contributing reason is that a better mimic of viral Env would include protein that is present in oligomeric form.[117-120] Several oligomeric HIV Env proteins (dimers and trimers) have recently been expressed, and they are known to be covalently associated as a dimer or trimer through disulfide bonds.[53, 121] This surprising result implies that the disulfide bonding network in recombinant oligomeric Env protein must be different from that in the previously characterized monomers, since at least one cysteine must be used for the inter-subunit disulfide bond.

Previous studies have identified the location of inter-chain disulfide bonds between two subunits of Env proteins, by deleting certain domains and/or loops that

are suspected to be involved in the connecting disulfide bond and detecting the changes in the number of domains that are covalently linked in the new protein.[121-123] Although deletion mutations on a protein are useful to identify which domains and/or loops are involved in the inter-subunit contact of a protein, a possibility that truncating these segments influences the protein conformation and indirectly inhibits inter-subunit association cannot be ruled out.[121-123] Additionally, these studies do not address the disulfide bonding which is not associated with the inter-subunit linkage.

The study presented herein is the first investigation to fully characterize the disulfide bonding network of an oligomeric Env protein, CON-S gp140 ΔCFI, and identify the exact location of an inter-subunit disulfide bond in HIV Env protein, using high resolution FTICR mass spectrometry. Our results show that two functional domains previously identified in a monomeric Env protein, the third and forth variable regions (V3, V4), are also conserved in the disulfide bonding in CON-S gp140 ΔCFI. Among these two regions, V3 is the immunodominant region that is responsible for inducing neutralizing antibodies.[53] One cysteine residue Cys^{225} was identified as forming an inter-subunit disulfide bond between two Env monomers, accounting for the oligomeric nature of CON-S gp140 ΔCFI. Interestingly, five free cysteine residues are present in the N-terminal region (defined by amino acid residues 1-250) of CON-S gp140 ΔCFI. Our results demonstrate that the oligomeric form of an HIV Env protein possess a different disulfide bonding network, compared to the monomeric HIV Env protein. This information will facilitate understanding how the disulfide bond arrangement correlates to immunogenetic activities of the oligomeric form of HIV Env protein. This study also sets the foundation for further work: Assessing the differences in disulfide bonding patterns of recombinant Env proteins and comparing

them to the disulfide bonds pattern on Env isolated from virions; these studies would make it possible to determine what types of recombinant proteins best mimic the native viral Env protein. Such studies would greatly aide in the generation of an effective vaccine against the HIV-1 virus.

5.2 Experimental Section

Materials and reagents

Albumin from bovine serum (BSA), 4-Vinylpyridine, acetonitrile, formic acid, acetic acid, and ammonium bicarbonate were all obtained in high purity from Sigma-Aldrich (St. Louis, MO). The HIV envelope glycoprotein CON-S gp140 ΔCFI was expressed and purified in the laboratory of Dr. Barton F. Haynes, Duke Human Vaccine Research Institute (Duke University, Durham, NC), using the method described elsewhere[53]. Peptide *N*-glycosidase F (PNGase F) from *Elizabethkingia meningosepticum* and proteomics grade trypsin were purchased from Calbiochem (San Diego, CA) and Promega (Madison, MI), respectively. Ultra-pure water was obtained from a Millipore Direct-Q3 filtration system. (Billerica, MA).

N-deglycosylation of CON-S gp140 ΔCFI

A sample containing approximately 100 μg of HIV envelope protein CON-S gp140 ΔCFI was dissolved in 50 mM ammonium bicarbonate buffer (pH 7.0) and treated with 1 μL of PNGase F enzyme solution (≥ 4500 units/mL). The reaction was incubated at 37 °C for one week.

Protein digestion

The protein, either BSA or deglycosylated CON-S gp140 ΔCFI, was dissolved in 50 mM ammonium bicarbonate buffer (pH 7.0). Prior to enzymatic digestion,

unpaired cysteine residues in BSA or deglycosylated CON-S gp140 ΔCFI were alkylated with 4-Vinylpyridine at a protein:alkylating reagent ratio of 1:6 (molar ratio). The resulting solution was incubated in the dark for 1 hour at ambient temperature. Proteins were then digested at 37°C with trypsin at an enzyme-to-substrate ratio of 1:20 (w/w) for 18 hours, followed by a second trypsin addition under the same conditions. The digestion was stopped by the addition of 1μL concentrated acidic acid and the resulting protein digest mixture was analyzed by reverse phase-HPLC/ESI-FTICR MS.

LC/ESI-FTICR MS analysis

The tryptic digestion mixtures were subjected to reverse phase high performance liquid chromatography (RP-HPLC, Dionex, Sunnyvale, CA) coupled with a hybrid linear ion trap-Fourier transform ion cyclotron resonance mass spectrometer (LTQ-FTICR-MS) equipped with a 7 Tesla actively shielded magnet (ThermoElectron Corp, San Jose, CA). The mobile phase A was 99.9% water with 0.1% formic acid. Mobile phase B was 99.9% acetonitrile with 0.1% formic acid. Approximately 10 μL of the sample was injected and separated on a C18 PepMap 300^{TM} column (150mm×300 μm i.d. 5 μM, 300Å; LC Packings, Sunnyvale, CA) at a flow rate of 5μL/min. The tryptic peptides were eluted using the following gradient, which was modified from the method described in the literature[124]: The mobile phase initially contained 2% B and the level of B increased linearly to 40% over 30 min, then ramped to 90% B over 20 min. The column was re-equilibrated after holding at 90% B for 10 min.

The samples were infused into the electrospray ion source, and the hybrid LTQ-FTICR data acquisition was performed in a data-dependent scanning mode.

Briefly, the MS^1 spectra were recorded in FT-MS scan and the three most intense peptide ions in MS scan were sequentially selected for CID experiment performed in the LTQ mass analyzer, with 25% normalized collision energy and a 3 min dynamic exclusion window. Electrospray ionization was achieved with a spray voltage of ~ 4.0 kV. Nitrogen was used as nebulizing gas and set at a pressure of 10 psi. The capillary temperature was maintained at 200 °C. All the data were acquired in the positive ion mode and analyzed using Xcalibur 1.3 software (ThermoElectron Corp, San Jose, CA).

5.3 Results and Discussion

To demonstrate the effectiveness of our approach in disulfide mapping using LC/ESI-LTQ-FTICR-MS analysis, a disulfide-rich protein, bovine serum albumin (BSA), was chosen as a model protein to optimize experimental conditions. This approach was subsequently applied in the determination of disulfide bond arrangement of HIV Env protein CON-S gp140 ΔCFI.

Disulfide mapping of bovine serum albumin

Bovine serum albumin (primary accession number P02769 from Swiss-Prot) contains ~600 amino acid residues, 77 potential cleavage sites for trypsin, and 35 cysteine residues.[125] The putative disulfide bond arrangements[126] are shown in Figure 1, in which 17 inter- and intra-chain disulfide linkages are formed. One unpaired cysteine residue, Cys^{58}, has a free thiol group, and it could promote the disulfide bond rearrangement at neutral pH ~7.0.[100] To preclude disulfide scrambling, the thiol groups in the unpaired cysteine residues were masked with the addition of excess alkylating reagent, 4-Vinylpyridine. 4-Vinylpyridine is an ideal alkylating agent

because the modified peptides containing *S*-*β*-(4-pyridylethyl)-cysteine can be readily identified, due to the presence of characteristic ion, *S*-pyridylethyl moiety,

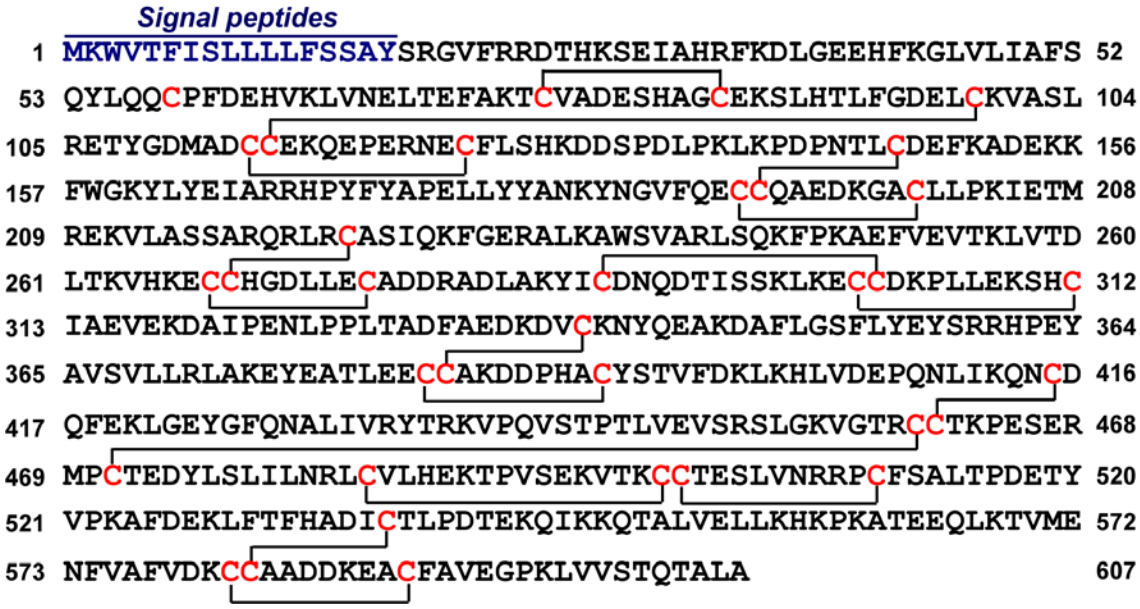

Figure 1. Protein sequence and theoretical disulfide-linkage arrangement in bovine serum albumin; Disulfide linkages are indicated with a solid line and cysteine residues are shown in red.

upon CID experiments in mass spectrometry.[127] The protein was then digested with trypsin at neutral pH ~7.0. Trypsin was used for generating the disulfide-linked peptides due to its substrate specificity and its capability to produce relatively simple mass spectra, compared to other proteases (e.g. pepsin).[100] The resultant tryptic peptides containing disulfide linkages and modified unpaired cysteine residues were then subjected to reverse-phase HPLC followed by ESI-FTICR MS and MS/MS analysis, as shown in Figure 2.

When the tryptic digestion mixtures were separated, several clusters of peptides with inter- or/and intra-disulfide linkages were identified. A representative reverse-phase HPLC chromatogram and LC/ESI-FTICR MS data of tryptic peptides

from BSA are shown in Figure 3A and B, respectively. The FTICR-MS spectrum of the HPLC fraction eluting between 16-17 min (the red bar shown in Figure 3A) shows two peaks at *m/z* 925.8946 and *m/z* 1234.1892 with different charge states. Figure 3 inset shows the zoomed-in spectra used to identify the monoisotopic peaks at *m/z* 925.3933, *m/z* 1234.5219 and their corresponding charge states (+4, and +3, respectively). By comparing the observed masses resulting from the tryptic protein digests with the theoretically calculated masses of the putative disulfide-linked peptides, the peaks at *m/z* 925.3933 and *m/z* 1234.1892 were identified as corresponding to a three-chain disulfide-linked peptide found in BSA. This is the third entry in Table 1, which summarized all the experimentally determined disulfide linkages in BSA. All the 35 cysteines have been identified by LC/ESI-FTICR MS analysis. Each cluster of peptides containing disulfide linkages or unpaired cysteine residues has been identified with high mass accuracy, which is consistent with the known disulfide linkages in BSA, as described in literature.[108, 126]

To further verify the disulfide linkages and peptide sequences of these peptide clusters, MS/MS analysis was performed using data dependent acquisition in the linear ion trap. Representative LC/ESI-LTQ-FTICR MS/MS data are shown in Figure 4. Three classes of peptides containing disulfide-linkages or unpaired cysteine residues have been identified by the product ions observed in MS/MS analysis. Figure 4A depicts the CID data of a peptide that contains a cysteine capped with 4-Vinylpyridine. The major ions in the spectrum are consistent with the expected peptide sequence that retains the chemically modified thiol group on the cysteine. Figure 4B represents an intra-chain disulfide-linked peptide from BSA. For the product ions at *m/z* 407.22, 438.09, 566.39, 849.24, and 860.88, in which the

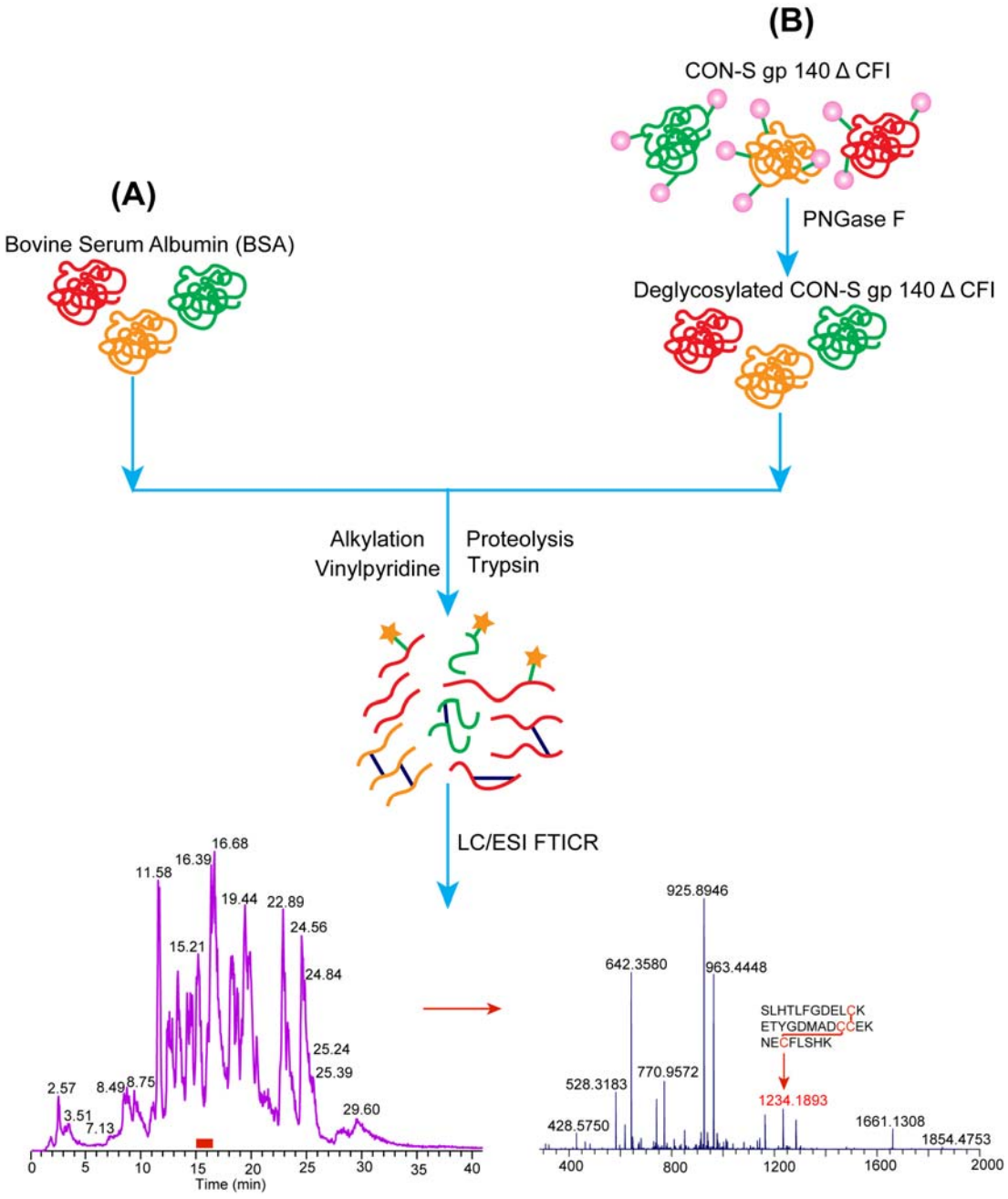

Figure 2. Schematic representation of disulfide bond mapping work-flow in (A) bovine serum albumin and (B) CON-S gp140 ΔCFI; The pink ball represents the glycans on CON-S gp140 ΔCFI. The yellow star indicates the free cysteines alkylated by 4-Vinylpyridine.

disulfide bonds are dissociated, the termini of the cysteine residues were detected as thiol groups (-SH), as expected.[98] Again, the MS/MS data is highly consistent with the depicted peptide sequence. Figure 4C demonstrates the identification of a three-chain disulfide-linked peptide. The product ions denoted y/b were generated from the peptide chain containing an N- terminal serine (S), whereas product ions denoted Y/B and $y_{n'}/b_{n'}$ (n'=1-7) were produced from the peptide chains with N terminal glutamic acid (E) and asparagine (N), respectively. As demonstrated here, in addition to using high mass accuracy data in FTICR-MS analysis to identify the disulfide-linked peptides in BSA, the peptide sequences and disulfide linkages in these peptides were also confirmed with MS/MS experiments, which significantly increases the confidence level in the mass assignments and implicates that our approach is an effective way to determine the disulfide bonds in complex protein digests.

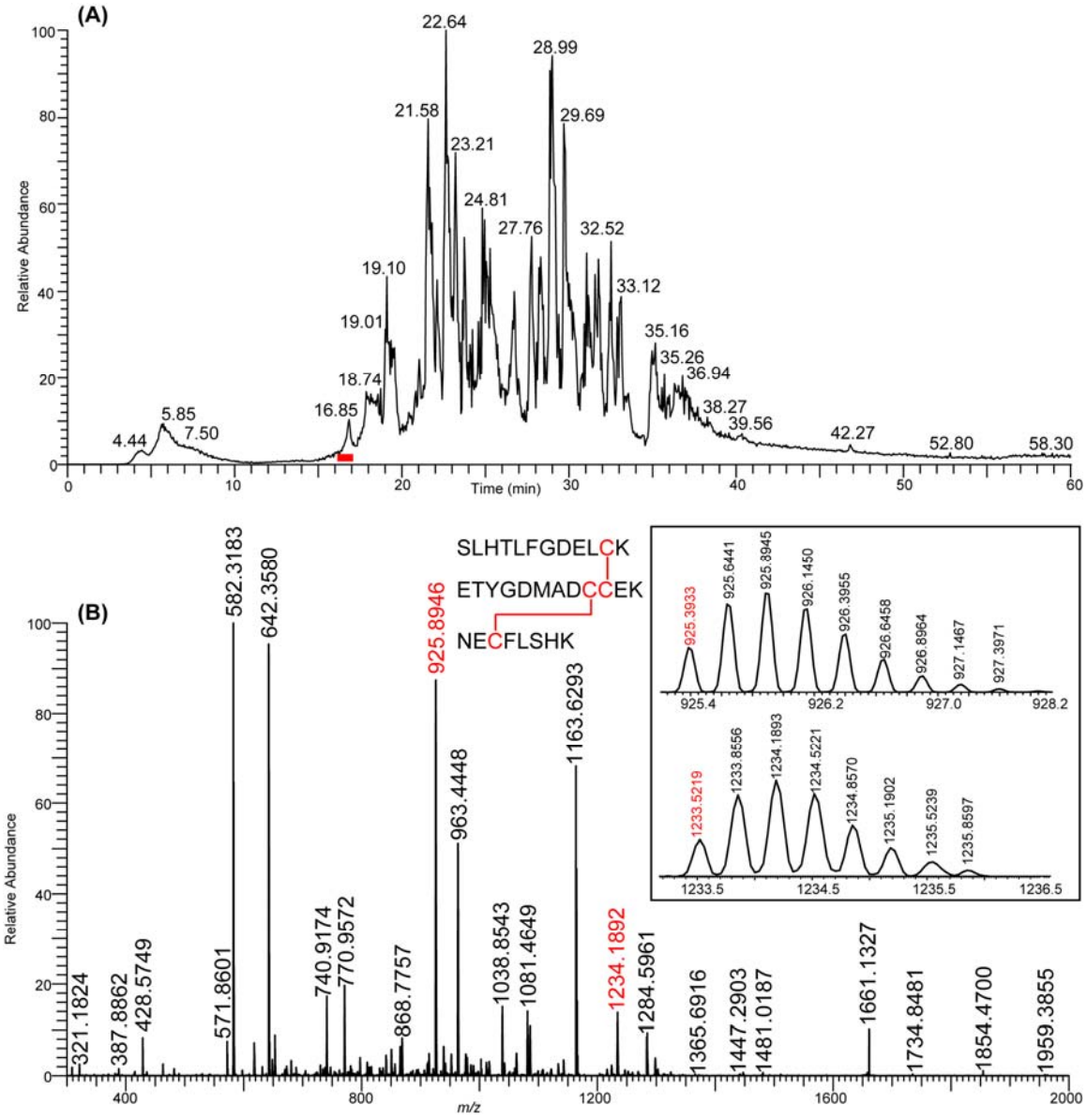

Figure 3. Representative (A) reverse-phase HPLC chromatogram and (B) LC/ESI-FTICR MS data of tryptic peptides from bovine serum albumin; The tryptic peptides are separated within a 60-min gradient. The mass spectrum of HPLC fraction eluting at 16-17 min (labeled with a red bar in A) shows two peaks (in red) with different charge states corresponding to the tryptic peptides with two inter-chain disulfide linkages. Inset: The zoomed-in spectra of detected disulfide-linked peptide peaks, used to identify the monoisotopic peaks and charge states.

Table 1. Summary of the disulfide linkages in bovine serum albumin

Cys-containing peptides from BSA	Theoretical *m/z*	Experimental *m/z*	Mass error ppm	Charge State
GLVLIAFSQYLQQC*PFDEHVK	847.4384 635.8307	847.4376 635.8303	0.94 0.63	3+ 4+
TCVADESHAGCEK	1347.5305 674.2689	1347.5283 674.2680	1.63 1.33	1+ 2+
SLHTLFGDELCK ETYGDMADCCEK NECFLSHK	1233.5242 925.3950	1233.5219 925.3934	1.86 1.73	3+ 4+
LKPDPNTLCDEFK YNGVFQECCQAEDK GACLLPK	1283.5929 962.9465 770.5587	1283.6040 962.9460 770.5576	8.65 0.52 1.43	3+ 4+ 5+
CASIQK ECCHGDLLECADDR	1111.9505 741.6361 556.4789	1111.9495 741.6351 556.4783	0.90 1.35 1.08	2+ 3+ 4+
YICDNQDTISSK ECCDKPLLEK SHCIAEVEK	1191.8788 894.1610 715.5302 596.4431	1191.8763 894.1600 715.5289 596.4403	2.10 1.12 1.82 4.69	3+ 4+ 5+ 6+
DVCK EYEATLEECCAK DDPHACYSTVFDK	1115.4628 836.8490	1115.4625 836.8484	0.27 0.72	3+ 4+
QNCDQFEK CCTKPESER MPCTEDYLSLILNR	1242.5507 932.1649 745.9333 621.7790	1242.5502 932.1635 745.9327 621.7783	0.40 1.50 0.80 1.13	3+ 4+ 5+ 6+
LCVLHEK CCTESLVNR RPCFSALTPDETYVPK	1228.5945 921.6977 737.5596 614.8009	1228.5937 921.6966 737.5589 614.8007	0.65 1.19 0.95 0.33	3+ 4+ 5+ 6+
LFTFHADICTLPDTEK CCAADDK EACFAVEGPK	905.9068 724.9269	905.9069 724.9261	0.11 1.10	4+ 5+

*: The free Cysteine is alkylated by 4-vinylpyridine.

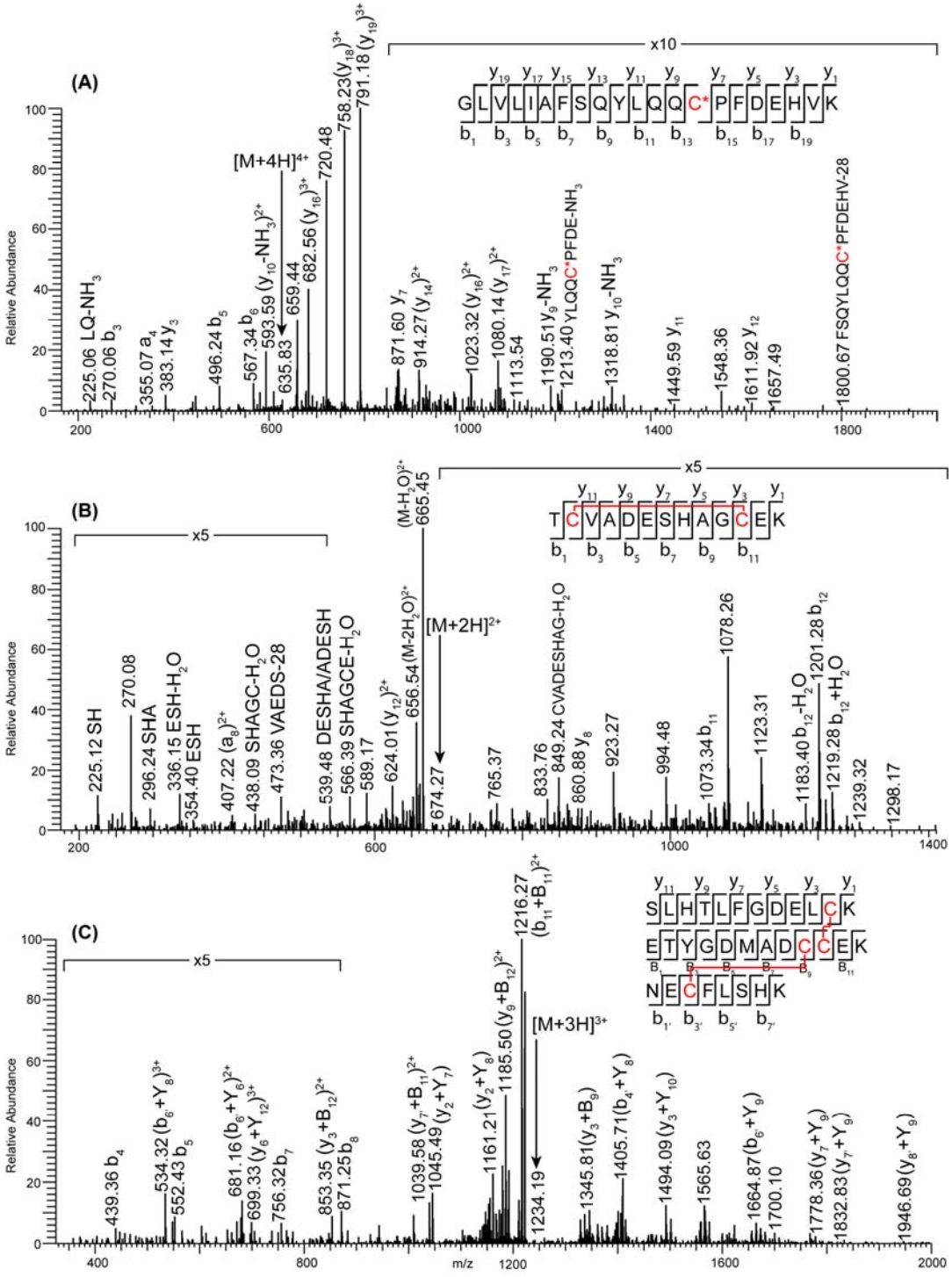

Figure 4. Representative LC/ESI-FTICR MS/MS data for the disulfide-linked tryptic peptides from bovine serum albumin; (A) peptide with a free cysteine residue; (B) peptide with an internally linked disulfide bond; (C) peptides with two inter-chain disulfide linkages.

Disulfide mapping of CON-S gp140 ΔCFI

Owing to the successful application of this approach in disulfide mapping of bovine serum albumin, we extend its utility to a structurally complex protein CON-S gp140 ΔCFI.

CON-S gp140 ΔCFI is a synthetic form of the HIV-1 Env protein; in small animal vaccine trials, it was shown to induce type I and limited type II neutralizing antibodies against the HIV-1 virus.[53] This protein contains ~600 amino acid residues[53], 52 potential cleavage sites for trypsin, 18 cysteine residues, and 31 potential N-linked glycosylation sites, attached with a heterogeneous population of glycans.[128] It is expressed mainly as a dimer. According to the disulfide connectivity in a previously analyzed recombinant, monomeric HIV Env protein,[96] nine disulfide bonds should be present for each monomeric unit of CON-S gp140 ΔCFI, if the disulfide bonding pattern is conserved. This "expected" disulfide connectivity for the monomeric form of CON-S gp140 ΔCFI is shown in Figure 5A, in which the disulfide bonds define the boundaries of the variable regions (V1-V5) as well as conserved domains in HIV Env protein.[96, 129] Since CON-S gp140 ΔCFI used in this study is an oligomeric form of Env, we accounted for the possibility that the disulfide bonding pattern could be significantly different. Therefore, many possibilities for the disulfide connectivity were considered and investigated in data analysis, including free cysteine residues, the disulfide bonding pattern observed previously,[96] new disulfide bonds within the monomeric unit and inter-chain disulfide bonds between two monomeric units.

One final obstacle in analyzing disulfide bonds of CON-S gp140 ΔCFI is dealing with

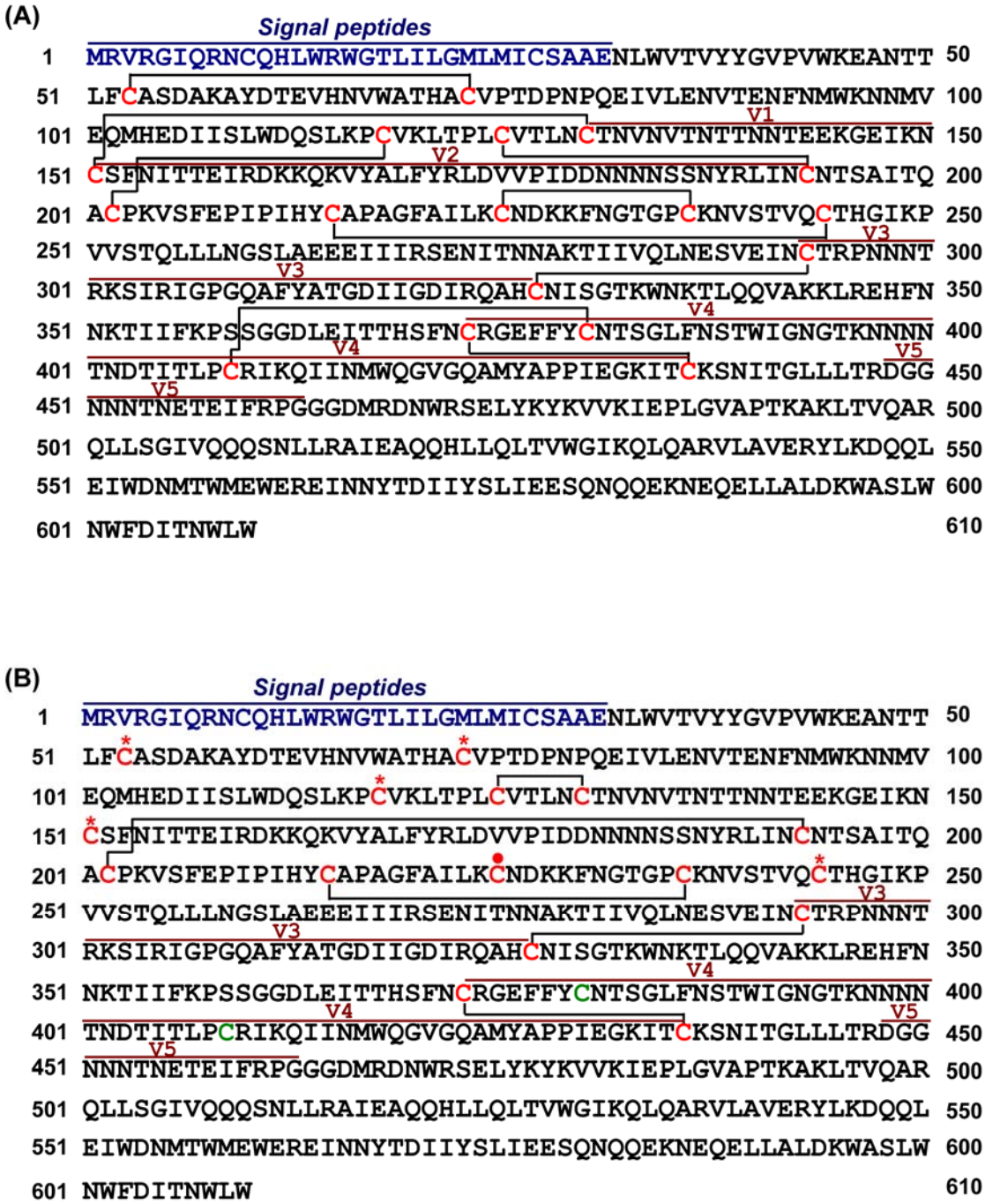

Figure 5. Overview of (A) “Expected” disulfide-linkages based on the disulfide bond arrangement of a previous analysis of a monomeric form of HIV Env protein expressed in CHO cells.[96] and (B) experimentally determined disulfide linkages in CON-S gp140 ΔCFI. (A): disulfide linkages are indicated with a solid line and cysteine residues are shown in red; (B): cysteine residues shown in red and green represents the identified and non-identified cysteines, respectively. The cysteines

labeled with a star represent the free cysteines. The cysteine labeled with a circle indicates a formed inter-subunit disulfide bond to connect two monomeric units in CON-S gp140 ΔCFI. The disulfide linkages are indicated with a solid line and the variable regions (V1 to V5) are labeled.

protein glycosylation. This protein is extensively glycosylated. The glycans are bulky and block proteases from accessing the peptide backbone. This would result in multiple missed cleavage sites during enzymatic digestion, thus producing complicated spectra in MS analysis. As a result, the glycans attached to CON-S gp140 ΔCFI were cleaved prior to the disulfide mapping, to facilitate trypsin digestion.

Control experiment to validate the deglycosylation step in disulfide mapping of CON-S gp140 ΔCFI

While the deglycosylation step is essential in assigning the disulfide bond arrangement of CON-S gp140 ΔCFI, it is possible that this process would result in disulfide scrambling. Herein, we introduced a control experiment to investigate this possibility. The validation protein, bovine serum albumin, was incubated with PNGase F at 37 °C for one week, followed by alkylation with 4-Vinylpyridine and tryptic digestion. The resultant tryptic peptides containing inter-/intra-disulfide linkages were subjected to LC/ESI-FTICR-MS analysis. Our study shows that the same disulfide connectivity in BSA is obtained, compared to the results described in the previous section. This demonstrates that the conditions described herein for the extra deglycosylation step do not affect the determination of disulfide linkages in glycoproteins.

Determination of disulfide bonds in CON-S gp140 ΔCFI

A schematic work-flow of disulfide-mapping in CON-S gp140 ΔCFI is shown in Figure 2B. The glycoprotein was enzymatically deglycosylated with PNGase F by incubating the protein:enzyme solution at 37°C for one week. The enzymatic release of glycans converts asparagine in the peptide consensus sequence NXT/S to aspartic acid, which results in a mass shift of 1 Da; see Scheme 1.

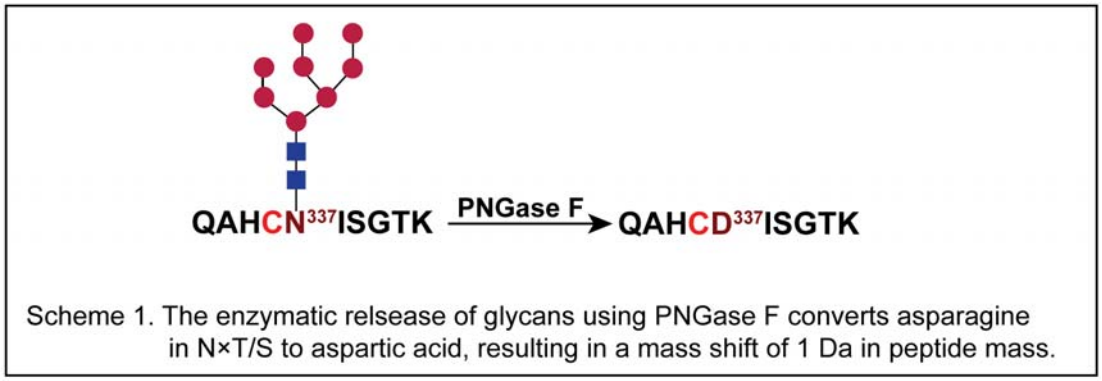

Scheme 1. The enzymatic relsease of glycans using PNGase F converts asparagine in N×T/S to aspartic acid, resulting in a mass shift of 1 Da in peptide mass.

It is necessary to know which asparagines (N) would be converted to aspartic acids (D) during deglycosylation, so that the theoretical masses of each peptide would be elucidated; therefore, the glycosylation site occupancy of the protein must be known or determined. The determination of glycosylation site occupancy in CON-S gp140 ΔCFI was achieved and described in a previous work.[128] Accordingly, the cysteine-containing tryptic peptides from CON-S gp140 ΔCFI with fully or partially occupied glycosylation sites and their corresponding deglycosylated peptide masses are listed in Table 2. The masses in this table were used to generate theoretical masses for a wide variety of possible disulfide-linked peptides, as described above, and this list of theoretical masses was interrogated against the mass spectral data, in order to determine the disulfide connectivity of this protein.

Table 2. Glycosylation sites occupancy on the Cys-containing tryptic peptides of CON-S gp 140 ΔCFI

CON-S gp140 Δ CFI	Number of potential glycosylation sites	Number of sites occupied	Theoretical deglycosylated peptide mass (*m/z*)
EAN^{48}TTLFCASDAK	1	1	1371.6097
AYDTEVHNVWATHACVPTDPNPQEIVLEN^{87}VTENFNMWK	1	1	4413.0224
CNDKKFN^{237}GTGPCK	1	1	1412.6298
QAHCN^{337}ISGTK	1	1	1059.4889
GEFFYCN^{391}TSGLFN^{397}STWIGN^{403}GTK	3	3	2446.0545
LTPLCVTLN^{129}CTNVN^{135}VTN^{138}TTN^{141}NTEEK	4	2 and 3	2738.2860 and 2739.2700
N^{155}CSFN^{159}ITTEIR	2	1 and 2	1298.6046 and 1299.5886
LINCN^{201}TSAITQACPK	1	0 and 1	1576.7823 and 1577.7663
N^{245}VSTVQCTHGIKPVVSTQLLLN^{266}GSLAEEEIIIR	2	1 and 2	3562.9152 and 3563.8992
TIIVQLN^{293}ESVEIN^{299}CTRPNN^{305}NTR	3	1 and 2	2529.2726 and 2530.2566
NNN^{413}NTN^{416}DTITLPCR	2	1 and 2	1590.7176 and 1591.7016

The mass spectral data was acquired by first subjecting the deglycosylated CON-S gp140 ΔCFI to tryptic digest, then obtaining an LC/ESI-FTICR-MS analysis. Representative reverse-phase HPLC chromatogram and ESI-FTICR MS data of tryptic peptides from deglycosylated CON-S gp140 ΔCFI are shown in Figure 6A and B, respectively. The FTICR-MS spectrum of HPLC fraction eluting between 14-15 min (the red bar shown in Figure 6A) shows a doubly charged peak at *m/z* 788.8779 originating from an intra-chain disulfide linked peptide, LINCDTSAITQACPK. Figure 6 inset shows a zoomed-in spectrum of this peak, which is used to identify the monoisotopic peak at *m/z* 788.3805 and its corresponding charge state. The aspartic acid residue (labeled in green) was generated upon deglycosylation with PNGase F, as described above.

The summary of all the experimentally determined disulfide linkages in CON-S gp140 ΔCFI is shown in Table 3. Only two interchain disulfide linked peptides were detected as having a disulfide bonding pattern consistent with the disulfide bonding observed in the previous analysis of a monomeric form of Env protein.[96] These two

disulfide-linked peptides form the third and forth variable regions (V3, V4) in CON-S gp140 ΔCFI. It is worth noting that the V3 loop is an immunodominant region, which is responsible for the generation of a wide range of neutralizing antibodies.[53] Aside from these two disulfide-linked peptides, which are consistent with the "expected" disulfide-linkages for monomeric Env,[96] several peptides with unpaired cysteine residues, intra-, and inter-chain disulfide linkages were identified, which are also listed in Table 3. Most notable in this group of newly-described disulfide bonding is the tryptic peptide CNDKK, which forms an inter-subunit disulfide bond, where a disulfide bond connects the same peptide region present in two monomeric units. This disulfide-linked peptide demonstrates the exact cysteine residue responsible for the oligomerization of this protein.

To further verify each of the disulfide linkages and peptide sequences of these peptide clusters, MS/MS analysis was performed. In each case, the MS/MS data is consistent with the assignments presented in Table 3. Representative LC/ESI-LTQ-FTICR MS/MS data are shown in Figure 7. Three classes of peptides containing intra-, inter-, and self-linked disulfide bonds have been confirmed by the fragmentation ions observed in the MS/MS analysis. Figure 7A depicts the fragmentation of a peptide with an intra-chain disulfide linkage. For the product ions at *m/z* 779.74 and 874.77, in which the disulfide bonds are dissociated, the termini of the cysteine residues were detected as thiol groups (-SH), as expected, based on prior work.[98] The ion at *m/z* 975.50, with an intact disulfide bond, demonstrates that this peptide indeed contains an intra-chain disulfide linkage. All of the other major ions in the spectrum are also assignable, and consistent with the peptide sequence shown on the Figure.

Figure 7B and C represent the verification of an interchain disulfide-linked peptide and the peptides forming an inter-protein disulfide bond, connecting the two monomeric subunits in CON-S gp140 ΔCFI, respectively. In Figure 7B, the product ions denoted y/b were generated from the peptide chain with an N-terminal threonine (T), whereas product ions denoted Y/B were produced from the peptide chains with N-terminal isoleucine (I). As in Figure 7A, the data in 7B and 7C clearly show that the MS/MS data is highly consistent with the assignment for each precursor ion, further validating the data in Table 3.

An overview of the experimentally determined disulfide bonds from this study is shown in Figure 5B. In the N-terminal region (defined by amino acid residues 1-250) of CON-S gp140 ΔCFI, six cysteine residues form intra-, and inter-chain disulfide bonds; one cysteine residue forms an inter-protein disulfide bond which connects the same regions of two monomeric units in CON-S gp140 ΔCFI; and five unpaired cysteine residues are present in the early region of the protein. While the disulfide connectivity in the N-terminal region of the protein is completely different, the disulfide linkages from V3 and V4 regions are consistent with the putative disulfide bonds in a previous analysis of a monomeric form of Env protein.[96] Overall, out of 18 cysteine residues in CON-S gp140 ΔCFI, 16 cysteine residues have been identified by LC/ESI-FTICR MS analysis. Two cysteine residues within the V4 loop, Cys^{380} and Cys^{409}, were not detected. This is probably due to the fact that the tryptic peptide generated within V4 loop would be large, and it contains numerous acidic amino acid residues, so its ionization efficiency in MS would be problematic.

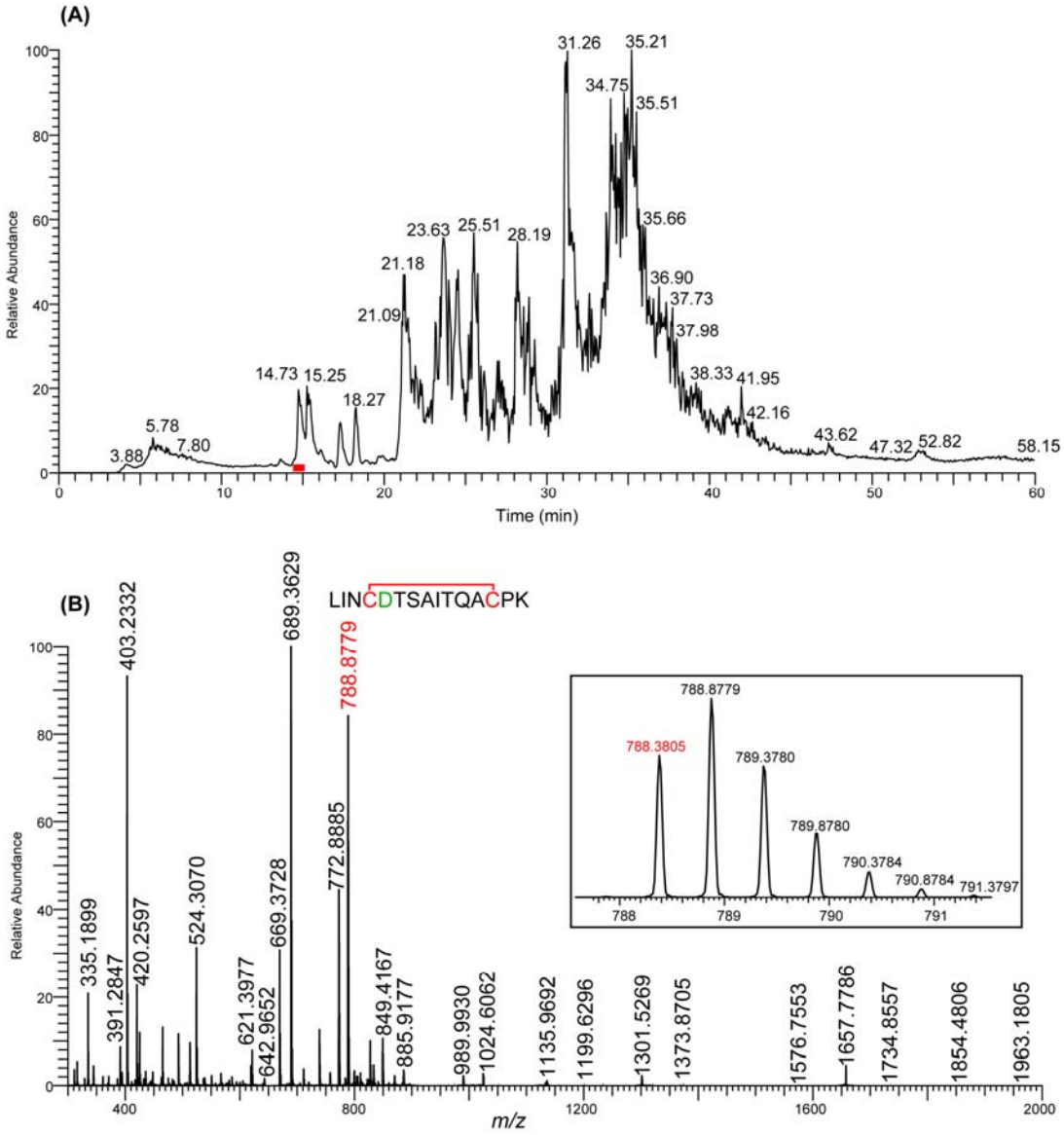

Figure 6. Representative (A) reverse-phase HPLC chromatogram and (B) LC/ESI-FTICR MS data of tryptic peptides from CON-S gp140 ΔCFI; The tryptic peptides are separated within a 60-min gradient. The MS spectrum of HPLC fraction eluting at 14-15 min (labeled with a red bar in A) shows a peak at *m/z* 788.8779 (in red) corresponding to the disulfide-linked tryptic peptides. Inset: The zoomed-in spectrum of the detected disulfide-linked peptide peak, which is used to identify the monoisotopic peak and charge state.

Table 3. Summary of the disulfide linkages in CON-S gp140 ΔCFI detected by LC-LTQ-FTICR

Peptides Peptides in V3 and V4 loops	Theoretical *m/z*	Experimental *m/z*	Mass error ppm	Charge State
TIIVQLDESVEIDCTRPNNNTR (PyroQ)AHCDISGTK	1190.5702	1190.5766	5.4	3+
TIIVQLDESVEINCTRPNNNTR (PyroQ)AHCDISGTK	1190.2422	1190.2416	0.5	3+
TIIFKPSSGGDLEITTHSFNCR ITCK	721.8639 577.6925	721.8649 577.6940	1.4 2.6	4+ 5+

Peptides that are capped with vinylpyridine	Theoretical *m/z*	Experimental *m/z*	Mass error ppm	Charge State
EADTTLFC*ASDAK	738.8374 492.8940	738.8386 492.8946	1.6 1.2	2+ 3+
AYDTEVHNVWATHAC*VPTDPNPQEIVLEDVTENFNMWK	904.4219	904.4226	0.8	5+
NNMVEQMHEDIISLWDQSLKPC*VK	988.1469 741.3620 593.2910	988.1521 741.3645 593.2925	5.3 3.4 2.5	3+ 4+ 5+
DC*SFNITTEIR	702.3349 468.5590	702.3360 468.5594	1.6 0.9	2+ 3+
DVSTVQC*THGIKPVVSTQLLLDGSLAEEEIIIR	1223.6572 917.9947 734.5972	1223.6643 917.9991 734.5991	5.8 4.8 2.6	3+ 4+ 5+
TIIFKPSSGGDLEITTHSFNC*R	843.4250 632.8206 506.4579	843.4267 632.8170 506.4588	2.0 5.7 1.8	3+ 4+ 5+

Peptides that are internally linked	Theoretical *m/z*	Experimental *m/z*	Mass error ppm	Charge State
LINCNTSAITQACPK	394.4472	394.4485	3.3	4+
LINCDTSAITQACPK	788.3790	788.3805	1.9	2+
LTPLCVTLDCTNVDVTNTTNNTEEK	912.7617 684.8231	912.7569 684.8188	5.3 6.3	3+ 4+

Peptides are proximal to each other	Theoretical *m/z*	Experimental *m/z*	Mass error ppm	Charge State
VSFEPIPIHYCAPAGFAILK	998.8346	998.8227	11.9	3+
FDGTGPCK	749.3778	749.3790	1.6	4+

Peptide that is self-linked	Theoretical *m/z*	Experimental *m/z*	Mass error ppm	Charge State
CNDKK CNDKK	1211.5509 606.2791	1211.5730 606.2890	18.2 16.3	1+ 2+

*: free cysteines are alkylated by 4-vinylpyridne; Asparagine in NXT/S is converted to aspartic acid upon deglycosylation and labeled in green.

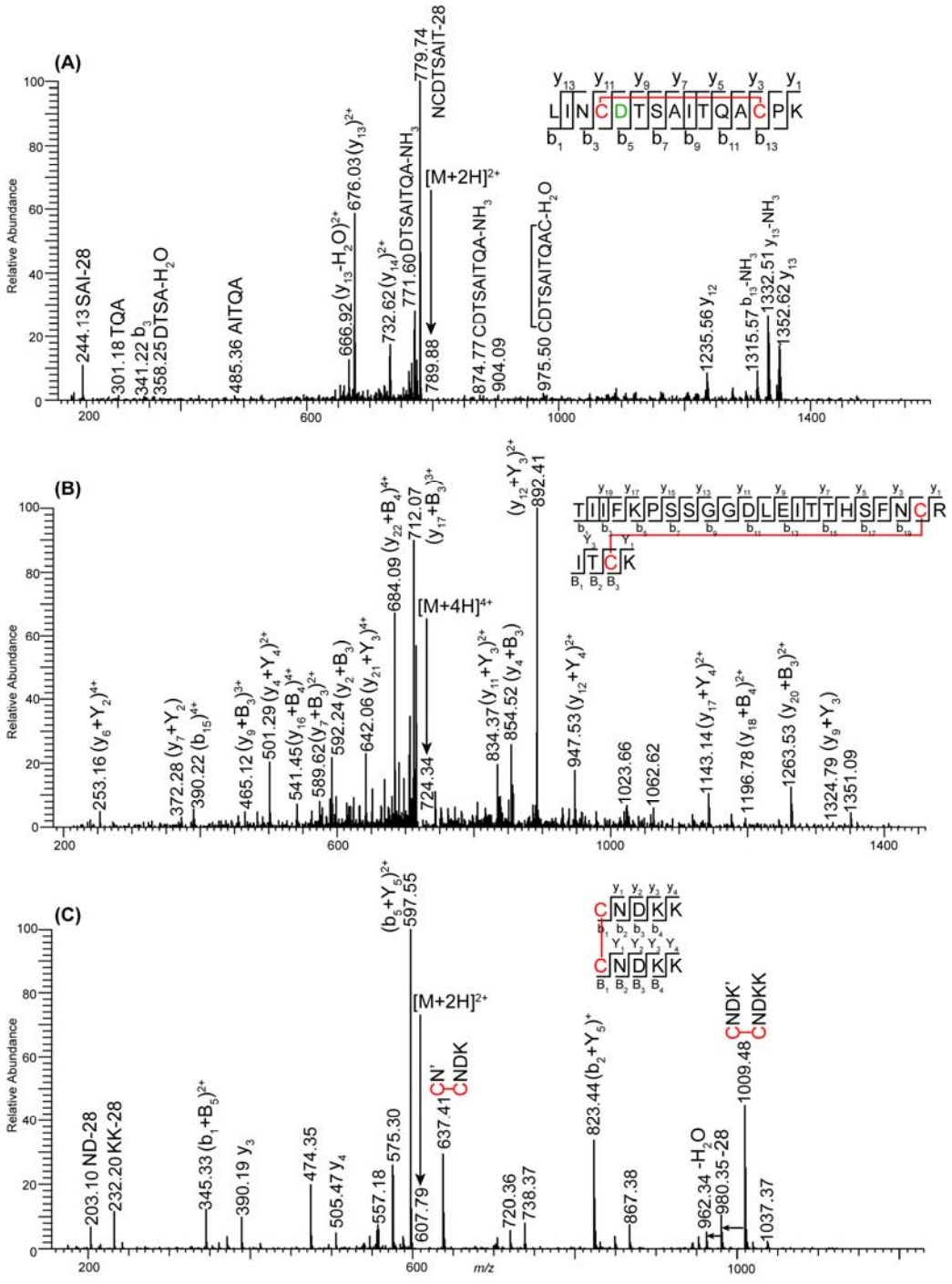

Figure 7. Representative LC/ESI-FTICR MS/MS data for the disulfide-linked tryptic peptides from CON-S gp140 ΔCFI (A) peptide with an internally linked disulfide bond; (B) disulfide-linked peptides within the V4 loop (C) peptide with a self-linked disulfide bond, showing where the inter-subunits contact point in CON-S gp140 ΔCFI is located. N' and K' indicate that the side chain of asparagine and lysine are cleaved, while the peptide backbone remains intact.

Biological implications of this study

The results obtained from this study demonstrate that the disulfide connectivity of CON-S gp140 ΔCFI is dramatically different than the disulfide linkages in the previously analyzed monomeric form of HIV Env protein expressed from CHO cells[96] (Figure 5A), especially in the N-terminal region of protein where the first and second variable regions (V1, V2) are normally formed.

Our findings complement a previous study by Jobes *et al*, which shows that the V1 and V2 regions of Env are highly variable, with the respect to the cysteine content.[129] These authors suggest that when the insertion or deletion of cysteine residues occurs in these regions, it could result in the disruption of normal disulfide bonds.[129] Both our work and this previous work show that the cysteine residues in the N-terminal region of Env can have a varying disulfide connectivity. The V1 and V2 region of the protein are important, because they shield the V3 region, preventing antibodies from directly accessing neutralizing epitopes present in V3.[129-131] Since the disulfide linkages of the V1 region in CON-S gp140 ΔCFI are connected differently than those described previously,[96, 111-114] and many unpaired cysteine residues are present, the disulfide connectivity in CON-S gp140 ΔCFI may cause the epitopes in the V3 region to be more exposed, facilitating immune response to this region.

In addition, our study identified an inter-subunit disulfide bond via the self-linked peptide, CNDKK. This peptide is near the V2 loop and is responsible for the oligomeric nature of CON-S gp140 ΔCFI.[53] This result can be used to support and further clarify previous studies that reported the deletion of the V2 domain on the HIV Env causes the disruption of dimeric protein conformation, implicating that this region

would be involved in the inter-subunit connection in the oligomeric form of Env protein.[122]

Aside from the disulfide linkages in V1 and V2 regions, the final interesting implication of this work relates to the disulfide linkage in the V3 loop, which is identified in our study to be consistent with the disulfide bonding established for monomeric Env.[96, 111-114] This is somewhat expected, since this region was determined to be immunodominant, and it contributes to the improved immunogenicity in CON-S gp140 ΔCFI.[53] As demonstrated here, the disulfide bond arrangement in the N-terminal region of CON-S gp140 ΔCFI is not in agreement with the putative disulfide linkages in literature;[96] however, marked improvement of immunogenicity in CON-S gp140 ΔCFI was obtained and described previously.[53] This implies that satisfactory immune response may rely on several factors including the presence of V3 loop, the degree of accessibility to the neutralizing epitopes on this region, and the oligomeric conformation of Env protein, etc. Further study of the correlation between the disulfide linkages in Env protein and its immune response will provide more information on understanding how the antigenic structures affect the immnogenicity. The disulfide bond mapping for other synthetic and wild-type recombinant Env proteins is on-going and will be presented separately.

5.4 Conclusions

Aiming to elucidate the correlation between the structure of the HIV-1 Env protein and its immunogenicity, we developed a MS-based approach, LC/ESI-FTICR, to characterize the disulfide linkages on the Env protein CON-S gp140 ΔCFI. Prior to applying this approach to the Env protein, the method was validated using a

disulfide-rich protein, bovine serum albumin. In this protein, all the 35 cysteine residues were detected. A total 17 disulfide-linked peptides and 1 unpaired half-cysteine residue were identified with high mass accuracy, and confirmed by MS/MS experiments. This data is in agreement with the putative disulfide linkages reported previously for BSA.[126]

This approach was then applied to elucidate the disulfide connectivity in CON-S gp140 ΔCFI. Out of 18 cysteine residues, 16 cysteine residues were identified. In the N-terminal region of CON-S gp140 ΔCFI, one cysteine residue Cys^{225} was identified as forming an inter-subunit disulfide bond, stabilizing the dimeric composition of this HIV-1 Env protein. Six cysteines are involved in forming disulfide bonds within the monomeric units. In addition to the cysteines that are utilized in disulfide bond connectivity, five free cysteine residues are present in the N-terminal region of CON-S gp140 ΔCFI.

Although the cysteine residues in the N terminal region of the protein are different from the putative disulfide linkages from an analysis of a monomeric form of HIV Env protein,[96] the V3 and V4 loops formed in the later region of the protein are indeed identified in CON-S gp140 ΔCFI. Among these two regions, the V3 loop is immunodominant and contributes to the improved immunogenicity of CON-S gp140 ΔCFI. The disulfide bond determination of CON-S gp140 ΔCFI indicates that the satisfactory immune response may depend on several factors including the presence of the V3 loop, the degree of accessibility to the neutralizing epitopes on this region, and the oligomeric conformation of Env protein, etc.

Acknowledgements

The authors acknowledge the National Institute of Health for funding (project number RO1GM077266, PO1AI61734) and a Collaboration for AIDS Vaccine Development Grant from the Bill and Melinda Gates Foundation to Dr. Barton F. Haynes.

5.5 References

1. Fukuyama, Y.; Iwamoto, S.; Tanaka, K.J. Rapid sequencing and disulfide mapping of peptides containing disulfide bonds by using 1,5-diminonaphthalene as a reductive matrix. *J. Mass. Spectrom.* **2006,** *41,* 191-201.

2. Leonard, C.K.; Spellman, M.W.; Riddle, L.; Harris, R. J.; Thomas, J. N.; Gregory, T. J. Assignment of intrachain disulfide bonds and characterization of potential glycosylation sites of the type 1 recombinant human immunodeficiency virus envelope glycoprotein (gp120) expressed in Chinese hamster ovary cells. *J. Biol. Chem.* **1990,** *265,* 10373-10382.

3. Wefing, S.; Schnaible, V.; Hoffmann, D. SearchXLinks. A program for the identification of disulfide bonds in proteins from mass spectra. *Anal. Chem.* **2006,** *78,* 1235-1241.

4. Zhang, M.; Kaltashov, I. A. Mapping of protein disulfide bonds using negative ion fragmentation with a broadband precursor selection. *Anal. Chem.* **2006,** *78,* 4820-4829.

5. Nguyen, D. N.; Bechker, G. W.; Riggin, R. M. Protein mass spectrometry: application to analytical biotechnology. *J. Chromatogr. A.* **1995,** *705,* 21-45.

6. Baneyx, F.; Mujacic, M. Recombinant protein folding and misfolding in *Escherichia Coli. Nat. Biotechnol.* **2004,** *22,* 1399-1408.

7. Gorman, J.J.; Wallis, T.P.; Pitt, J.J. Protein disulfide bond determination by mass spectrometry. *Mass Spectrom. Rev.* **2002,** *21,* 183-216.

8. Smith, D.L.; Zhou, Z. Strategies for locating disulfide bonds in proteins. *Methods Enzymol.* **1990,** *193,* 374-389.

9. Haniu, M.; Arakawa, T. Analysis of disulfide structures in proteins. *Curr. Top. Pept. Protein Res.* **1997**, *2*, 115-124.

10. Craik, D.J.; Daly, N.L. NMR as a tool for elucidating the structures of circular and knotted proteins. *Mol. Biosyst.* **2007,** *3,* 257-265.

11. Acharya, K. R.; Lloyd, M.D. The advantages and limitations of protein crystal structures. *Trends Pharmacol. Sci.* **2005,** *26,* 10-14.

12. Liu, H.; Hsu, J. Recent developments in structural proteomics for protein structure determination. *Proteomics*. **2005,** *5,* 2056-2068.

13. Andrews, P.C. Selective isolation of disulfide-containing peptides from trypsin digests using strong cation exchange HPLC. *Curr. Res. Protein Chem.* **1990,** 95-102.

14. Crimmins, D.L.; Analysis of disulfide-linked homo- and hetero-peptide dimmers with a strong cation-exchange sulfoethyl aspartamide column. *Pept. Res.* **1989,** *2,* 395-401.

15. Brown J.R.; Kauffman, D.L.; Hartley, B.S. Primary structure of porcine pancreatic elastase; The N-terminus and disulfide bridges. *Biochem. J.* **1967,** *103,* 497-507.

16. Haniu, M.; Arakawa, T.; Bures, E.J.; Young, Y.; Hui, J.O.; Rohde, M.F.; Welcher, A.A; Horan, T. Human leptin receptor. Determination of disulfide structure and N-glycosylation sites of the extracellular domain. *J. Biol. Chem.* **1998,** *273,* 28691-28699.

17. Irungu, J.; Go, E.P.; Dalpathado, D.S.; Desaire, H. Simplification of mass spectral analysis of acidic glycoprptides using GlycoPep ID. *Anal. Chem.* **2007,** *79,* 3065-3074.

18. Owusu-Apenten, R.K.; Chee, C.; Hwee, O.P. Evaluation of a sulphydryl-disulphide exchange index (SEI) for whey proteins ─ β-lactoglobulin and bovine serum albumin. *Food Chem.* **2003,** *83,* 541-545.

19. Liao, H.; Sutherland, L.L.; Xia, S.; Brock, M. E.; Scearce, R. M.; Vanleeuwen, S.; Alam, S. M.; McAdams, M.; Weaver, E. A.; Camacho, Z. T.; Ma, B.; Li, Y.; Decker, J. M.; Nabel, G. J.; Montefiori, D. C.; Hahn, B. H.; Korber, B. T.; Gao, F.; Haynes, B. F. A group M consensus envelope glycoprotein induces antibodies that neutralize subsets of subtype B and C HIV-1 primary viruses. *Virology* **2006,** *353,* 268-282.

20. Kwong, P.D.; Wyatt, R.; Robinson, J.; Sweet, R.W.; Sodroski, J.; Hendrickson, W.A. Structure of an HIV gp120 envelope glycoprotein in complex with the CD4 receptor and a neutralizing human antibody. *Nature* **1998,** *393,* 648-659.

21. Wyatt, R.; Kwong, P.D.; Desjardins, E.; Sweet, R.W.; Robinson, J.; Hendrickson, W.A.; Sodroski, J.G. The antigenic structure of the HIV gp120 envelope glycoprotein. *Nature* **1998,** *393,* 705-711.

22. Zhou, T.; Xu, L.; Dey, B.; Hessell, A.J.; Van, R.D.; Xiang, S-H.; Yang, X.; Zhang, M-Y.; Zwick, M.B.; Arthos, J.; Burton D.R.; Dimitrov D.S.; Sodroski, J.; Wyatt, R.; Nabel, G.J.; Kwong, P.D. Structural definition of a conserved neutralization of epitope on HIV-1 gp120. *Nature* **2007,** *445,* 732-737.

23. Chen, B.; Vogan, E.M.; Gong, H.; Skehel, J.J.; Wiley, D.C.; Harrison, S.C. Structure of an unliganded simian immunodeficiency virus gp120 core. *Nature* **2005,** *433,* 834-841.

24. Flynn, N. M.; Forthal, D. N.; Harro, C. D.; Judson, F. N.; Mayer, K. H.; Para, M. F. Placebo-controlled phase 3 trial of a recombinant glycoprotein 120 vaccine to prevent HIV-1 infection. *J. Infect. Dis.* **2005,** *191*, 654-665.

25. Gilbert, P. B.; Peterson, M. L.; Follmann, D.; Hudgens, M. G.; Francis, D. P.; Gurwith, M.; Heyward, W. L.; Jobes, D. V.; Popovic, V.; Self, S. G.; Sinangil, F.; Burke, D.; Berman, P. W. Correlation between immunologic responses to a recombinant glycoprotein 120 vaccine and incidence of HIV-1 infection in a phase 3 HIV-1 preventive vaccine trial. *J. Infect. Dis.* **2005,** *191,* 666-677.

26. Sharma, V.A.; Kan, E.; Sun, Y.; Lian, Y,; Cisto, J.; Frasca, V.; Hilt, S.; Stamatotos, L.; Donnelly, J.J.; Ulmer, J.B.; Barnett, S.W.; Srivastava, I.K. Structural characteristic correlate with immune responses induced by HIV envelope glycoprotein vaccines. *Virology* **2006,** *352,* 131-144.

27. Srivastava, I.K.; Stamatatos, L.; Legg, H.; Kan, E.; Fong, A.; Coates, S.R.; Leung, L.; Wininger, M.; Donnelly, J.J.; Ulmer, J.B.; Barnett, S.W. Purification and characterization of oligomeric envelope glycoprotein from a primary R5 subtype B human immunodeficiency virus. *J. Virol.* **2002,** *76,* 2835-2847.

28. Srivastava, I.K.; Stamatatos, L.; Kan, E.; Vajdy, M.; Lian, Y.; Hilt, S.; Martin, L.; Vita, C.; Zhu, P.; Roux, K.H.; Vojtech, L.; Montefiori, D.C.; Donnelly, J.; Ulmer, J.B.; Barnett, S.W. Purification, characterization, and immunogenicity of a soluble trimeric envelope protein containing a partial deletion of the V2 loop derived from SF162, an R5-tropic human immunodeficiency virus type 1 isolate. *J. Virol.* **2003,** *77,* 11244-11259.

29. Barnett, S.W.; Srivastava, I.K.; Ulmer, J.B.; Donnelly, J.J.; Rappuoli, R. Development of V2-deleted trimeric envelope vaccine candidates from human immunodeficiency virus type 1 (HIV-1) subtypes B and C. *Microbes Infect.* **2005,** *7,* 1386-1391.

30. Yuan, W.; Craig, S.; Yang, X.; Sodroski, J. Inter-subunit disulfide bonds in soluble HIV-1 envelope glycoprotein trimers. *Virology,* **2005,** *332,* 369-383.

31. Center, R.J.; Earl, P.L.; Lebowitz, J.; Schuck, P.; Moss, B. The human immunodeficiency virus type 1 gp120 V2 domain mediates gp41-independent intersubunit contacts. *J. Virol.* **2000,** *74,* 4448-4455.

32. Center, R.J.; Leapman, R.D.; Lebowitz, J.; Arthur, L.O.; Earl, P.L.; Moss, B. Oligomeric structure of the human immunodeficiency virus type 1 envelope protein on the viron surface. *J. Virol.* **2002,** *76,* 7863-7867.

33. Ihling, C.; Berger, K.; Hoefliger, M.M.; Fuehrer, D.; Beck-Sickinger, A.G.; Sinz, A. Nano-high-performance liquid chromatography in combination with nano-electrospray ionization Fourier transform ion-cyclotron resonance mass spectrometry for proteome analysis. *Rapid. Commun. Mass Spectrom.* **2003,** *17,* 1240-1246.

34. Schnaible, V.; Wefing, S.; Buecker, A.; Wolf-Kuemmeth, S.; Hoffmann, D. Screening for disulfide bonds in proteins by MALDI in-source decay and LIFT-TOF/TOF-MS. *Anal. Chem.* **2002,** *74,* 2386-2393.

35. Brown, J.R. Structure of serum albumin: disulfide bridges. *Fed. Proc.* **1974,** *33,* 1389-1389.

36. Moritz, R.L.; Hall, N.E.; Connolly, L.M.; Simpson, R.J. Determination of the disulfide structure and *N*-glycosylation sites of the extracellular domain of the human signal transducer gp130. *J. Biol. Chem.* **2001,** *276,* 8244-8253.

37. Go, E.P.; Irungu, J.; Zhang, Y.; Dalpathado, D.S.; Liao, H-X.; Sutherland, L.L.; Alam, S.M.; Haynes, B.F.; Desaire, H. Glycosylation site-specific analysis of HIV envelope proteins (JR-FL and CON-S) reveals major differences in glycosylation site occupancy, glycoform profiles, and antigenic epitopes' accessibility. *Submitted*

38. Jobes, D.V.; Daoust, M.; Nguyen, V.; Padua, A.; Michele, S.; Lock, M.D.; Chen, A.; Sinangil, F.; Berman, P.W. High incidence of unusual cysteine variants in gp120 envelope proteins from early HIV type 1 infections from a phase 3 vaccine efficacy trial. *AIDS. Res. Hum. Retroviruses.* **2006,** *22,* 1014-1021.

39. Mckeating, J.A.; Shotton, C.; Cordell, J.; Graham, S.; Balfe, P.; Sullivan, N.; Charles, M.; Page, M.; Bolmstedt, A. Characterization of neutralizing monoclonal antibodies to linear and conformation-dependent epitopes within the first and second variable domains of human immunodeficiency virus type 1 gp120. *J. Virol.* **1993,** *67,* 4932-4944.

40. Pinter, A.; Honnen, W.J.; He, Y.; Gorny, M.K.; Zolla-Pazner, S.; Kayman, S.C. The V1/V2 domain of gp120 is a global regulator of the sensitivity of primary human immunodeficiency virus type 1 isolates to neutralization by antibodies commonly induced upon infection. *J. Virol.* **2004,** *78,* 5205-5215.

Chapter IV

Conclusions

In order to understand biological functional properties of glycoproteins, several efficient MS-based approaches have been developed in this study to characterize glycans on the glycoproteins.

To identify the acidic functional groups (sulfate, and phosphate) on the carbohydrates and glycopeptides, an ion-pairing strategy in conjunction with ESI-MS/MS was developed on the model phosphorylated and sulfated monosaccharides to differentiate between these two functional groups. Since both sulfate and phosphate are highly acidic compounds with different proton affinities, differences in the chemical reactivities with the ion-pairing reagents can be used to differentiate these isobaric compounds in MS/MS experiments. This approach was subsequently applied to the other biological relevant molecules, such as mono-, di-saccharides, and sulfated glycopeptides to differentiate phosphorylation and sulfation on these species.

Aside from identification of acidic glycans on the glycoproteins, we also designed an experimental workflow that maximizes coverage of glycosylation heterogeneity on glycoproteins that vary in the number of glycosylation sites and their corresponding glycan profiles. All the features of glycopeptide-based MALDI-MS analysis, including sample preparation methods, mass spectral data acquisition, and data analysis were optimized. In doing so, we designed a work-flow for glycan profiling on heavily glycosylated glycoproteins, such as HIV virus envelope protein ─ JR-FL gp 140 ΔCF, which contains 27 glycosylation sites. Out of 27 glycosylation sites, 23 glycosylation sites and over 300 glycoforms have been detected on this

protein.

In addition to glycan profiling on glycoproteins, disulfide connectivity is another predominant feature in elucidation of chemical structure of a protein and define its functional domains. Aiming to elucidate the correlation between the structure of HIV Env protein and its immunogenicity, we validated a MS-based approach, LC/ESI-FTICR, by characterizing the disulfide linkages on bovine serum albumin to optimize the experimental conditions. This approach was subsequently applied in the determination of disulfide bonds in a HIV Env protein CON-S gp140 ΔCFI. In this protein, out of 18 cysteine residues, 16 cysteine residues were identified. Two functional domains previously identified in monomeric Env protein, the third and forth variable regions (V3, and V4), are also conserved in the disulfide bonding in CON-S gp140 ΔCFI. One cysteine residue Cys^{225} was identified as forming an inter-subunit disulfide bond to stabilize the oligomeric structure of CON-S gp140 ΔCFI. Aside from the cysteines that are utilized in disulfide bond connectivity, the peptides with free cysteine residues are also present in CON-S gp140 ΔCFI. The information obtained from this study will facilitate understanding how the disulfide bond arrangement correlates to immunogenetic activities of oligomeric form of HIV Env protein and may also provide the insights into the direction for the future vaccine development.